Exploiting macrophages and nanoparticles for targeted and controlled drug delivery

Von der Fakultät für Lebenswissenschaften

der Technischen Universität Carolo-Wilhelminazu Braunschweig

zur Erlangung des Grades

eines Doktors der Naturwissenschaften

(Dr. rer. nat.)

genehmigte

D i s s e r t a t i o n

von Sami Ullah
aus Dir Lower /Pakistan

1. Referentin: Professorin Dr. SusanneEngelmann
2. Referentin: Professorin Dr. Dagmar Wirth

eingereicht am: 27.11.2019
mündliche Prüfung (Disputation) am: 18.02.2020

Druckjahr 2020

Vorveröffentlichungen der Dissertation

Teilergebnisse aus dieser Arbeit wurden mit Genehmigung der Fakultät für Lebenswissenschaften, vertreten durchdie Mentorinder Arbeit, in folgenden Beiträgen vorab veröffentlicht:

Publikationen

1. S. Ullah, K. Seidel, S. Türkkan, D. P. Warwas, T. Dubich, M. Rohde, H. Hauser, P. Behrens, A. Kirschning, M. Köster and D. Wirth, Macrophage entrapped silica coated superparamagnetic iron oxide particles for controlled drug release in a 3D cancer model. *J. Controlled Release*, 2019, **294** , 327-336

Tagungsbeiträge

1. Exploiting macrophages and nanoparticles for targeted and controlled drug delivery, 8th annual retreat, Helmholtz Centre for Infection Research, Germany (2017)
2. Evaluation of magnetic hyperthermia induced drug release in cell culture system, 9th annual retreat, Helmholtz Centre for Infection Research, Germany (2018)
3. 2nd international symposium on Bio-fabrication in corporation with I4A, 31 Aug-01 Sep 2017, Hannover, Germany
4. Exploiting macrophages and nanoparticles as targeted and controlled drug delivery tools. HZI PhD retreat 2017, Braunschweig, Germany
5. On demand drug release by hyperthermia from superparamagnetic silica nanoparticles in a 3D tumour model, Annual meeting of the German society of biomaterials, Braunschweig, Germany (2018).
6. Exploiting macrophages and nanoparticles as targeted and controlled drug delivery tools. HZI PhD retreat 2018, Braunschweig, Germany

Posterbeiträge

1. Molecular mechanism of interferon activation by microparticles, 7th annual retreat, Helmholtz Centre for Infection Research, Germany (2016)
2. 4th International symposium of the virtual institute VISTRIE, 3rd June 2016, Braunschweig Germany
3. Evaluation of magnetic hyperthermia induced drug release in 3D cell culture system, International conference on nanomedicines and nanobiotechnology, Barcelona, Spain (2017)
4. Evaluation of magnetic hyperthermia-induced drug release in a cell culture system. HZI PhD symposium 2017, Braunschweig, Germany
5. On demand drug release by hyperthermia from magnetic silica nanoparticles in 3D cell culture, HIPS annual symposium, Saarbrücken, Germany (2019)

CONTENTS

SUMMARY

Targeted delivery of drugs is a major challenge in treatment of many diseases. Systemic administration of drugs poses limitations like demand for high doses, poor selectivity and off target effects. In this context, the development of a system that enables targeted administration and controlled release of drugs is sensible. In this study, a controlled delivery system is launched that combines macrophages as transporters for nanoparticle-coupled drugs and hyperthermia mediated release of cargo from the intracellular nanoparticles. Silica-coated superparamagnetic iron oxide nanoparticles (SPIONs) were used that were mounted with cargo via a thermo-sensitive linker. By exposing these nanoparticles to an alternating electromagnetic field (AMF) magnetic hyperthermia is generated that induces release of the cargo from both, the nanoparticles and the carrier cells. This concept was evaluated for two models: i) Anticancer activity of the ansamitocin derivative, Maytansin; ii) (Z)-4-Hydroxytamoxifen dependent activation of CreERT2-mediated reporter gene switch. Upon loading of the cargo-linked SPIONs macrophages maintained their intrinsic homing property enabling them to migrate to inflammatory sites. Using 2D and 3D carrier-target cell culture models, it was shown that drug release is tightly controlled by AMF exposure and the Maytansincargoachieves efficient cancer cell killing.

Finally, the property of macrophages to rapidly accumulate at sites of inflammation was exploited for targeted delivery of cargo molecules to specific sites in the living organism. It was shown in vivo that M2 macrophages accumulate within 24 hours at sites of LPS-induced inflammation irrespective whether they were loaded with nanoparticles or not. By using the reporter-based gene switch model it was shown that macrophages can deliver (Z)-4-Hydroxytamoxifen-loaded nanoparticles to disease sites in the body and the released cargo can act on surrounding target cells.

Together, a targeted and controlled drug delivery system has been developed which fulfills requirements of fast, precise, and controlled therapeutic interventions for treatment of disease conditions.

ZUSAMMENFASSUNG / KURZFASSUNG

Die gezielte Applikation von Arzneimitteln stellt eine große Herausforderung bei der Behandlung vieler Krankheiten dar. Die systemische Gabe von therapeutischen Wirkstoffen beinhaltet Einschränkungen wie die Notwendigkeit einer hohen Wirkstoffkonzentration, geringe Selektivität und Anreicherung in nicht betroffenen Organen. Dementsprechend ist die Entwicklung eines Systems, dass eine gezielte räumliche Verabreichung und Freisetzung des Wirkstoffes ermöglicht, von großer Bedeutung. In dieser Arbeit wurde ein System eingeführt, welches die Verwendung von Makrophagen als Tranporter für Nanopartikel-gekoppelte Wirkstoffe mit deren gezielter Freisetzung aus diesen Zellen mittels Hyperthermie kombiniert. Hierzu wurden Silica-beschichtete superparamagnetische Eisenoxid-Nanopartikel(SPIONs) verwendet, an die der Wirkstoff über einen Hitze-sensitiven Linker gekoppelt ist. Sobald diese Nanopartikel einem alternierenden magnetischen Feld (AMF) ausgesetzt werden, entsteht Hitze. Dies führt zur Freisetzung des Wirkstoffes. Dieses Konzept wurde für zwei Modellmoleküle evaluiert: 1. Maytansin, daseine hohe zytotoxische Wirkung gegen Krebszellen aufweist; 2. (Z)-4-Hydroxytamoxifen, das über die Cre-Rekombinase die Aktivierung eines Reportergens induziert. Die Beladung mit diesen Wirkstoff-gekoppelten SPIONs verändert nicht die Fähigkeit von Makrophagen in inflammatorische Regionen im Mausmodell einzuwandern. In 2D und 3D-Zellkulturmodellen konnte gezeigt werden, dass die Freisetzung des Maytansin-Wirkstoffs aus den Makrophagen strikt erst nach AMF-Behandlung der Zellen erfolgt und dies zu einem effektiven Absterben von Krebszellen führt. Abschließend wurde die spezifische Anreicherung von SPION-beladenen Makrophagen in einem in vivo Inflammationsmodell untersucht. Es konnte gezeigt werden, dass SPION-beladene M2 Makrophagen innerhalb von 24 Stunden mit vergleichbarer Effizienz in Regionen mit LPS-induzierter Inflammation in der Maus einwandern. Mittels (Z)-4-Hydroxytamoxifen-beladener Nanopartikel wurde der Nachweis erbracht, dass Makrophagen den Wirkstoff in spezifischen inflammatorischen Bereichen in der Maus freisetzen und dieser in Zielzellen wirken kann.

Zusammenfassend kann festgestellt werden, dass die Kombination aus Makrophagen als Transportvehikel und die thermosensitive Kopplung von Wirkstoffen ansuperparamagnetischeNanopartikeln zukünftige Anforderungen an eine gezielte Vor-Ort-Freisetzunghoch-wirksamer Therapeutika innerhalb des Körpers ermöglichen kann.

1 INTRODUCTION

1.1 Drug delivery

The pharmacological properties of drugs are an important determinant of their therapeutic efficacy. Drug-target affinity, turnover of the molecule in the body, accumulation in target and off-target tissues as well as off-target activities are important parameters that specify the therapeutic effect and biological side effects. To achieve a high drug-target interaction, the drug is required at a particular concentration for a particular time at a specific site in the body [1]. Conventional drug delivery strategies like injections or oral delivery (tablets, suspension or capsules) have certain basic disadvantages. For example, systemic applications of drugs in the form of intravenous injections ensure delivery of the drug to the target site but in a minimal amount, while most of the drug injected is distributed systemically, potentially affecting also different other organs. Similarly, oral delivery of drugs possesses the chance that the drug might be either degraded and/or un-specifically absorbed within the gastrointestinal tract [2]. Local administration of drugs in the form of creams and ointments or direct injection into affected tissue do have the advantage that the required amount of drug is delivered site specifically. However, this is not applicable for many diseases and infections where internal organs are the target sites. Apart from these, there are additional factors, which are taken into consideration in current drug delivery approaches. These include bioavailability, absorption, timing of delivery and pharmacokinetics [3]. Therefore, there is a need to devise a controlled and targeted drug delivery (TDD) approach to increase therapeuticefficacy.

A typical successful TDD approach has four main properties:

- Retention: the drug should be retained in the delivery system without any non-specific released
- Evasion: the system should be able to evade the immune system
- Targeting: only the pathologically damaged sites should be targeted
- Release: the drug should be released on demand

Together this means that the formulation should circulate in the body in a way that its nonspecific degradation is reduced and its circulation time in the body is increased. This, in turn gives the advantage that the drug will reach its target site and there it should be specifically released in a controlled manner.

1.2 Advances in drug delivery

An important component of a successful TDD is the controlled release (CR) of a therapeutic molecule. With advances in nanotechnology, many breakthroughs have been made in both controlled and targeted drug release systems. With the use of such systems, certain side effects like off target release can be limited. Nanoparticles gives an extra advantage when CR or TDD is in question. With the use of nanoparticles as drug carriers, not only the drug can be targeted specifically to the pathogenic tissues and off-target effects be avoided but also the residence of a drug at a target site can be increased. Further, it is shown that certain nanoparticles improve the cellular uptake and thereby higher drug stability in vivo is achieved [4]. Based on the therapeutic goal, a number of different types of materials can be used to make nanocarriers. A schematic overview of different nanoparticle based drug delivery strategies has been shown in Figure 1.1. Some of these are discussed in the following chapter.

1.3 Polymer-based drug delivery systems

Polymers can provide a better blood circulation (retention) time to the drugs as compared to their conventional delivery. Polymers have been the first choice in targeted and controlled drug delivery systems in the form of liposomes or hydrogels. Polymers have the advantage that the drug can be easily attached and that the release is generally based on simple diffusion. In other circumstances like hydrogels, usually, solvents activate the release of the drug from them. Polymers used in drug delivery research can be biodegradable or non-biodegradable [5]. For instance, Polyester based polymers which are one of the most extensively used polymers in drug delivery research. These include polylactic acid (PLA), polyglycolic acid (PGA) or co-polymers like poly lactic-co-glycolic acid (PLGA). The stereochemistry of these polymers can be modified to give more biological or thermal and mechanical properties to the material [6]. The release mechanism from such particles is usually based on diffusion, although, temperature or pH can enhance the release as well, based on their formulation [7]. On the other hand, polyamino acids have been extensively explored for delivery of small molecules. The release from polyaminoacid based systems depends on proteolytic enzyme activity such as polylysines are degraded by trypsin. Although, due to their immunogenic nature, care must be taken during its selection as drug delivery tool [8].

Hydrogels that are also called ‘smart polymers’ represent a relatively new concept introduced for the delivery of therapeutic and imaging agents. Hydrogels have relatively high water absorbing capacity conferring them with high permeability. Thereby, these nanoparticles are more responsive to chemical, biological or physical stimuli, hence given the name, stimuli responsive hydrogels [9]. Recently, polyacrylamide-based hydrogels have been shown to respond to antigens like bacteria which trigger a mechanism for release of drugs like antibiotics enclosed in them [10].

Apart from these, a number of different polymers like cellulose, micelles, polyanhydrides, silicones, acrylic polymers etc. have been fabricated and investigated to achieve better targeting and release[11].

1.4 Liposomes as a drug delivery system

Liposomes are one of the first to be investigated as a drug delivery tool. Liposomes range in sizes from nanometers to micrometers in diameter (20-1000nm). Typically, they are spherical structures consisting of phospholipids bilayers. The formation of liposomes is relatively easy as they can be formed by simply dissolving certain lipids in specific aqueous media or by sonication. They have characteristics of a typical good delivery tool, like high drug solubility which in turn increase pharmacokinetics [12]. Drugs are usually encapsulated inside liposomes and their release depends on liposome composition (spontaneous release), pH, or surrounding environment (stimuli responsiveness). Liposomes are internalized by a variety of cell types and by different mechanisms. In turn, the surface of liposomes can be engineered with specific receptors, antibodies or antigens that makes the approach promising for targeted delivery [13]. However, release of drugs from liposomes is still not tightly controlled.

1.5 Inorganic nanoparticles as drug delivery tools

A promising TDD tool has the property of targeted and site specific drug release to minimize collateral damage usually associated with conventional delivery approaches. Nanoparticles have an edge as they can be engineered in a way to make the release more controlled. Inorganic nanoparticles have been used in vaccine and anticancer drug delivery research quite extensively. Nanoparticles have been generated from a variety of inorganic materials like silica, gold, silver, lanthanide and other metals for different applications with drug delivery research [14]. Inorganic nanoparticles impart a number of advantages over

organic nanoparticle based drug delivery systems. For example, organic nanoparticles can be used as reservoirs for drugs while inorganic nanoparticles can be used not only to enclose drugs but also can be used as contrast agent and as exothermic reactors. Some of the inorganic nanoparticles being used in TDD are listed in the following chapter.

1.5.1 Iron oxide nanoparticles

In late 1980s, iron oxide nanoparticles (IONs) with sizes range from 50 to 100 nm were first synthesized to be used as contrast agents for negative imaging of hepatocellular carcinoma [15]. Generally, IONs are engulfed by Kupffer cells in the liver. As hepatocellular carcinoma sites have fewer Kupffer cells than healthy liver, injection of IONs can visualize hepatocellular carcinoma tissue by negative imaging [16]. When exposed to an alternating magnetic field, the iron oxide nanoparticles start oscillation. This oscillation is based on Neel relaxation and Brownian rotation of the particles in suspension. This in turn leads to elevation of temperature at the residence site of these nanoparticles. Literature suggests that within the tumor site, this elevation of heat can be as much as 41-45 °C, sufficient to induce bio-molecular changes within the microenvironment and induce cell death by apoptosis or necrosis [17]. In addition, when shelled with materials like liposomes, hydrogels or silica, drugs can be encapsulated inside or attached to them. Such strategy gives the option for dual therapy of cancer by, i.e, release of an anticancer drug (chemotherapy) and hyperthermia-mediated killing of cancer cell [18]. However, depending on the size and coating of iron oxide nanoparticles, these might be cleared or retained inside the body. For instance, PEGylated IONs of larger size are most likely opsonized by macrophages in the blood and to some extent they are trapped in the liver and spleen. Although they are cleared in more than 2 weeks by the renal system, their efficacy in context of drug delivery is already hindered. Nevertheless, drugs can be either absorbed or chemically linked on the surface of IONs. To stabilize the drug-ION complex, polymers like starch is coated on them. When injected intravenously, the drug is belatedly released in 60 minutes. Although some of the drug-IONs can accumulate at the site of cancer and slow down tumor progression, the vast majority of the nanoparticles still accumulates in off-target organs, in particular the liver, where they can pose serious health problems [19]. One approach to overcome the drawbacks is to double coat IONs. Oleic acid is normally used for emulsification of IONs which are then further coated with PEG copolymers. The double coated IONs can not only entrap drugs but also can slowly release them over time. Another approach is to covalently attach the drugs to IONs by using carbodiimide [20].

1.5.2 Gold nanoparticles

Gold nanoparticles have an immense importance in the field of drug delivery. Previously, gold nanoparticles (AuNPs) has been used for gene delivery to different cells as well. One of the many advantages of using gold is that they can be easily synthesized in different sizes (1 to 100 nm) and in different shapes like spherical, rod like and so on. Because AuNPs contain a negatively charged surface, different kinds of biomolecules including drugs or targeting agents can be attached to them. Further, AuNPs are non-toxic and biocompatible [21]. Drugs and proteins can be easily conjugated with AUNPs by simple ionic or covalent bonding or even by physical absorption. Successful conjugation of the anti-cancer drugs such as methotrexate and doxorubicin has been already reported. At least in vitro, these functionalized AuNPs halt the growth of cancer cells [21]. In some studies, drugs have been linked with AuNPs via pH-sensitive linkers. Such linker systems allow the nanoparticles to release the drug intracellularly. Once inside the cells, the acidic environment within endosomes cleaves the pH-sensitive linker, making the drug available for action. In addition, AuNPs have been layered with poly ethylene glycol (PEG) and in turn PEG has been functionalizedwith NH_2 groups. Such approaches gave better attachment of drugs to the functional groups. Also, AuNPs have been tethered with platinum for example which improves the biocompatibility as compared to naked AuNPs [22]. These systems have been tested on a variety of cancer cell lines like A549, HCT15 and have been shown very effective in vitro [23].

1.5.3 Carbon nanotubes

Carbon nanotubes are graphite nanomaterials with a hollow and well-ordered structure. Recently, carbon nanotubes have attained much attention in vaccine and drug delivery research. They can be produced as single layer sheets or multiple layers cylindrical structures. These nanotubes are usually insoluble which poses a major health hazard as their clearance from the body is a major obstacle. However, they are modified by functionalization. They can be ideally oxidized using acids which expose or generate carboxylic groups in them, increasing their solubility in aqueous solution. Additionally, such functionalization can also support the attachment of drugs or peptides on their surface [24]. Such functionalized nanotubes have been tested for example in vaccine delivery. Immunogenic peptides (for instance the B cell epitope of foot and mouth disease virus) have been covalently attached to the amine groups generated on the surface of carbon

nanotubes. Immunization of mouse models with such vaccines elicits strong antibody responses as compared to free peptide treated animals. In addition, these nanotubes were able to activate the complement system in the mice which helped the generation of better immune response against the antigen. An important feature of carbon nanotubes is that they can be easily internalized by the cells passively as well as by classical endocytosis. This property also makes them suitable candidates for drug delivery [25]. It has been shown in a range of mammalian cells that antibiotics attached on the surface of nanotubes can be internalized by the cells and protect from bacterial and/or fungal infections.

1.5.4 Silica nanoparticles

Mesoporous silica nanoparticles (MSNs) are also inorganic nanomaterials with hollow, porous channels arranged in a 2D network. MSNs are favored because of their tunable size, pore volume, diameter, structure and high surface area, which increases drug loading capacity. They can be directly used for delivery of different biomolecules where the biomolecules are released spontaneously by diffusion depending on the pore size. Unlike liposomes and polymers, drugs are usually protected inside the MSNs as they cannot be easily degraded by the harsh environment in the blood stream or intracellularly [26]. In addition, MSNs can also be surface modified with different functional groups, thus allowing covalent attachment of different biomolecules to the surface. This gives extra stimuli responsive release system to MSNs. In vitro, MSNs are readily taken up by a variety of different cell types. Once inside the cells, they are usually kept in endosomes. If the surface of MSNs is modified with pH-responsive linkers, the drug can be released from endosomes. In addition, other functionalizations support the release the drug upon specific stimulus. This includes the application of an electromagnetic field, ultrasound light or any enzymatic activity, depending on the nature of the linker. MSNs have been used for delivery of drugs to different cancers in mouse models. However, the research is at its infancy and much work is needed before testing the system in clinic [27].

1.6 Core-shell superparamagnetic iron oxide nanoparticles (SPIONs) and hyperthermia

In the present study, silica shell superparamagnetic iron oxide nanoparticles were utilized. Therefore, these will be discussed in detail in this section.

Iron oxide nanoparticles have been introduced in section 2.5.1. Depending on their magnetism and phase transition induced by temperature, there are eight different forms of iron oxides[28]. Among these hematite, maghemite and magnetite are very popular and promising candidates for drug delivery applications. Hematite which occurs naturally as α-Fe_2O_3 is the most widely used catalyst and n-type semiconductor[29]. It is also used as a starting material for synthesis of maghemite and magnetite nanoparticles. Maghemite nanoparticles (γ- Fe_2O_3) are considered as fully oxidized and occur in cubic structure with closely packed arrays of ferric ions. Although ideal candidates for fabrication of luminescent and magnetic dual properties nanoparticles, they have genotoxic properties[30]. Magnetite nanoparticles (Fe_3O_4) are cubic spinel nanoparticles with superparamagnetic properties. Among the other forms of iron oxides, magnetite nanoparticles have emerged as the most promising because of their biocompatibility with biological systems as well as their superparamagnetic properties[31].

Frequently, superparamagnetic iron oxide nanoparticles are surface modified to increase the drug loading capacity, improve the targeting of nanoparticles, enhance the surface activity and to augment the biocompatibility of the nanoparticles. Such modifications include polymer coating as well as decoration of iron oxide core with inorganic shells[32]. Silica is one of the most commonly used surface modification agent for iron oxide nanoparticles. Silica shell coating not only reduce the agglomeration but also improve stability by preventing oxidation of iron oxide and hence minimize the cytotoxicity. Silica shells are also proven to be more biocompatible with high hydrophilicity. Moreover, the size and thickness of silica shell can be controlled by the use of appropriate method for its preparation[33]. Further, silica nanoparticles are well dispersed in aqueous suspension and can be negatively charged with pH change. The negative charge on silica shell allow the possibility to covalently link ligand molecules on surface or conjugate drugs on shell. Dugs can be also encapsulated inside the nanoparticles within the interface of iron oxide core and silica shell. Such drug loaded nanoparticle systems are particularly best when mesoporous or nonporous silica shell is used. The iron oxide core can be used as magnetic agent to accumulate the nanoparticles at a particular site where magnet is placed on the body and the drug can be spontaneously released from the pores within the shell[34].

Recently, heat sensitive linkers have been conjugated on the silica shell of magnetic silica nanoparticles to achieve a controlled drug delivery system. A prototype system relies on

thermo-labile covalent linkers which are conjugated on one side with silica shell and on the other side with drugs of interest. The linkers are attached to the shell via retro-Diels-Alder reaction mechanism and can be cleaved by exposure to higher temperatures. When such nanoparticles are exposed to an alternating magnetic field, magnetic hyperthermia is induced utilizing Neel-Brownian relaxation mechanism. This hyperthermia is as high as 110°C at the surface of nanoparticles, sufficient to induce cleavage of the drug from nanoparticles[35].

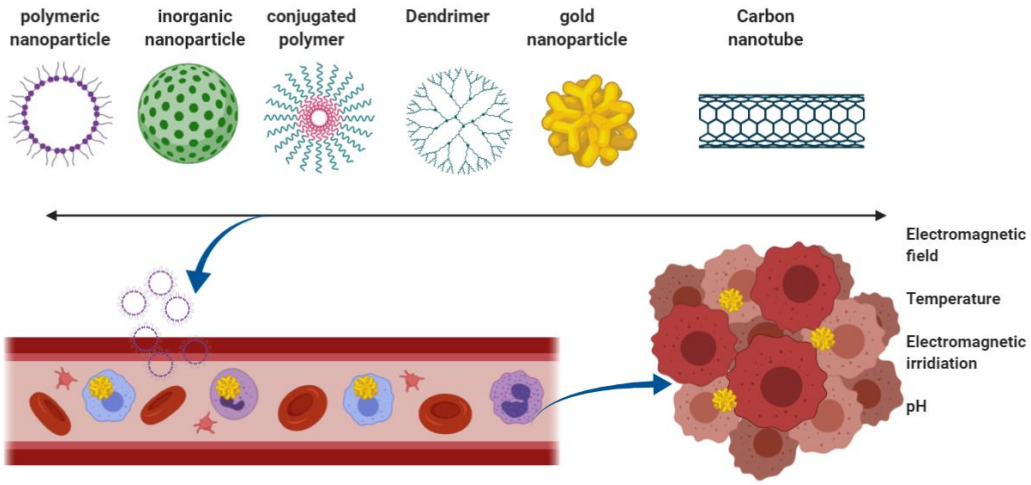

Figure 1-1Nanoparticle assisted drug delivery. Organic, inorganic and polymeric nanoparticles when injected systemically are taken up by professional phagocytic cells or if conjugated with targeting moieties, migrate to site of cancer. Different stimuli can be used to release the drug from nanoparticles at target site.

1.7 Cell-mediated drug delivery

Site-specific drug delivery without off-target toxicity is the prime goal of any TDD approach. Although there is much advancement in biomaterial sciences for this purpose, specific targeting still remains a largely unsolved question. Some hard to achieve goals within TDD includes crossing biological impermeable membranes such as the blood brain barrier (BBB) and penetration of carriers within deep tissues or tumors. Cells, in particular immune cells such as dendritic cells, neutrophils, lymphocytes, macrophages and monocytes are mobile in nature and possess properties which make them attractive candidates as carriers for therapeutic loads. Immune cells as well as mesenchymal stem cells have intrinsic ability of homing to infection or tumor sites and so are of interest to be used as Trojan horses to deliver drugs targeted with much more precision [36]. These cells can be used for therapeutic approaches in two ways:

- Genetically modified cells, which express recombinant proteins of pharmaceutical interest or
- Carrier cells, which can be directly loaded with drugs or with drug containing nanoparticles.

1.7.1 Genetically modified cells

With the development in genetic engineering, attempts have been made to genetically modify cells for better cell therapy. Usually genes are incorporated into the cells either to track the cells in vivo (fluorescent and/or luminescent proteins) or express protein of therapeutic interest. In other cases, genes encoding proteins which can make the cells susceptible to certain drugs are also transduced into the cells. One such example is thymidine kinase which convert the antiviral prodrug Ganciclovir to its toxic metabolite which in turn induce killing of bystander cells [37].

1.7.2 Carrier cells

Till today, there is a high demand to develop a drug delivery system that can targetedly distribute drugs to the site of action with minimal effects on healthy cells or tissues. Such a system would definitely enhance the therapeutic effect of drugs and minimize the dose used for therapy. In fact, immune cells along with other cells have been investigated for their use to be loaded with drugs and used as delivery vehicles. Such a system would work as a Trojan horse and could not only increase the circulation time of the drug but also limit the toxicity towards off-target cells. Some of the cell types being used for the purpose are discussed here.

1.7.2.1 Erythrocyte-based drug vehicles

Red blood cells (RBSs) or erythrocytes are the most abundant blood cells that carry oxygen to tissue via the circulatory system. In addition, they are involved in homeostasis and pathophysiology like thrombosis. They develop in bone marrow, have a diameter of 6.2-8.2 μm and a half-life of 120 days. Their biconcave shape makes it easy for them to be squeezed through the capillary network. They lack the nucleus as well as most cell organelles for maximum accommodation of hemoglobin bound oxygen. Thus, they are natural carriers for the vascular delivery [38]. The first use of erythrocytes as carrier cells was reported in 1973 when Ihler et al., encapsulated enzymes into RBCs and since then

there have been attempts to load anti-viral, anti-inflammatory and anti-cancer drugs in to them [39].

Drugs can be loaded into RBCs either by direct encapsulation into isolated erythrocytes ex vivo or coupling the drug to RBC membrane. Loaded erythrocytes can then be used as drug reservoirs for sustained release in circulatory system or they can be directed towards reticuloendothelial system of spleen, liver and bone marrow. The idea is that RBCs are normally degraded spontaneously at these sites and hence can release the encapsulated drug at site. They are attractive drug carriers as they are biocompatible, biodegradable and has a longer life span. In addition, relatively higher doses of drugs can be loaded in the cells. Nevertheless, RBCs cannot migrate through endothelial barriers and therefore their use as Trojan horses is limited [36].

1.7.2.2 Immune cell-based drug vehicles

In contrast to erythrocytes, immune cells can cross physiological barriers like inter-endothelial passages actively. Some of the immune cells can even cross the blood brain barrier (BBB). Apart from this, upon onset of infections or inflammation, immune cells like neutrophils, monocytes, lymphocytes, dendritic cells and macrophages migrate to the site of action to initiate an immune response. Therefore, immune cells have been explored by loading them with drugs so they could act as Trojan horses and deliver loaded material site specifically.

Neutrophils are the most abundant leukocytes and are attractive delivery system. They accumulate at sites of inflammation in very large numbers. Neutrophils have been loaded with therapeutic albumin nanoparticles ex vivo and have been shown to deliver them at inflammation sites in lipopolysaccharide (LPS)-induced inflammation models. They have also been shown to deliver nanoparticles to lungs against Pseudomonas aeruginosa infection [40]. Alternatively, neutrophils can take up intravenously injected albumin nanoparticles in vivo and deliver them to inflammation sites as well. Neutrophils when loaded with liposome containing anti-cancer drugs have been shown to cross the blood brain barrier and deliver the drug to cancer site in glioma mouse models [41]. The inflammatory environment in the brain then trigger the release of drugs from liposomes and reduce tumor growth significantly. Apart from this, they have been shown to be effective in diseases where neutrophil infiltration is necessary for prognosis such as multiple sclerosis, stroke, Alzheimer’s disease, and traumatic brain injury [41]. However, the short life span of

neutrophils and the need to be used immediately upon isolation limits their use as drug carriers.

Lymphocytes which originate from in the central lymphoid organs can be classified broadly into T and B cells and represent the major arm of the adaptive immune system, can also serve as carrier cells. The ability of T and B cells to attack diseased cells can be exploited in a way that the drug can be directed to target site. Lymphocytes has a number of advantages as drug carriers such as they can target locally, complement and amplify cytotoxic T cell response, detect and attack tumors at an early age and can generate memory cells. Using T and B cells to carry nanoparticles conjugated drugs to diseased sites can be a promising strategy for targeted drug delivery. However, their short life span and hurdles in harvesting limits their ability to be loaded with drug and manipulated for drug delivery [42].

Besides lymphocytes also monocytes and macrophages are found in abundance in the tumor microenvironment both in hypoxic and necrotic regions of the tumor. Therefore, the tumor homing and deep tumor penetration properties of leukocytes can be exploited for ideal drug delivery system. Encapsulation of drugs in monocytes and macrophages is easy as they naturally phagocytose materials whether in the blood or in the tissues [43]. This property has been utilized to deliver a variety of drug-loaded nanoparticles to tumors or infections. This has been shown in experimental cancer models, for instance, where they deliver and release liposome containing anti-cancer drugs in lungs as soon as 24 hours after intravenous injection. They also have the ability to cross the blood brain barrier and have been shown effective in mouse models of Parkinson disease where bone marrow derived macrophages delivered almost 2.1% of injected catalase to brain. Catalase once at glioma site, has antioxidant activity and protect the tissues from oxidative stress and neurodegeneration [44]. A schematic overview of uptake and migrationof immune cells to cancer site has been shown in Figure 1.2.

1.7.2.3 Macrophage-based drug delivery vehicles

Macrophages are specialized types of immune cells that are considered to be bridge between innate and adoptive immune systems. Macrophages detect, phagocytose and present antigens and initiate immune response referred to as inflammation. In the process, they also release cytokines that activate other immune cells. Macrophages reside in almost all type of tissues within the body [45]. Primarily, they are originated from monocytes within the peripheral blood. Monocytes migrate towards inflammatory signals and mature

into macrophages at inflammation site. The monocytes in turn develop from common myeloid progenitor cells in bone marrow. During development, the myeloid progenitor cells in the bone marrow commonly known as granulocytes/macrophage colony forming units give rise to monoblast, pro-monocytes and then monocytes which are finally released in to blood circulation. Monocytes then migrate to different tissues and differentiate into tissue resident macrophages (such as Kupffer cells, alveolar macrophages, histiocytes and osteoclast) [46]. In the blood, the monocytes heterogeneity is not well understood, but it is generally believed that monocytes develop and mature in the blood stream. The point when they are leaving the blood stream and migrating to specific tissue, determines the fate of these monocytes whether to become tissue resident or inflammatory monocytes. Macrophages respond to endogenous stimuli produced from pathological conditions or injury. They can also respond to signals produced by the immune cells and in turn themselves produce cytokines which can affect their own physiology [47].

1.7.2.3.1 Macrophage polarization

In general, three predominant forms of macrophages exist in context of their activation status:

- Classically activated macrophages (also called M1 macrophages) refer to the macrophages activated from cell mediated immune responses. They are generally believed to be produced in response to interferon-γ and tumour necrosis factor which are secreted by natural killer cells. These macrophages have in general microbicidal and tumoricidal properties and secretes elevated amount of pro-inflammatory cytokines. Although these pro-inflammatory cytokines help in clearly antigens by activating other immune cells but their activation should be tightly controlled [48].

- Wound healing macrophages (also called M2 macrophages) are also activated in during adaptive and innate immune response. During tissue injury, IL-4 is believed to be released first by basophils and mast cells. This IL-4 converts tissue resident macrophages in to M2 macrophages. Originally, macrophages activated by IL-4 were referred to as alternatively activated macrophages because these can upregulate their mannose receptor expression. Although, there role in host defence is poorly

understood, there is strong evidence that they help in clearing parasitic infections like the one caused be nematodes and helminths [49].

- Regulatory macrophages are also produced following adaptive or innate immune response. These macrophages produce TGF-β when they phagocytose an apoptotic cell. Production of TGF-β in turn contributes to their immune regulatory role [50].

Unlike other cells, which undergo immense epigenetic changes, macrophages keep a certain level of plasticity during differentiation and development. They respond to environmental signals and change their phenotype accordingly. That being the reason, most of the time it is problematic to identify macrophage population based on biochemical markers [51]. For instance, IL-4 activated wound healing or M2 macrophages can be converted to regulatory macrophages by adding immune complexes to macrophage cultures that help them produce more IL-10 and low level of IL-12. Such macrophages then exhibit both the properties of M2 and regulatory macrophages [52].

1.7.2.3.2 Macrophages as carrier cells

Because of their particular properties, macrophages have been explored extensively to be used as drug carrying vehicles. One important aspect of a macrophage based drug delivery system is that macrophages phagocytose foreign particles easily [53]. Nanoparticles when added to macrophage cultures can be readily taken up and maintained in phagosomes and later endo-lysosome inside the macrophages. Maturation of phagosome in to endo-lysosome results in drop in pH of the vesicle which can be used as a stimulus for drug release from the nanoparticles [54] as discussed in previous sections. Although, much care should be taken when loading the macrophages with drug loaded nanoparticles. Drugs poorly attached on nanoparticles can be released pre-maturely and hence can be toxic to the macrophages themselves. Thus, more sophisticated developments would be required to exploit these cells for controlled drug delivery [55].

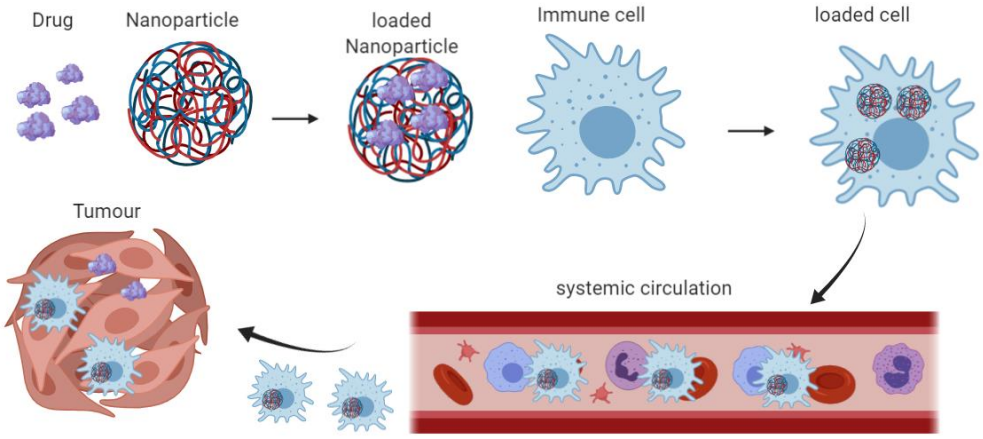

Figure 1-2Immune cells as drug carriers: Nanoparticles are loaded with drugs in vitro and then are incorporated into immune cells (e.g. macrophages). The loaded immune cells when injected systemically, migrate to tumor site, release the nanoparticles, and in turnthe drug at the target site.

The in vivo the fate of these macrophages largely depends on their activation status. Literature suggests that although M1 macrophages have a high phagocytic and pro-inflammatory activity, their migration to the cancer site in vivo is poor. M2 macrophages on the contrast have a low phagocytic and high anti-inflammatory activity but are recruited to the inflammation site rapidly [56]. Based on the plasticity of macrophage in vivo, much care should be taken when considering macrophages as drug delivery tool.

The final step in macrophage based drug delivery system is the expulsion of cargo from the macrophages once it reaches its destination. Within the phago-lysosomes, the low pH could help in degradation of the materials inside. The re-usable material such as amino acids and proteins then diffuse to the cytosol through phago-lysosome membrane. However, the insoluble components of the phago-lysosomes are secreted out from the cell by the endoplasmic reticulum-Golgi complex secretion pathway [57]. Some of the insoluble material can be presented by the macrophages on their surface by a mechanism depending on calcium and vesicle membrane associated protein 7 [58]. However, while such release strategy can contribute to drug release from the macrophage based drug delivery system, more controlled release system is desired for better outcome.

1.8 Controlled drug release

Drug delivery to pathogenically damaged areas without affecting healthy tissue has been focus of medical research since decades [59]. With the advent of nanotechnology, many nanoparticles or smart therapeutics have been proposed that can prevent the drug from affecting the host. Nanoparticles provide a shield to the drug and hence delays the exposure

of healthy tissues to the action of the drugs. Hence, with proper targeting of these nanoparticles and the encapsulated drugs, a proper controlled delivery system can be achieved [60]. Many nanoparticles such as micelles or hydrogels have been proposed that can be degraded upon exposure to specific stimuli such as pH changes, raise in temperature or even exposure to specific enzymes [3]. These hydrogels can be easily decorated with ligands that helps targeting to specific cells or tissues. Nevertheless, hydrogels or micelles pose the hazards of non-specific release and in some cases; a slight physiological change can induce spontaneous release of the drug [61]. Inorganic nanoparticles such as silica provide a promising platform to overcome non-specific release. Different approaches such as encapsulation of drugs in nanoporous or mesoporous silica nanoparticles have already been explored but spontaneous release from nanoparticles remains the obstacle [62]. Recently, drugs have been attached with silica nanoparticles using heat sensitive linkers via covalent bonds. Covalent bonding of the drugs with silica ensures that the drugs are neither released non-specifically nor released upon normal physiological changes such as fever or immune response to pathogens [63]. The heat sensitive linkers can be cleaved from the nanoparticles at elevated temperatures. Heat-based drug release systems have previously been explored using a variety of materials such as zinc or iron oxide nanoparticles [64]. For example, particles composed of a spherical silica core coated with a thin gold layer have also been shown to release enclosed drugs upon exposure to near infrared light, a process that generates heat and hence induces dissociation of the drug from silica-gold nanoshells. One such strategy is the exposure of iron oxide nanoparticles to an alternating magnetic field that induces hyperthermia [65]. Although much work has been done to achieve controlled drug release, there is still need to develop a tightly controlled release system.

1.9 Aim of study

Site specific and controlled delivery of drugs to pathogenically damaged sitesis stilla challenge that limits many therapies. In conventional drug delivery approaches, drugs are not only systemically administered but also undergo biological degradation in vivo. This is accompanied withlack of targeting and a low therapeutic index at the target site. In addition, systemic distribution leads to increased off target effects that excludes the application of many drug candidates. For an optimal drug delivery system, primary objectives are to increase the half-life of the drug and target its activity specifically to the diseased site. Nanoparticles have been recently explored for designing optimal delivery systems. Although nanoparticles can protect the drug from biological degradation,their targeting to the diseased site is still a problem. As well, depending on the nanoparticle nature, controlled release of drugs has been a hurdle. Recently, evidence was given that drugs covalently attached to shells of magnetic nanoparticles via heat sensitive linkers were released upon induction of hyperthermia. However, targeting of the nanoparticles to the diseased site is an unmet challenge.

Thus, the current study was designed to develop a sophisticated drug delivery system that will target drugs to inflamed/infected sites and allow its controlled release in response to an external stimulus. To address this aim, drug-entrapped silica-coated superparamagnetic iron oxide nanoparticles (SPIONs) were used upon loading to macrophages. SPIONs were coupled to two different model drugs via a thermo-sensitive linker: i) the anti-cancer drug Maytansin; ii) the model drug (Z)-4-Hydroxytamoxifen, which can be visualized upon a Cre-dependent reporter gene switch. The efficiency of controlled cargo release from SPION loaded macrophages upon induction of magnetic hyperthermia should be determined in 2D and 3D cell culture models in vitro. Finally, theapplicability of macrophages for targeted delivery of drug loaded SPIONs tosites of inflammation should be investigated in vivo.

2 MATERIALS AND METHODS

2.1 Materials

2.1.1 Equipment and consumables

Table 2-1: List ofequipment

Equipment	Manufacturer	Model
Autoclave	Santer, BeliMed	
Table top centrifuges	Eppendorf	5417C
	Biozyme sprout	
Cooling Centrifuges	Thermo scientific	Multifuge X3 FR
Photometer	Nanodrop Spectrophotometer, Peqlab	ND-1000
Eliza Reader	Berthold Technologies	Tristar 2, multimode reader, LB942
Gel Electrophoresis Chambers	Life Technologies	Horizon 5P
Power Supplies	Life Technologies	ST305
PCR Machine	T3 Thermocycler, Biometra	-
Micropipettes	Gilson	-
Microscopes	Leica Labovert FS Nikon Olympus CellM Zeiss LMS 510 META	-
Gel Documentation system	NTAS UV Spectrum	-
Luminometer	Berthold Lumat LB	9507
Cell Counter	Casy-DT 1, Schaerfe Systems	-
CO_2 Incubators for CellCulture	Labotect	C200
Sterile Work Benches	Heraeus	

In vivo, Bioluminescence Imaging Machine	Xenogen IVIS system, PerkinElmer IVIS system	IVIS 200
Thermomixer	Eppendorf	5436
pH meter	Beckman	M340
Vortex	Scientific Industries Vortex Genie 2	-
Shaker	Heidolph	-
Deionized Water Supply	Millipore MilliQ	-
Precision Weighing Scale	Sartorius	-
Microwave	Whirlpool	-
Water Bath	Rowalabortechnische Anlage Gmbh	-
4 °C refrigerator	Liebherr	-
-20°C freezer	Liebherr	-
-80°C freezer	Thermo Scientific	-
Sonicator	Branson	1200
Magnetic field inductor	Himmel	Hu5000+

Table 2-2listofconsumable

Consumable	Manufacturer
Cell culture plates (96 well, 48 wells, 24 wells, 12 wells, 6 wells)	Nunc, Corning
Tissue Culture dishes (100mm)	Corning, Greiner Bio-one
Falcon tubes (15, 50 ml)	Greiner bio-one
FACS / luciferase measurement tubes (5 ml)	Sarstedt
Tissue Culture flasks (25 cm^2 and 75 cm^2)	Nunc
Syringes (1 ml, 5 ml, 20 ml)	Omnifix®
CombiTips (0.5ml, 1.25ml, 2.0ml, 2.5ml, 5 ml)	Eppendorf
PCR tubes	Biozym
Cryogenic Vials	Corning
Pipette tips (20 µl, 200 µl, 1000 µl)	Star Labs
Syringe Filters (0.2µM and 0.45µM)	Sartorius

2.1.2 Plasmids and oligonucleotides

Table 2-3List ofplasmids

Plasmid	Nr.	Description
pEF1 VenusGFPlox	4152	Encodes VenusGFP flanked with inverted LoxP sites is in reverse orientation and under EF1α promotor
pCre-ERT2[66]	2456	Encodes SV40 promotor driving Cre-ERT2 expression

Table 2-4listofoligonucleotides

Oligonucleotides	Sequence	Purpose
iNOS-F	GGCAGCCTGTGAGACCTTTG	qRT-PCR
iNOS-R	GCATTGGAAGTGAAGCGTTTC	qRT-PCR
Arg1-F	GGAATCTGCATGGGCAACCTGTGT	qRT-PCR
Arg1-R	AGGGTCTACGTCTCGCAAGCCA	qRT-PCR
TNF-F	CCAGTGTGGGAAGCTGTCTT	qRT-PCR
TNF-R	AAGCAAAAGAGGAGGCAACA	qRT-PCR
IL-4R-F	CTAGCTCCGTGCCCTTATTTAC	qRT-PCR
IL-4R-R	GGTTGGCTTCTGGTGGTATT	qRT-PCR
M-Act-F	TGTCCACCTTCCAGCAGATGT	qRT-PCR
M-Act-R	AGCTCAGTA ACAGTCCGCCTAG	qRT-PCR
Cre1	GCCTGCATTACCGGTCGATGCAACGA	Genotyping PCR
Cre2	GTGGCAGATGGCGCGGCAACACCATT	Genotyping PCR
Luc2	TCAAAGAGGCGAACTGTGTG	Genotyping PCR
R26F	AAAGTCGCTCTGAGTTGTTAT	Genotyping PCR

2.1.3 Chemicals, medium and kits

Table 2-5List of chemicals, medium and kits

Chemicals, Medium and Kits	Supplier	Catalogue Nr.
PKH26 red fluorescent cell linker kit	Sigma Aldrich	Mini26
Apoptosis/necrosis assay kit	Abcam	Ab176749
Cell Tracker red CMTPX dye	ThermoFisher Scientific	C34552
Recombinant Human Complement Component C5a Protein	R&D systems	2037-C5-025
Recombinant Murine IL-4	Peprotech	214-14
Recombinant mouse IL-10 protein	Abcam	Ab9736
Insulin, Human Recombinant	Fisher Scientific	MP219390025
(Z)-4-Hydroxytamoxifen	Sigma Aldrich	H7904-5MG
Blasticidin S (hydrochloride)	Cayman chemical	14499
IMDM culture media	Gibco	I2911-500ML
DMEM culture media	Gibco	88364
RPMI culture media	Gibco	21875034
Sodium Pyruvate Solution	SIGMA-ALDRICH	S8636-100ML
2-Mercaptoethanol	Gibco	21985023
Fetal bovine serum	Biowest	S1810-500
Lipofectamine 2000	ThermoFisher scientific	11668019

2.1.4 Cell lines and mouse strains

The cell lines were used in the following conditions:

J774a.1[67], **RAW264.7**[68], **IC21**[69] macrophage cells were cultured in DMEM media supplemented with 10% FBS and 1% penicillin and streptomycin. The cells were split in 1:10 after each 3 days culture.

NIH3T3 mouse fibroblastoid cells were cultured in DMEM media supplemented with 10% FBS, 1% penicillin and streptomycin, 1% sodium pyruvate and 1% HEPES.

Cre-Luc cells were generated as follows: Mouse fibroblast cells were isolated from Rosa26-CreERT^2-Luclox mice and immortalized with SV40 large T-Ag. Cells were

cultured in DMEM media supplemented with 10% FBS, 1% penicillin and streptomycin, 1% sodium pyruvate, 1% HEPES, 1% 100xMEM and 0.1% β-marceptoethanol.

Bone marrow derived macrophages (BMDMs) were cultured in IMDM media supplemented with 10% FBS, 1% penicillin and streptomycin, 1% glutamine, 1% HEPES and 0.1% β-mercaptoethanol.

KSHV infected endothelial cells(K-EC)[70] were cultured in endothelial growth media supplemented with 2µg/mL doxycycline and 5µg/mL of puromycine.

MCF-7[71] human breast carcinoma cells were cultured in DMEM media supplemented with 10% FBS, 1% penicillin and streptomycin, 1% human recombinant insulin.

U937[72] human monocytes cells were cultured in RPMI media supplemented with 10% FBS and 1% penicillin and streptomycin.

2.1.4.1 Mouse strains

The following mouse lines were used for the thesis. All mouse lines were bred and maintained at the animal facility of HZI according to the ethical guidelines for animal experiments.

- Mx2-Luc transgenic mouse line with C57BL/6 background [66],
- Cre-Luc mouse line was generated upon breeding of Rosa26-CreERT^2[73] mouse line with RosaAntiLuc mouse line [74], both on C57BL/6 background
- Rag2-/-γC-/- mouse line with C57BL/6 background [75].

Methods

2.1.5 Nanoparticle preparation and suspension

Magnetic silica nanoparticles (blank, maytansin-loaded and (Z)-4-Hydroxytamoxifen-loaded) were kindly provided by the lab of Andreas Kirschning, Leibniz University of Hannover. The detailed synthesis of nanoparticles has been published elsewhere [35]. The nanoparticles suspension was prepared by suspending 2mg of nanoparticles in 1mL of PBS and sonicating for 10 minutes in dark. For (Z)-4-Hydroxytamoxifen loaded nanoparticles, 2mg/mL of large pore silica nanoparticles (Peter Behrens, Leibniz University Hannover) were suspended in double distilled water. The nanoparticles were directly mixed with 2mg/mL of (Z)-4-Hydroxytamoxifen and incubated in dark at 4℃ for 24 hours. The loaded nanoparticles were washed 3 times with double distilled water before further use.

2.1.6 Isolation of bone marrow derived macrophages

The bone marrow derived macrophages were isolated from femur bone of mice according to established protocol [76]. Briefly, the femur bone was isolated after sacrificing the animals with carbon dioxide. The bones were flushed with 10mL of IMDM media (supplemented with penicillin and streptomycin). The filtrate was collected in 15mL tubes and centrifuged at 400g for 5 minutes at 4℃. The supernatant was discarded and the pellet was suspended in 5mL of erythrocytes lysis buffer. The suspension was kept at room temperature for 5 minutes and centrifuged at 400g for 5 minutes at 4℃. Supernatant was discarded and the pellet was suspended in IMDM media supplemented with penicillin and streptomycin and distributed in 100mm petri dishes. The cells were incubated for 2.5 hours and then fresh media (with M-CSF) was added. After 4 days of culture, fresh media was added (without M-CSF) and cultured for additional 3 days.

2.1.7 Generation of the Cre-GFP cell line

NIH3T3 cells were transfected with pCre-ERT^2[77] and pEF1VenusGFPlox plasmids by lipofectamine 2000 as per manufacturer's protocol. Briefly, 1 x 10^6 NIH3T3 cells were seeded in a 6 well plate one day before transfection. Lipofectamine solution was prepared by mixing 150µL of Opti-MEM with 10µL of Lipofectamine 2000. In a separate tube, 2µg each of pCre-ERT^2 and pEF1VenusGFPlox DNA was mixed in 150µL of MEM. Bothe suspensions were incubated for 3 minutes and then mixed together by pipetting a few times.

The mix was incubated for 15 minutes and then added to the cells. After 5 minutes, 1 mL of complete media was added to the cells and incubated at 37℃, 95% humidity and 5% CO_2 for 6 hours. Afterwards, the cells were washed with PBS and fresh media was added to the cells. The cells were selected by culturing the cells in media supplemented with 3ng/mL of Blasticidine antibiotic. After 2 weeks of culture, the cells were seeded at a density of 100 cells per 35 x 10 mm cell culture dish. Single colonies were picked under a light microscope and cultured in 96 well plate. Silent clones that can be induced by (Z)-4-Hydroxytamoxifen were isolated.

2.1.8 Cellular uptake assay

For cellular uptake assays, macrophages (40,000 cells per well) were cultured in a 24-well plate. Nanoparticles suspension was prepared by mixing 20ug/mL of nanoparticles in 700uL of media (without FCS). The nanoparticle suspension was added on top of the cells and incubated for 2 hours. After 2 hours, the cells were washed 3 times with PBS and fresh media (with FCS) was added.

2.1.9 Magnetic field induced magnetic hyperthermia and drug release

Macrophage (10^5 cells per well of 24 well plate) were cultured with 30µg of SPIONs or T-SPIONs or OH-TAM-SPIONs for 2 hours in serum free culture media. The cells were trypsinized and suspended in 150µL culture media in a 200µL tube. The cells were exposed to magnetic field with constant amplitude of 4.8kA/m, 6mT or 60Oe for up to 40 minutes with a constant frequency of 779kHz using magnetic field inductor as described previously [35]. The cells with SPIONs were cultured for 24 hours after magnetic field while T-SPIONs and OH-TAM-SPIONs were placed in transwell inserts and co-cultured with targets cells for 48 hours.

2.1.10 Viability assays

For apoptosis assays, 10^5 cells were suspended in 500µL of binding buffer and 5µL of Annexin V-FITC reagent (Abcam) was added. The cells were kept in dark for 5 minutes at room temperature and subjected to flow cytometry.

For WST-1 based assay, 10^4 cells were cultured in 96 well plates and 10µL of cell proliferation reagent was added. The cells were incubated for 30 minutes at 37℃, 5% CO_2 and 95% humidity in incubator and the absorbance was measured with ELISA plate reader

at 420-480nm wavelength. The viability of the cells was measured with the following formula;

$$Survivalrate(\%) = \frac{Asample - ABlank}{Acontrol - Ablank} \times 100$$

2.1.11 Flow cytometry

For flow cytometry analysis, LSR II flow cytometry platform was used. For uptake studies, macrophages were labelled with FITC-labelled silica nanoparticles for 2 hours. For apoptosis assays, FITC-labelled Annexin V was used. To confirm release of (Z)-4-Hydroxytamoxifen, NIH3T3 cells expressing venusGFP were used. For each analysis, the cells were suspended in 300µL of FACS buffer.

2.1.12 Transwell assay

The transwell system was used for release assays. Briefly, 30,000 carrier cells were culture in upper well of transwell in 300µL of culture media. In the lower well of transwell, 70,000 target cells were cultured in 600µL culture media. The co-culture was separatedby 0.4µm tanswellmembrane.

2.1.13 Spheroid assay

4000 KSHV infected endothelial cells (K-EC) [70] per well were cultured on 0.5% agarose coated 96 well plate for 24 hours. For co-culture assays, K-EC and macrophages were cultured in a ration of 40:1. The spheroids were isolated after 24 hours, subjected to AMF for 30 minutes and placed again on agarose coated wells. Confocal microscopy was done after 48 hours of culture or co-culture.

2.1.14 Macrophage polarization

Macrophages were polarized to either M1 phenotype by culturing in media supplemented with 50ng/mL of IFNγ and 100ng/mL LPS or to M2 phenotype by cultring in media supplemented with 20ng/mL IL4 and 20ng/mL of IL10 for 48 hours. Macrophages were also treated with 30µg/mL of SPIONs for 48 hours. The cells were washed and collected by treatment with 0.05% trypsin. M1 and M2 markers expression was analyzed with qRT-PCR.

2.1.14.1 RNA isolation

RNA was isolated from macrophages using RNeasy minikit (Qiagen), following manufacturer protocol. Briefly, 10^7 were harvested and suspended in 350µL RLT buffer and 350µL of 70% ethanol. The sample was mixed by pipetting and transferred to RNeasy mini spin column with 2mL collection tube. The sample was centrifuged for 15 seconds at 8000 × g, the flow through was discarded and 700µL RW1 buffer was added. After centrifugation at 8000 × g for 15 seconds, the flow through was discarded and 500 µL RPE buffer was added. Again the flow through was discarded and 500µL RPE buffer was added. After centrifugation at 8000 × g for 2 minutes, the column was placed in fresh collecting tube and 30µL RNase free water was added. The column was spined at 8000 × g for 1 minute and RNA was collected. The RNA concentration was measuredwithnanodrop.

2.1.14.2 cDNA synthesis

For reverse transcription of isolated RNA, Revert aid first strand cDNA synthesis kit was used according to manufacturer protocol. Briefly, to 300ng of mRNA, 1µL Oligo $(dT)_{18}$ primers (0.5ng) were added. The total volume was raised to 12µL by adding nuclease free water. 8µL of reaction master mix containing 4µL of 5x reaction buffer, 1µL RNase inhibitor, 2µL of 10mM dNTP and 1µL RevertAid M-MuLV RT (200U/µL) was added. The mixture was kept at 42℃ for 60 minute and the reaction was terminated by incubation at 70℃ for 5 minutes.

2.1.14.3 Quantitative real time PCR

BioRadSsoFastEvaGreenSupermix kit was used for quantitative real time PCR reactions according to manufacturer's instruction. Briefly, 5µL cDNA was mixed with 10µL EvaGreen, 1 µL of both forward and reverse primers and 3 µL RNase/DNase free water. The reaction was prepared on 96 well plate LightCycler 480 multiwell plate (Roche) in triplicates. The following program was used in LightCycler 480 (Roche) for all genes:

StepNr	Program	Temperature	time	Cycles
Step 1	Pre-incubation	95℃	15 Seconds	1
Step 2	Amplification	95℃	15 second	40
		58℃	20 seconds	
		72℃	30 seconds	
Step 3	Meltingcurve	95℃	05 seconds	1
		65℃	60 seconds	
		97℃	Continuous	
Step 4	Cooling	40℃	30 seconds	1

2.1.15 *In vitro* chemotaxis assay

The in vitro chemotaxis assay was performed with µ-slide chemotaxis (ibidi) per manufacturer instructions. Briefly, 6µL of 3 x 10^6 were applied in the observation area while filling out the larger reservoirs with plugs. Closing the filling ports of observation area, 65µL of serum free media was put in one larger reservoir and 65µL of culture media with 100ng/mL of C5a (Abcam). All the filling ports were closed with plugs and migration of macrophages was observed towards C5a filled compartment by time lapse microscopy (Olympus) for 24 hours.

2.1.16 Confocal laser-scanning microscopy

Spheroid co-cultures were placed into Lab-Tek Chamber Slides (Nunc). Confocal analysis was performed with a Zeiss LSM 510 META inverted laser-scanning microscope using a 10x objective. Cells expressing EGFP were excited with an argon laser at 488 nm, and emission was collected using a 505-530 nm filter. Macrophages stained with PKH26 were excited with a laser at 543 nm and a 560-610 filter was used to collect emitted light.

2.1.17 Animal treatment

2.1.17.1 Local inflammation induction

Local inflammation was induced in Mx2-Luc or Rag2-/-γC-/- or Rosa26Cre-Luc mice by subcutaneous injection of 30µg/mL of silica nanoparticles and 20µg/mL LPS in a 100µL injection volume. The induction of inflammation was visualized in Mx2-Luc animals after injection of 100µL luciferin (intraperitoneal), at different time points post inflammation induction (12 hours, 24 hours, 48 hours).

2.1.17.2 Macrophage adoptive transfer

For tracking macrophages at inflammation site, one million bone marrow derived macrophages (M0 or M2) isolated from M2-Luc, either loaded or not loaded with nanoparticles were injected by tail vein injection, 1-hour post inflammation induction. For in vivo release studies, one million bone marrow derived macrophages were loaded with 40µg/mL of (Z)-4-Hydroxytamoxifen loaded large pore silica nanoparticles. Inflammation was induced in Cre-Luc mice using 30µg/mL of silica nanoparticles and 20µg/mL LPS in a 100µL injection volume. The loaded macrophages were injected by tail vein injection, 1 hour post inflammation induction. The macrophages or the release of (Z)-4-

Hydroxytamoxifen at inflammation site were visualized after intraperitoneal injection of 100µL D-Luciferin by in vivo imaging system (IVIS-200 Xenogen or IVIS spectrum PerkinElmer).

2.1.17.3 Genotyping

Rosa26Cre-Luc animals were generated by cross breeding Rosa26CreERT^2 and Rosa26antiLuc mice. The offspring's were genotyped for CreERT^2 and LucLoxP using DNA isolated from ear clips.

2.1.17.3.1 DNA isolation

The ear clips were lysed using 150µL direct-PCR lysis buffer supplemented with 2.5µL Proteinase K. The mixture was incubated at 40°C for 6 hours and 80°C for one hour. The samples were directly used for PCR.

2.1.17.3.2 Genotyping PCR

For genotyping of CreERT^2 1µL and for LucLoxP 2µL of lysate was used in 15µL and 20µL master mix respectively. The master mix was preparedasfollows

Components	CreERT^2	LucLoxP
PJK PCR Buffer	7.5 µL	10 µL
Forward primer	1.25 µL	1 µL
Reverse primer	1.25 µL	1 µL
water	3.5 µL	5.5 µL
DMSO	0.5 µL	0.5 µL
DNA	1 µL	2 µL
Total volume	15 µL	20 µL

The PCR conditions were as follows;

	CreERT^2			LucLoxP		
Step	**Temperature**	**Time**	**Cycles**	**Temperature**	**Time**	**Cycles**
1	95 °C	5 minutes	1	95°C	5 minutes	1
2	68°C	10 minutes	1	72 °C	10 minutes	1
3	95°C	30 seconds	35	95°C	30 seconds	35
	58°C	45 seconds		58°C	45 seconds	
	68°C	2 minutes		72°C	90 seconds	
4	68°C	10 minutes	1	72°C	10 minutes	1
5	16°C	Pause		16°C	Pause	

The PCR products were visualized on 1% agarose gel supplemented with Mandori Green dye.

2.1.18 Computer analysis and softwares

Microsoft office package including Word, PowerPoint and Excel was used for manuscript writing. Data analysis, statistical analysis and graphs were generated using GraphPad Prism version 8. Microscopic images and time lapse microscopy was analyzed using ImageJ version 1.50e. Images from IVIS were analyzed using Living Image version 4.7.2.

3 RESULTS

In the present study, a novel targeted and controlled drug delivery system was developed exploiting magnetic nanoparticles and macrophages. In general, the study is divided into two parts, controlled drug release from SPIONs loaded into macrophages and targeted delivery of drug-loaded nanoparticles frommacrophages in the mouse system. A schematic representation of the overall study is shown in Figure 3.1.

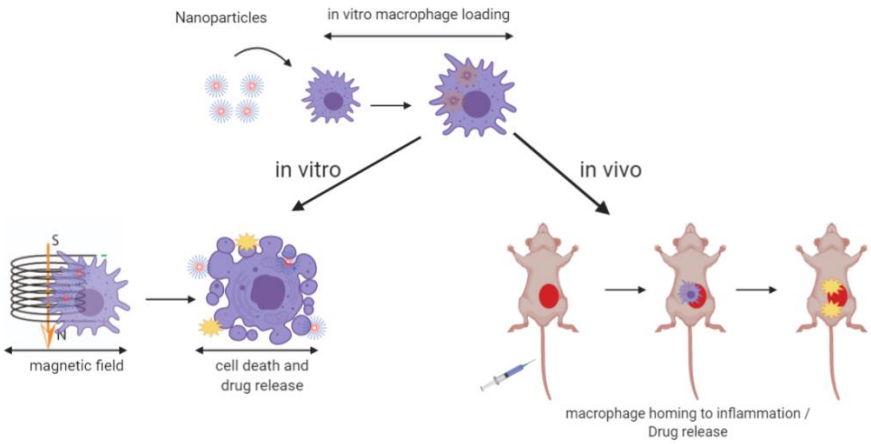

Figure 3-1Schematic outline of the study. Macrophages are loaded with nanoparticles in vitro. Application of a magnetic field induces hyperthermia, kills cells and releases the drug previously linked to nanoparticles. When the loaded macrophages are injected by tail vein, they accumulate at sites of inflammation and releases the linked drug at target site.

3.1 Controlled drug release from cargo loaded SPIONs

3.1.1 Uptake of superparamagnetic silica nanoparticles (SPIONs) by macrophages

The uptake of nanoparticles was tested in a variety of macrophage cell lines, namely J774a.1, RAW264.7, IC21, and U937 monocytes as well as in primary bone marrow derived macrophages (BMDM). RAW264.7 cells, J774a.1 cells, U937 cells, and IC21 cells represent different macrophage cell lines while BMDMs were used as a primary source of cells. Cells were incubated for 2 hours in serum free media with FITC-labelled magnetic silica nanoparticles and excessive particles were removed by extensive washing. To determine uptake efficacy, cells were analyzed by flow cytometry (Figure 3.2a). Results indicate that J774a.1, IC21, BMDM and U937 cells take up SPIONs with an efficiency of more than 95% while uptake in RAW264.7 cells was found to be 80%. Confocal microscopy (Figure 3.2b) and transmission electron microscopy (TEM) (Figure 3.2c) was used to confirm internalization of SPIONs. Indeed, as exemplified for J774a.1 cells, confocal images show that the macrophage cells effectively internalized particles. TEM

verified a massive accumulation of these SPIONs in intracellular compartments. Together the results indicate efficient SPION loading in primary and immortalized macrophage cell lines.

(a)

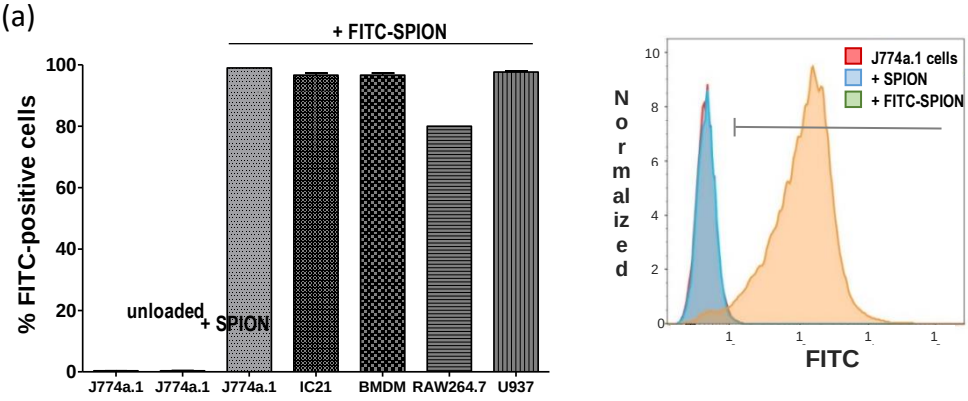

(b)

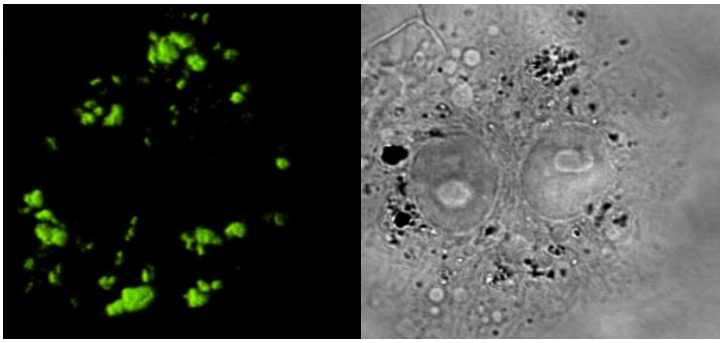

(c)

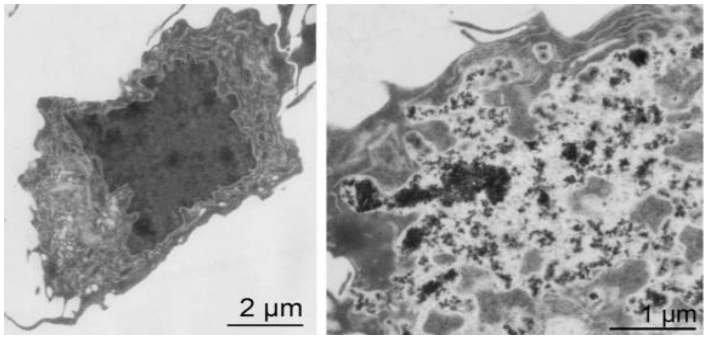

Figure 3-2 Uptake of SPION by macrophages. Different macrophage cell lines as well as primary BMD macrophages were cultured with 20µg of FITC-labelled SPIONs for 2 hours. The uptake of FITC-SPIONs was analyzed by flow cytometry (a), confocal microscopy(b) and transmission electron microscopy (c). Transmission electron microscopy was performed by Manfred Rhode, HZI. All the experiments were performed in triplicates and experiment (a and b) were repeated 3 times.

3.1.2 Biocompatibility of SPIONs with macrophages

The cytotoxicity of SPIONs under in vitro conditions in the various macrophage cell lines and in the BMDMs was examined in terms of the effect of these particles on cell proliferation by the WST-1 assay and the induction of intermediate stages of apoptosis by externalization of phosphatidylserine. The cells were exposed to a concentration of 20, 50,

or 100 µg/mL nanoparticles for 2 hours and excessive particles were removed. After 48 hours of cultivation in standard growth medium, the cells were analyzed for signs of apoptosis and for metabolic activity. As a positive control for toxicity, the cells were treated with Raptinal, an apoptosis inducing agent while untreated cells were used as negative control. As shown in Figure 3.3a, all cell lines, as well as primary macrophages showed no obvious signs of apoptosis even when the cells were loaded with the highest amounts of nanoparticles (100µg/mL). In contrast, Raptinal decreases viability of J774a.1, RAW264.7, and U937 cell lines more than 60% and of BMDMs to 5% of control cells. Interestingly, exposure of IC21 cells to Raptinal did not result in an increased number of cells undergoing apoptosis or decrease metabolic activity (Figure 3.3b), suggesting a higher resistance of these cells to apoptosis induction. In line with the apoptotic assay, SPION loading did not show a notable drop in metabolic activity in J774a.1, RAW264.7, and U937 cell lines (Figure 3.3b). In conclusion, these results indicate high biocompatibility of the tested macrophage lines and the BMDMs upon internalization of SPIONs.

(a)

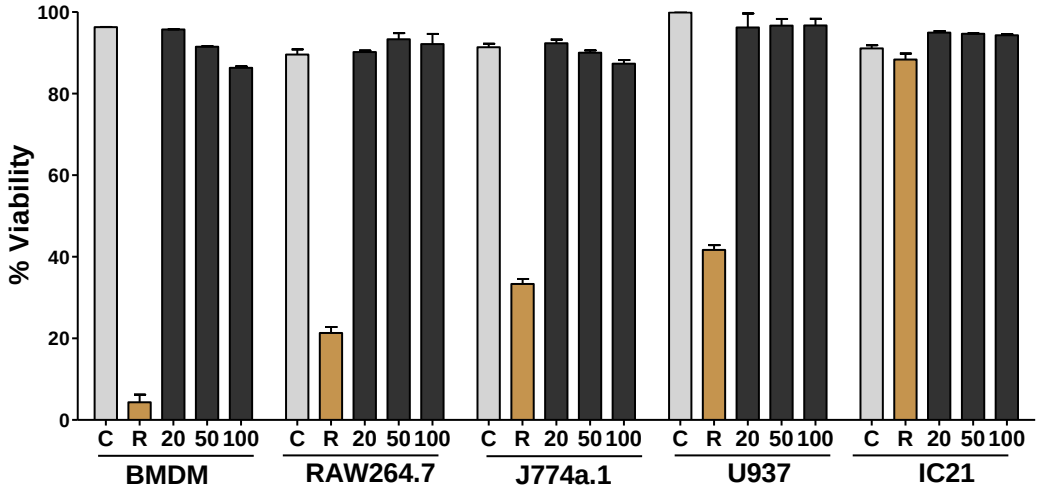

(b)

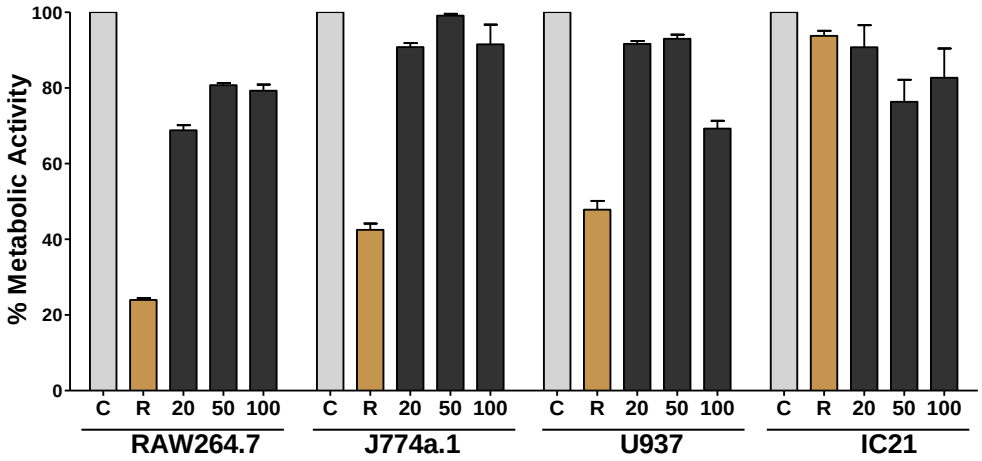

Figure 3-3Biocompatibility of SPIONs with different macrophage cell lines. Different macrophage cell lines as well as primary macrophages were treated with varying concentration of SPIONs for 48 hours. Control (c) were left untreated while Raptinal (R) treated cells served as positive control. After 48 hours, the viability of the cells was analyzed by staining phosphatidylserine on the cell surface by a fluorescent conjugate of Annexin V and subsequent flow cytometry (a). The metabolic activity of the cells was assessed by determining the activity of mitochondrial dehydrogenase using the WST-1 assay (b). Representative results from 3 experiments (n=3).

3.1.3 Magnetic hyperthermia induced macrophage cell death

SPIONs generate heat upon exposure to an alternating magnetic field (AMF). Thus it was tested whether the application of an AMF to cells loaded with SPIONs generates temperatures that are sufficient to induce significant cellular damage that finally lead to cell death. First, it was determined which load of SPIONs is required for magnetic hyperthermia (MHT) induced cell death. Therefore, J774a.1 cells were treated with varying concentrations of SPIONs (0µg/mL to 40µg/mL) and subsequently exposed to an AMF with a frequency of 779kHz in a 2-coil AMF inductor. The viability of cells was evaluated after 24 hours using the WST-1 based metabolic activity assay. Figure 3.4a indicates that AMF-induced magnetic hyperthermia reduced cell viability in SPION-loaded cells in a dose dependent manner. A reduction of metabolic activity of 79% was observed in cells loaded with 40µg/mL. WST-1 assay demonstrated a drop of cell viability of 53%, 45%, and 14% for 30, 15, and 5 µg/mL SPIONs, respectively. In essence, the results indicate that AMF induces magnetic hyperthermia that leads to cell death in SPION-loaded macrophages in a dose dependent manner.

Next, it was evaluated whether the duration of AMF given to SPION-loaded macrophages would have an effect on the viability of loaded cells. For this purpose, J774a.1 cells were loaded with 30 µg/mL SPIONs and then subjected to a magnetic field for varying periods of time (from 0 minutes to 35 minutes). As shown in Figure 3.4b, exposing the SPION-loaded cells to AMF for 5 minutes reduced cell viability to 55% compared to control cells. Prolonged exposure of cells to AMF for 25, 30, and 35 minutes further decreased cell viability similarly to 40%. However, differences were not statistically significant.

(a) (b)

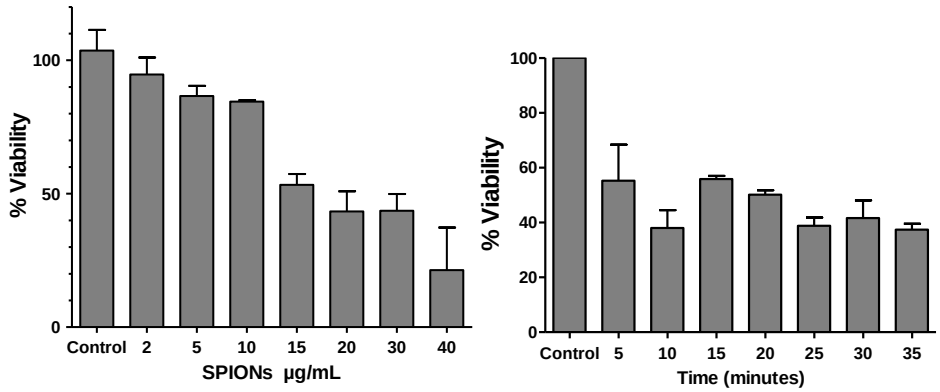

Figure 3-4Effect of SPION concentration and AMF duration on MHT induced cell death. (a) Effect of SPION concentration on magnetic MHT-induced cell death. J774a.1 macrophages were loaded by incubation with indicated concentrations of SPIONs and subjected to AMF for 30 minutes. The viability of cells was analyzed with WST-1 basedmetabolic activity assay after 24 hours. (b) Effect of AMF duration on MHT-induced cell death. J774a.1 cells were loaded with 20µg/mL of SPIONS and subjected to 779 kHz frequency of AMF for the indicated time. The viability of the cells was analyzed with WST-1 based assay. Both experiments were performed in triplicates.

Finally, it was tested whether magnetic hyperthermia induced cell death varies in different cell lines and in primary cells. Cells were incubated for 2 hours with 20 µg/mL SPIONs and exposed to AMF for 30 minutes in a 2-coil AMF inductor. Cell viability was determined by the WST-1 analysis and Annexin V based apoptosis assay after 24 hours of cultivation (Figure 3.5). Unloaded macrophages subjected to AMF and SPION-loaded macrophages without AMF exposure were used as controls. AMF exposure of SPION-loaded primary mouse macrophages, RAW264.7 and J774a.1 cells resulted in a dramatic decrease of the metabolic activity (Figure 3.5a) and a comparably strong apoptotic reaction (Figure 3.5b); BMDMs showed highest sensitivity towards magnetic hyperthermia (3% live cells in apoptotic assay) followed by RAW264.7 cells (17% live cells) and J774a.1 cells (25% live cells). U937 cells showed a 60% drop in the WST-1-based proliferation assay but only a modest reaction towards induction of an apoptotic program (70% viability, Figure 3.5b). Notably, the different sensitivities towards AMF-induced apoptosis correlate with the activity of Raptinal in these cell types. Raptinal was found to be a rapid inducer of apoptosis in multiple cell lines (Palchaudhuri et al., 2015). Treatment with 1 µM Raptinal ended in 3% live BMDMs in apoptotic assay followed by 18% live RAW264.7 cells, 37% live J774a.1 cells and 46% live U937 cells. Importantly, all unloaded cell types exposed to AMF or SPION-loaded macrophages without AMF application did not show a notable drop in metabolism and apoptosis. The application of the AMF to SPION loaded IC21 cells neither changed their metabolic activity nor induced apoptosis (Figure 3.5a/b) suggesting a higher

resistance of these cells to apoptosis induction. This is supported by the observation that the treatment with 10 µM Raptinal did not induce an apoptotic program in these cells.

(a)

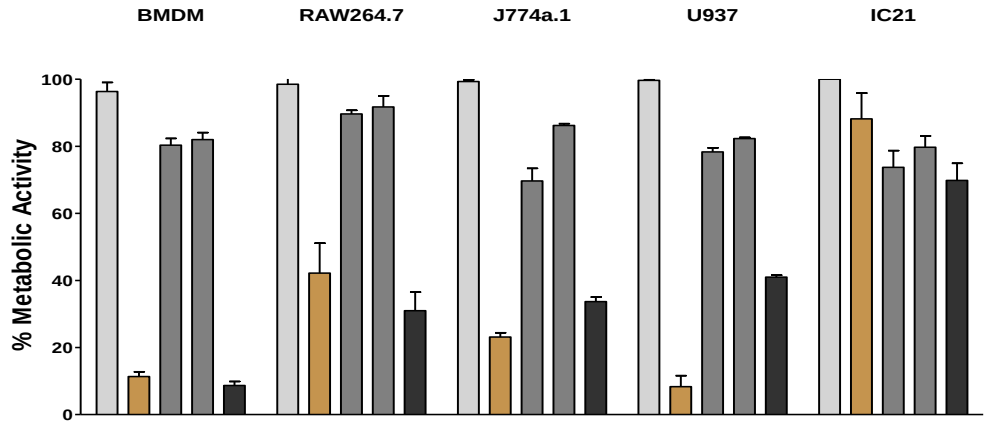

(b)

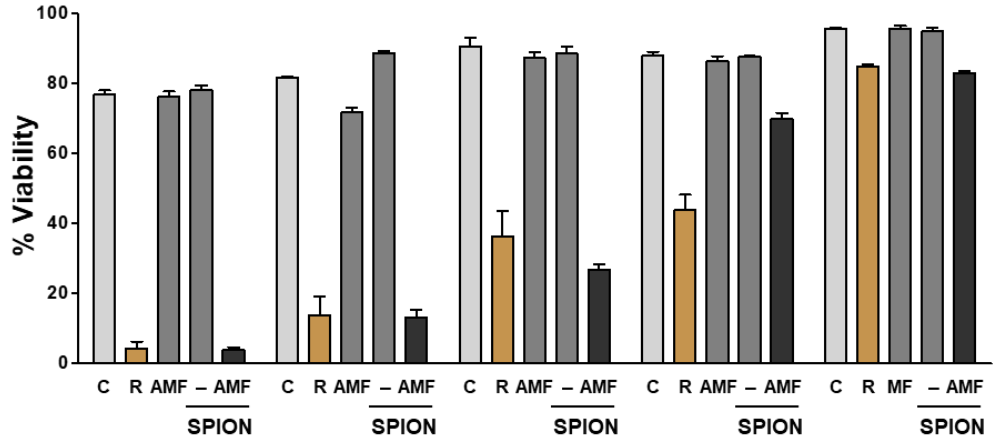

Figure 3-5Magnetic hyperthermia-induced macrophage cell death. Different macrophage cell lines were loaded with 30µg of SPION for 2 hours. AMF was applied for 40 minutes at frequency of 779kHz. The cells were incubated for 24 hours after AMF exposure and viability was analysed with (a) WST-1 based metabolic activity assay and (b) flow cytometry based Annexin V apoptosis assay. R (raptinal) treated cells served as positive control and c (macrophages without SPIONs) as negative control. Both experiments were repeated 3 times with n=3.

Scanning electron microscopy was used to evaluate the effect of magnetic hyperthermia on morphology of SPION-loaded macrophages (J774a.1 cells) (the analysis was performed by Manfred Rhode, HZI). Unloaded cells and SPION-loaded cells without AMF application showed distinct lamellipodial extensions and an amoeboid shape, typical characteristics of macrophages. In contrast, SPION-loaded macrophages exposed to magnetic field showed a characteristic apoptotic morphology such as membrane blebbing and cell shrinkage (Figure 3.6). Together these results indicated that magnetic hyperthermia is induced in response to exposure of SPIONs loaded macrophages to AMF in 4 out of 5 tested cell lines.

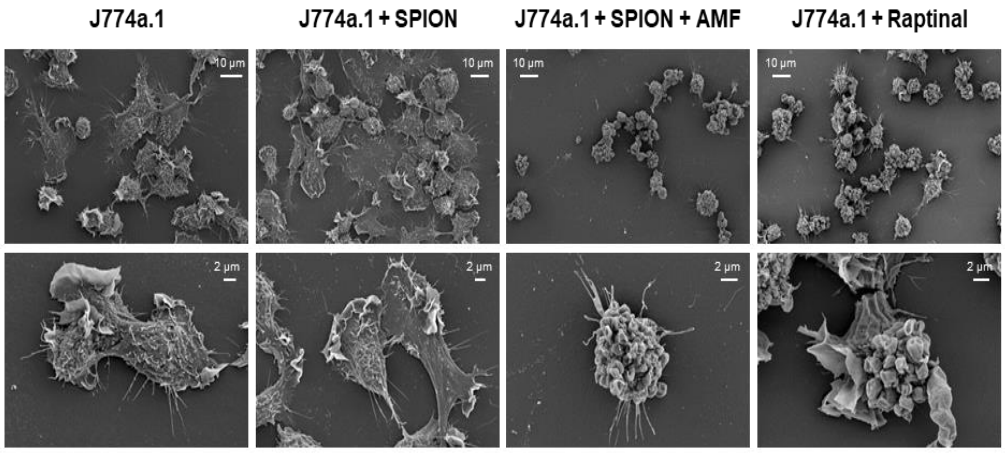

Figure 3-6Transmission electron microscopic depiction of macrophage cell death. SPIONs loaded J774a.1 macrophages exposed to 779kHz frequency AMF were incubated for 24 hours at standard cell culture conditions. The cells were then analyzed with transmission electron microscopy. Typical round apoptotic cells and apoptotic bubbles on cell surface were visible in treated cells. The results are shown as representative images from 2 independent experiments with n=3. At least 5 images were taken per sample. Analysis was performed by Manfred Rhode, HZI.

3.1.4 Magnetic hyperthermia induced controlled release of cargo

To investigate MHT induced release of compounds, in this thesis, SPIONs with covalently, heat-sensitively linked Maytansin (hereafter referred to as T-SPIONs) were used. To evaluate whether the release of the Maytansin cargo from T-SPIONs entrapped in macrophages could be achieved, first, the efficacy of Maytansin to induce cell death in two model cell lines were determined: Kaposi's sarcoma associated herpes virus (KSHV) infected endothelial cells (K-EC) [70]and the human breast cancer cell line MCF-7. Both cell lines were treated with varying concentrations of Maytansin (0-100nM) for 48 hours and cell viabilities were analyzed using the WST-1 assay. Figure 3.7a indicates that as low as 5nM toxin can induce 25% decrease in K-EC cell viability while 20nM Maytansin reduced K-EC cell viability to ca. 50%. For MCF-7 cells an IC50 value of 24nM Maytansin was determined (Figure 3.7b). Next, I evaluated the release of cargo through 2D transwell assay and 3D spheroids assay.

(a)

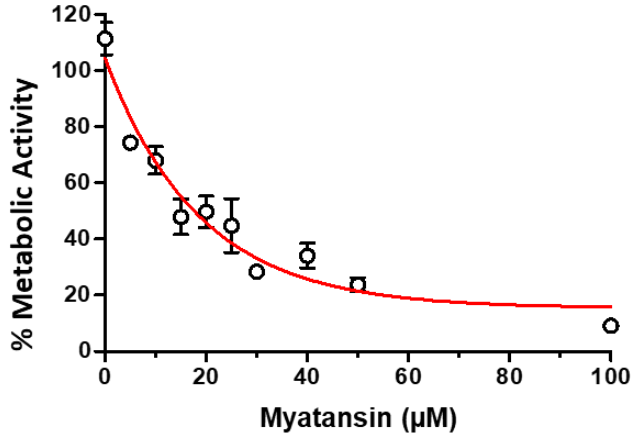

(b)

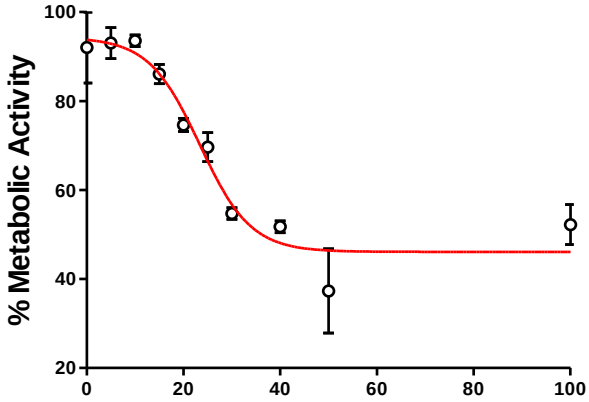

Figure 3-7Maytansin titration in (a) K-EC (b) MCF-7 cells. The IC50 values of Maytansin in K-EC cells and MCF-7 cells were determined by treating the cells with varying concentration of Maytansin for 48hrs. For K-EC cells an IC50 value of 20µM while for MCF-7 cells an IC50 of 25µM was calculated. These are representative results of 2 independent experiments (n=3).

3.1.4.1 Controlled and minimal non-specific cargo release

As shown in Figure 3.5, all tested cell lines were responsive to magnetic hyperthermia but IC21 macrophages showed complete resistance. Thus, IC21 cell line was used as a carrier cell line to test exclusively for the release of Maytansin toxin from T-SPIONs. IC21 cells were loaded with T-SPIONs while unconjugated SPIONs act as a control. Next, half of the T-SPION loaded cells as well as SPION control cells were subjected to AMF. Subsequently all conditions including mock-treated cells were cultivated for 48 hours and cell viability was determined by WST-1 assay (Figure 3.8a). Addition of 20 µM Maytansin strongly reduced the viability of IC21 cells. Importantly, exposing the T-SPION-loaded IC21 cells but not cells containing the drug-free SPIONs to AMF induced a significant cell killing (28% versus 87% remaining metabolic activity). Further, internalization of T-SPIONs did not decrease IC21 cell viability without AMF application. This observation was confirmed

by J774a.1 cell loading. After internalization of T-SPIONs or drug-free SPIONs, J774a.1 cells were cultivated for 48 hours and assayed for cell viability. WST-1 assay demonstrated a minor drop in metabolic activity of J774a.1 cells loaded with T-SPIONs (Figure 3.8b). However, this level in reduction showed no significant difference to cells loaded with drug-free SPIONs. Together these results indicate that internalization of drug-coated T-SPIONs is highly biocompatible and no unspecific release (without AMF application) of conjugated toxin affecting viability of the carrier cells is obvious.

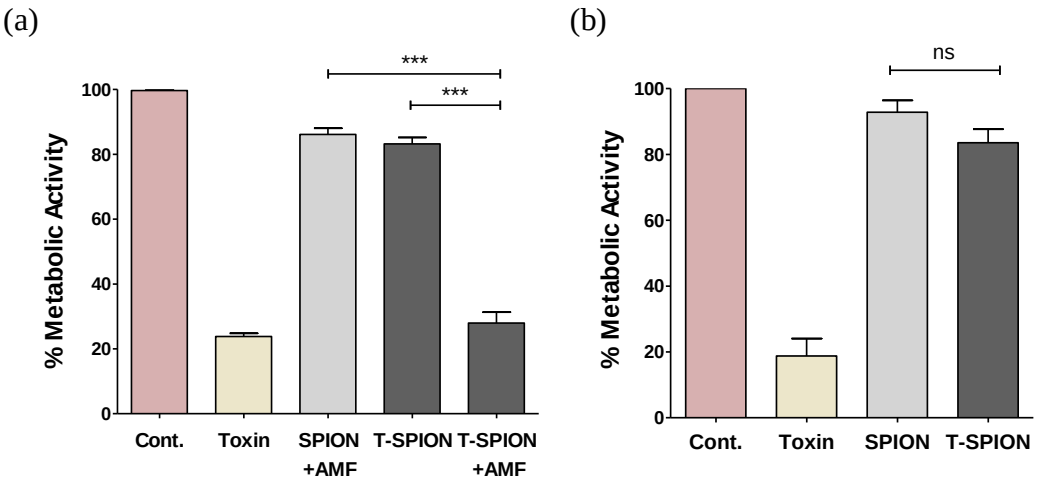

*Figure 3-8Biocompatibility of T-SPIONs with. (a) IC21 cells were loaded with SPIONs or T-SPIONs (20 µg/mL) and exposed to AMF or were mock treated. Metabolic activity of cells was measured after 48 hours using the WST-1 assay. ***p<0.001 (t-test) (b) J774a.1 cells were loaded with SPIONs or T-SPIONs (20µg/mL) and the viability of loaded cells was evaluated with WST-1 assay after 48 hours of cultivation. n.s.: non-significant. Both experiments were repeated 3 times and representative results are shown.*

3.1.4.2 AMF dependent drug release and killing of neighboring target cells

Next, it was investigated whether toxin released from T-SPIONs inside the carrier macrophages would induce cell killing of neighboring target cells. J774a.1 cells were used as T-SPION carriers. Since this cell line undergo apoptosis when exposed to AMF-induced hyperthermia, an effective toxin-release can be expected. As target cells, K-ECs and MCF-7 cells were used. Both cell lines were tested for their sensitivity to Maytansin and it was shown that the LC50 values were 15nM and 24nM respectively.

To separate carrier macrophages and target cells transwell inserts were used. The pore size of transwell membrane was 0.4µm, which allows the passage of toxin through membrane but does not allow transfer of carrier cells. MCF-7 and K-EC target cells were seeded in the lower chamber, while the upper chamber contained either cell-free T-SPIONs or T-SPION-loaded J774a.1 macrophages previously exposed to AMF or left untreated. As controls, the unloaded J774a.1 cells or the released toxin was used. Metabolic activity of target cells was

analyzed after 72 hours in transwell co-culture by WST-1 assay. The experimental set up is schematically shown in Figure 3.9a. As expected, addition of unconjugated toxin into the upper chamber resulted in a remaining metabolic activity of 20% for the MCF-7 cells and 30% for the K-ECs, compared to control cells (unloaded J774a.1) (Figure 3.9b/c). When T-SPIONs alone or J774a.1 cells loaded with T-SPIONs were added to the upper chamber without prior application of AMF, a slight reduction of MCF-7 cells and K-ECs activity (85% and 80% of control) was detectable. Importantly, the activity of target cells strongly dropped to 40% when free T-SPIONs or T-SPION-charged J774a.1 macrophages were subjected to AMF before loading onto transwell inserts.Together, these results indicate that toxin release from conjugated SPIONs can be induced by AMF application. Of note, AMF induced release of the toxin from free and cell-entrapped T-SPIONs resulted in a comparable reduction of the target cells' viability, both for MCF-1 cells and for K-ECs. This indicates that the activity of the toxin which was released from carrier cells was not altered by the cellular environment. All in all, these experiments prove a tightly controlled release mechanism of the toxinfrom T-SPION entrapped cells and subsequent death of exposed tumour cells.

3.1.4.3 Controlled release in 3D macrophage/tumor cell co-culture

In the previous chapter transwell cultures were used to separate carrier cells from target cells and prove AMF induced toxin release from T-SPIONs. However, such 2D cell cultures miss some tumor's physiological properties, like cellular layered assembling. Thus, three-dimensional (3D) growth of tumor cell lines is regarded as a more stringent and representative model to mimic features of human solid tumors, e.g. hypoxia as well as intricate cell-cell and cell-matrix interaction (Rasheena et al., 2014). Further, 3D cultures restrict unrestrained proliferation which is dominant in standard 2D cultures. Thus, AMF induced toxin release from T-SPION loaded macrophages was examined in a spheroid culture system. K-ECs when cultured in agarose coated cell culture plates tends to form spheroids, which have invasive properties, indicating tumorigenic status of cells (Dubich et al., 2019). To enforce close contact of carrier and target cells spheroid co-cultures of loaded macrophages and K-ECs were performed.

(a)

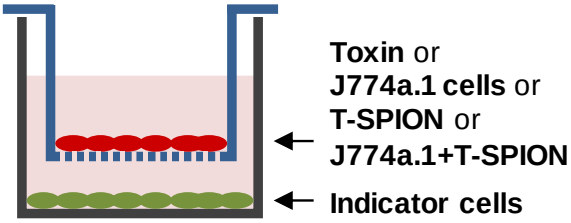

(b)

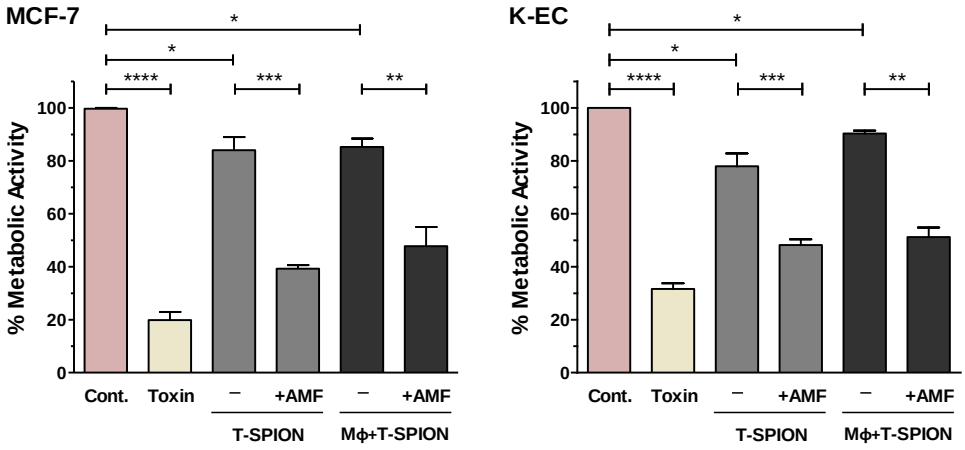

*Figure 3-9Effect of MHT induced Maytansin release on MCF-7 and K-EC cells. (a) Schematic representation of experimental procedures. (b) MHT-induced release of Maytansin in transwell system and subsequent effect on co-cultured MCF-7 and K-EC cells. 70,000 MCF-7 orK-ECs were cultured in the lower well while 30,000 loaded or unloaded J774a.1 macrophages were cultured in the upper transwell. The loaded macrophages were either exposed to AMF for 30 minutes prior co-culture or left as such. Also, 20µg/mL of T-SPIONs either exposed or not exposed to AMF were added into the upper transwell. As a controlled 24nM of toxin was directly suspended in media in the upper transwell. Viability of cells in the lower well was analyzed with WST-1 assay after 48 hours ofco-cultivation. Both experiments were repeated 3 times (n=3) and representative results are shown. ***p<0.001,**p<0.01,*p<0.05 (t-test).*

3.1.4.4 Controlled release in 3D macrophage/tumor co-culture

In the previous chapter transwell cultures were used to separate carrier cells from target cells and prove AMF induced toxin release from T-SPIONs. However, such 2D cell cultures miss some tumor's physiological properties, like cellular layered assembling. Thus, three-dimensional (3D) growth of tumor cell lines is regarded as a more stringent and representative model to mimic features of human solid tumors, e.g. hypoxia as well as intricate cell-cell and cell-matrix interaction (Rasheena et al., 2014). Further, 3D cultures restrict unrestrained proliferation which is dominant in standard 2D cultures. Thus, AMF induced toxin release from T-SPION loaded macrophages was examined in a spheroid culture system. K-ECs when cultured in agarose coated cell culture plates tends to form spheroids, which have invasive properties, indicating tumorigenic status of cells (Dubich et al., 2019). To enforce close contact of carrier and target cells spheroid co-cultures of loaded macrophages and K-ECs were performed.

3.1.4.4.1 Effect of Maytansin on K-EC spheroids

First, the sensitivity of K-EC spheroids towards Maytansin was determined. K-EC cells were cultured in agarose coated 96 well plates and after overnight cultivation different concentrations of Maytansin (0 to 100 µM) were directly added to the cell culture media. The cell aggregates were cultured with toxin for 48 hours and integrity of spheroids was determined by microscopic inspection. In the absence of drug, K-EC spheroids growth as compact structures. Exemplary brightfield images shown in Figure 3.10indicate that a Maytansin concentration of 20µM induced signs of loss of integrity indicated by spheroid swelling and increased cell debris around the spheroid structure. Higher concentrations resulted in complete spheroid disaggregation indicating death of cells. However, as shown in Figure 3.10, even at 100µM toxin concentration small aggregates of cells were still present.

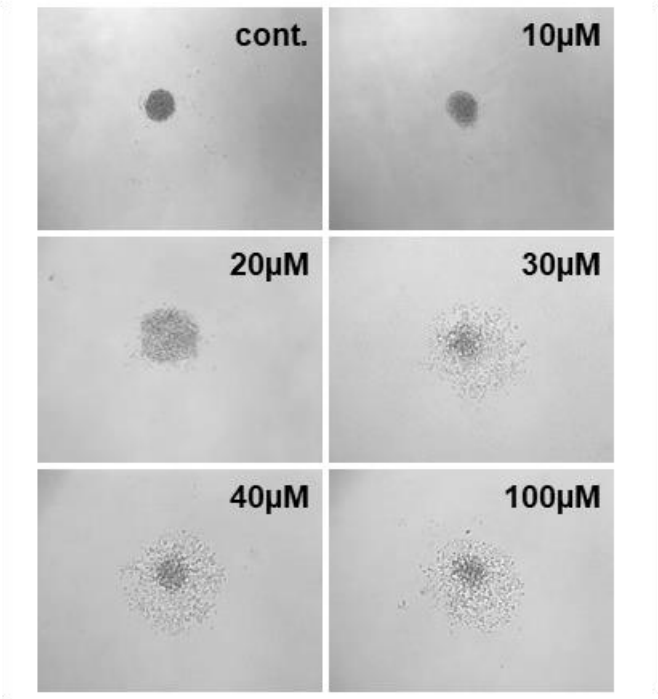

Figure 3-10Effect of Maytansin on K-EC spheroids. Spheroids were generated by culturing 4000 K-ECs on an agarose coated 96-well plate. The spheroids were treated with indicated concentrations of Maytansin for 48 hours. Representative pictures from 3 independent experiments (n=3) are shown.

3.1.4.4.2 AMF induced controlled release in 3D co-culture

To examine if toxin release from macrophages loaded with T-SPIONs is possible in a 3D environment and affect viability of target cells, 3D spheroid co-cultures of K-ECs and J774a.1 cells were formed. Therefore, J774a.1 cells were loaded immediately before spheroid formation with T-SPIONs, toxin-free SPIONs or left unloaded. Subsequently, K-ECs were mixed with J774a.1 cells in a ratio of 40 to 1. After spheroid formation, cells

were exposed to an AMF and cultivated for 48 hours. First, spheroids integrity was compared between the different conditions by brightfield microscopy. As shown in Figure 3.11, spheroids that comprised of K-ECs alone, together with unloaded J774a.1 cells or with SPION loaded J774a.1 cells showed comparable integrity in the absence of magnetic field application. Interestingly, when the AMF was applied to spheroids with SPION loaded macrophages, a partial loss of compactness and some cells outgrowing from central structures were observed. This can be attributed to heat induced killing of macrophages within the spheroid structure leading to partial disaggregation of the spheroids. Of most importance, when AMF was applied to spheroids containing T-SPION loaded macrophages a complete disruption of the spheroid structure was detected (Figure 3.11). In contrast, spheroids containing T-SPION loaded macrophages without AMF application showed only a partial loss of structural integrity and outgrowth of cells. However, the AMF-induced complete disruption of spheroids containing T-SPIONs was not seen even in in K-EC spheroids treated with the highest amount (100µM) of free toxin (compare Figure 3.10).

To quantify the extent of cell death, the metabolic activity of cells within spheroids was measured using the WST-1 assay. Only a marginal loss of metabolic activity (around 5% reduction) was observed when T-SPION containing spheroids were cultured for 48 hours without prior magnetic field application (Figure 3.12). Importantly, AMF treatment of this co-culture condition reduced cell viability to 35% compared to control K-EC spheroids. The WST-1 assay further indicates that cell viability in spheroids containing toxin-free SPIONs was not affected at all without AMF application and a partial loss of metabolic activity (20% reduction) was observed in spheroids that were subjected to AMF. This reduction can be explained by the heat-induced killing of carrier macrophages and side effects of cell debris to the growth rate of target cells. Together, these results indicate that AMF application leads to a controlled release of Maytansin toxin from macrophages in the 3D spheroids and efficient killing of target cells.

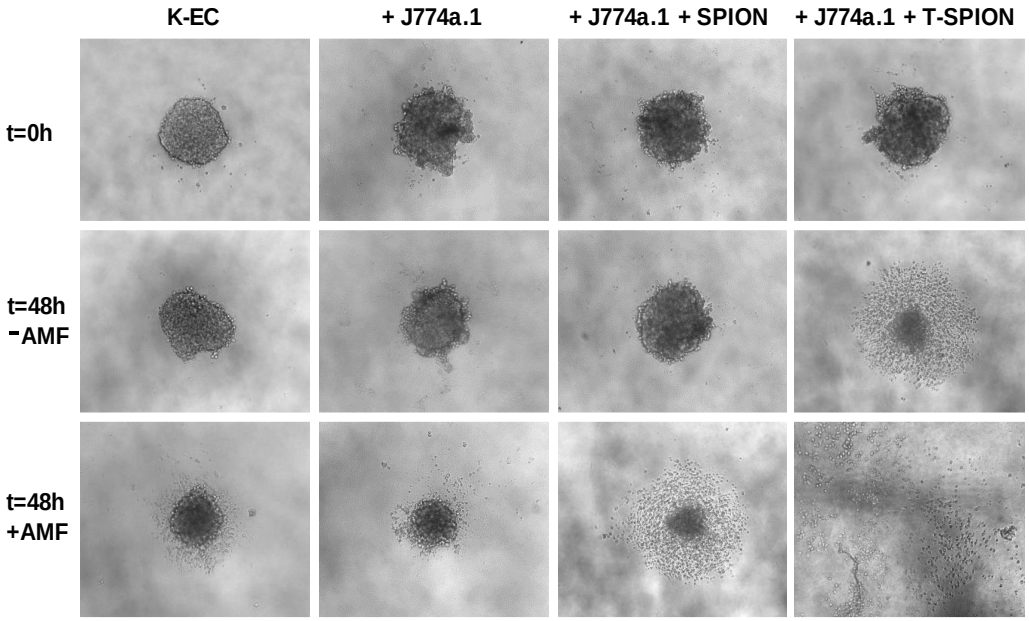

Figure 3-11AMF-induced Maytansin release in K-EC spheroids system. Spheroids were generated by co-culturing J774a.1 cells loaded with SPIONs or T-SPIONs with K-ECs in a ratio of 1:40 on an agarose-coated 96 well plate. The spheroids were exposed to AMF for 30 minutes (+AMF). The status of spheroids 48h after AMF exposure as well as of non-treated controls (-AMF) is depicted (representative photographs from 3 independent experiments (n=3)).

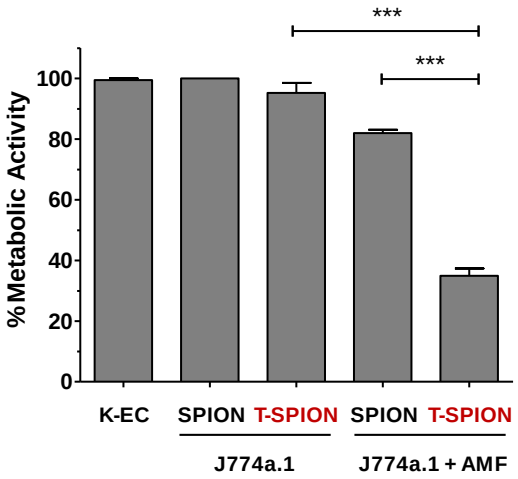

Figure 3-12Quantitative analysis of metabolic activity of spheroids after AMF-induced Maytansin release. The spheroids from figure 3.11 were disintegrated by pipetting several times and the viability was analyzed using WST-1 assay.

3.1.4.4.3 Macrophages infiltration in 3D tumor spheroids

Witnessing such a difference in toxin efficacy in case when it is released from carrier cell co-cultured with target cells in a 3D culture model or added directly into growth media, the hypothesis was tested that macrophages efficiently infiltrate 3D spheroids mainly formed by K-ECs. To test this hypothesis, GFP expressing K-ECs were co-cultured with J774a.1 cells labelled with cell tracker red. After overnight incubation of the co-culture, spheroids were analyzed by confocal microscopy. Optical sectioning revealed that J774a.1 cells were able

to integrate into the spheroids formed by the endothelial cells, which mimics in vivo tumor infiltration of macrophages (Figure 3.13). The strong effect of AMF-induced toxin release seen in Figure 3.11 and Figure 3.12 can be attributed to the phenomenon that the toxin is readily available for action on cancer cells in the spheroid and is not diluted in the media unlike free toxin treated cells.

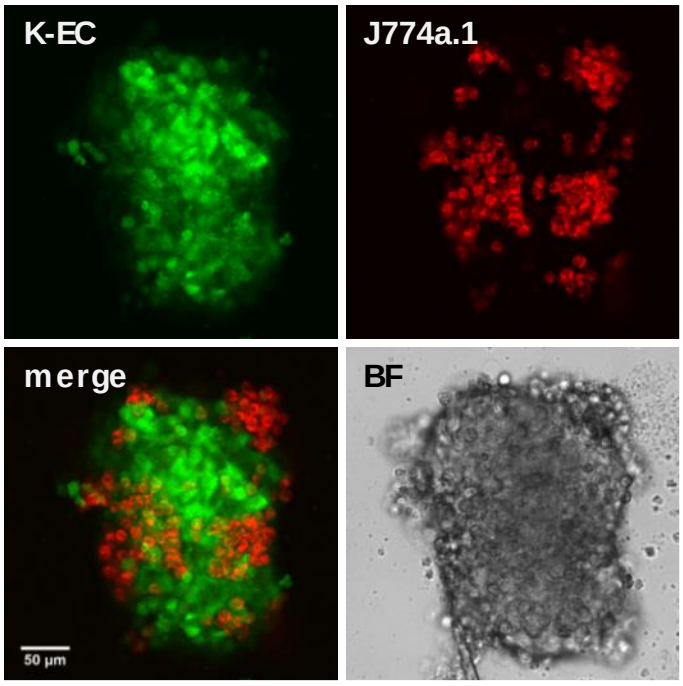

Figure 3-13Macrophage infiltration into K-EC spheroids. J774a.1 cells were stained with cell tracker red dye while K-ECs were expressing GFP. J774a.1 and K-ECs were mixed in a ration of 1:20 (200 J774a.1 cells and 3800 K-ECs).. Deep infiltration of macrophages in K-EC spheroids was observed with confocal microscopy. BF represents the brightfield image of the spheroid. Representative images are shown (n=3).

3.2 Targeting macrophages to inflammation sites

Based on the finding that an efficient release of cargo from intracellular SPIONs is possible, a novel strategy utilizing macrophages as a nanoparticles carrier to migrate to inflammatory sites in vivo was explored. Macrophages have the natural tendency to accumulate at the site of inflammation. They are one of the first cells that respond to inflammatory reaction. In this study, highly sensitive reporter systems were developed to determine a. the efficacy of cargo release in vitro and b. macrophage mediated transport and local cargo release within living mice. The loaded macrophages were produced by direct incubation of SPIONs or cargo linked SPIONs with bone marrow derived macrophages. In addition, in another strategy, macrophages were loaded with both SPIONs and cargo loaded large pore silica

nanoparticles. The ability of macrophages to migrate and to target local inflammation sites and strategies of cargo release were evaluated.

3.2.1 In vitro macrophage chemotaxis to inflammation signals

First, in vitro chemotaxis experiments were performed to determine the migratory capacity of loaded macrophages to an inflammatory signal. Therefore, IBIDI chemotaxis chambers (Figure 3.14) were used. Briefly, J774a.1 cells were cultivated in the middle chamber (observation area). On one side of the chamber (C_0), media without serum was added and on the other side of the chamber (C_{100}), complete media containing the chemotactic factor C5a was added. The chamber was placed under a confocal microscope and time-lapse analysis was performed overnight. Results were processed by ImageJ software. As shown in Figure 3.15a and 15b macrophages do respond to C5a by migrating towards it. The average distance covered by J774a.1 cells (unloaded) was 1100 µm but when the cells were loaded with SPIONs, the cells were migrating for much less distance, observed for the same amount of time. The average distance covered by SPION-loaded macrophages was 400µm. The same was true for the velocity of cells as well. The velocity of unloaded J774a.1 cells was higher (4µm/sec) as compared to loaded cells (3µm/sec).

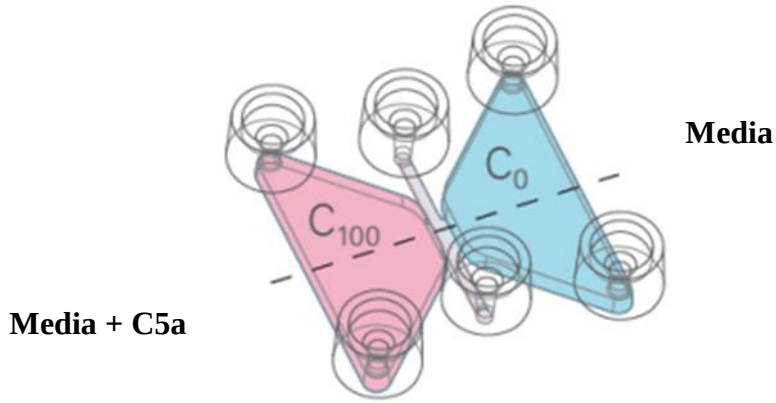

Figure 3-14Schematics of the in vitro chemotaxis assay. C100 represents the chamber with chemoattractant in media, C0 without chemoattractant but with media, while the middle chamber is the observational area where cells were cultivated.

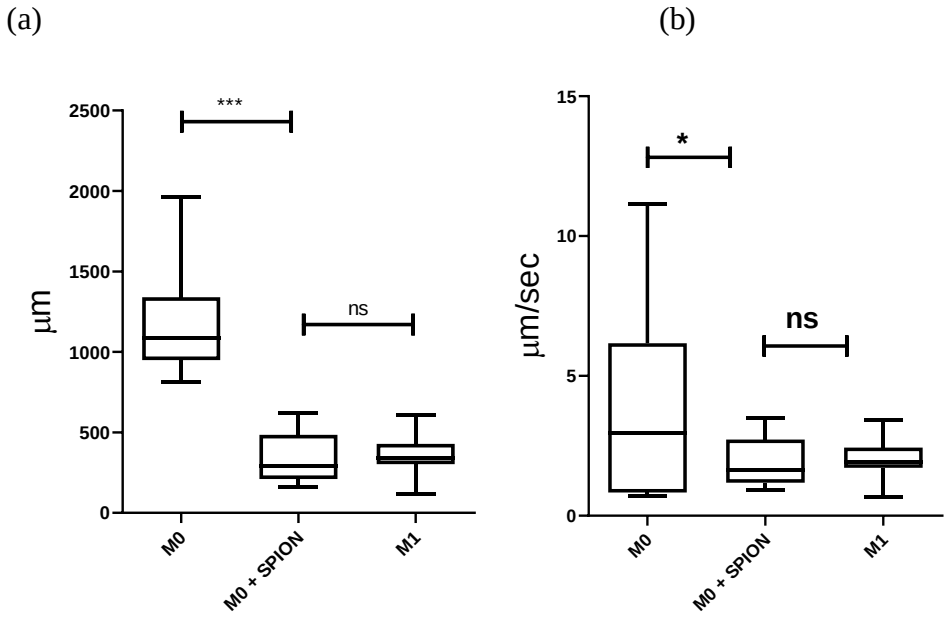

Figure 3-15In vitro chemotaxis of SPION-loaded macrophages. M0 represents M0 state macrophages, M0+ SPION represents SPION-loaded M0 macrophages while M1 is M0 macrophages polarized to M1 state by treatment with LPS and IFNγ. Briefly, 5000 cells were placed in the observation area and a minimum of 100 cells were followed using manual track option in ImageJ.(a) distance (b) velocity. The experiment was repeated 3 times and at least 30 cells were followed in each experiment.

Nanoparticles are known to serve as mechanical stimuli to activate certain signaling pathways in macrophages and thus alter the polarization status of these cells. It was hypothesized that SPIONs induce J774a.1 cells toward M1 polarization. Thus, M1 or M2 polarization markers were assessed in macrophages loaded with SPIONs for 48 hours using quantitative real time PCR. As a control, J774a.1 cells were treated either with LPS and IFN-γ to induce reprogramming to an M1 profile or with IL4 and IL10 to induce M2 polarization. M2 polarized macrophages were either assessed directly or loaded with SPIONs and checked for expression of M1 or M2 markers. As shown in Figure 3.17,

untreated J774a.1 cells neither express elevated levels of the M1 marker genes, TNF-α and iNOS nor of the M2 markers, IL-1 and Arg1, thus representing an unpolarized M0 status. However, upon loading of the M0 cells with SPIONs polarization towards M1 became evident. In contrast, once polarized to the M2 state, the macrophages retained their polarization status even after SPION loading.

The migration efficiency of M2 or SPION-loaded M2 macrophages was assessed using IBIDI in vitro chemotaxis assay. Interestingly, M2 macrophages traveled over a longer distance as compared to M0 macrophages (700µm versus 300µm) and showed higher velocity (4.05 versus 1.8µm/sec). Compared to unloaded M2 conditions SPION loaded M2 cells showed a reduced traveled distance (550µm) and velocity (3.1µm/sec) (Figure 3.18a/b). However, both parameters were still higher compared to loaded M0 cells.

Together, these results indicate that naïve macrophages when treated with SPIONs, are polarized to the M1 state which has less migratory capacity as compared to M0 or M2 polarization. However, the macrophages can retain their M2 phenotype when loaded with SPIONs and that M2 loaded macrophages travel faster and over a longer distance as compared to either SPION-loaded M0 cells or unloaded macrophages.

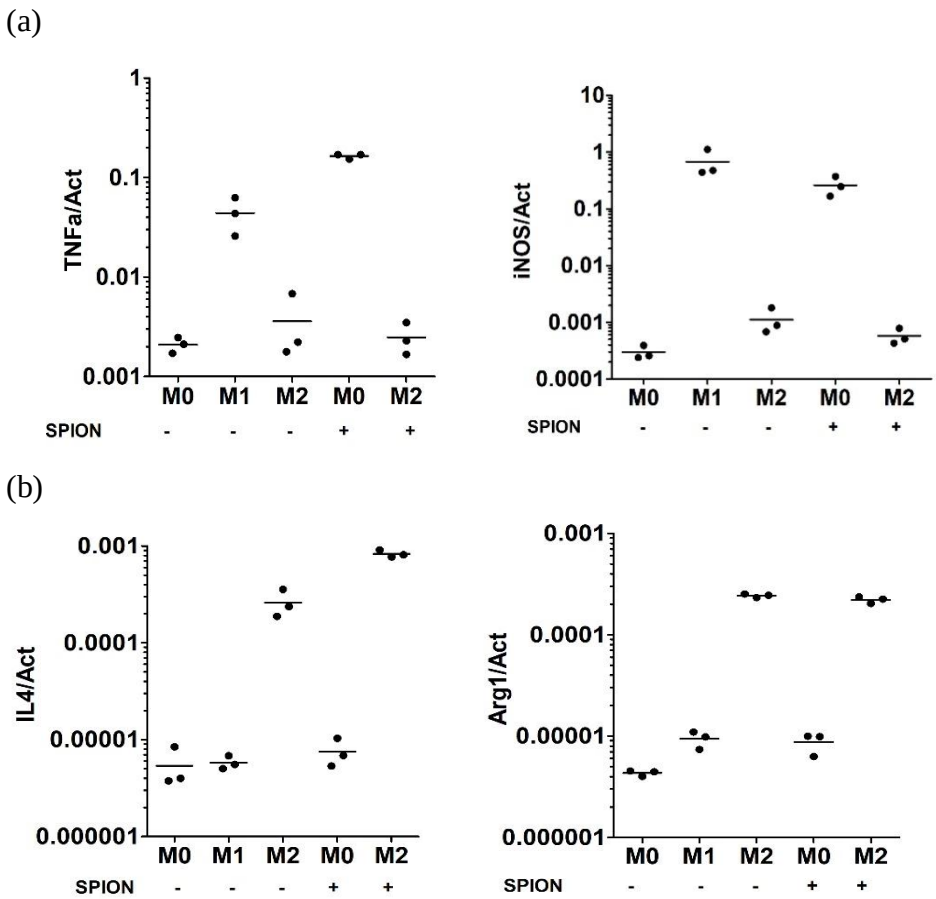

Figure 3-16SPION-induced macrophage polarization. (a) Expression profile of M1 polarization markers. (b) M2 polarization markers. The expression of marker genes was analyzed using qRT-PCR. The data was normalized to the expression of β-Actin(n=3)

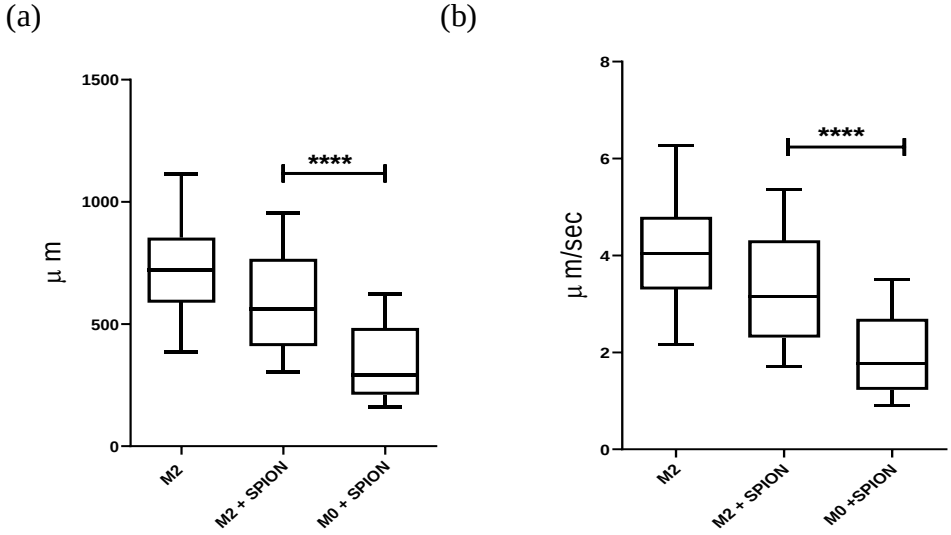

Figure 3-17In vitro chemotaxis of loaded macrophages. (a) Distance (b) Velocity of loaded M2 macrophages. 5000 cells were placed in the observation area and a minimum of 100 cells were followed using manual track option in ImageJ.

3.2.2 Development of a local inflammation model based on silica nanoparticles

To assess the migration of macrophages to inflammation site in vivo, a local inflammation mouse model was developed. For the purpose, the Mx2-Luc mouse model was used[66]. Briefly, in the mouse model the luciferase gene is under control of the Mx2 promotor, which is an IFN-stimulated gene (ISG). During inflammation, IFNs are produced which leads to the activation of the MX2 promotor and triggers the expression of luciferase. MX2-Luc mice were injected with 20µg/mL of LPS mixed with 40µg/mL of SPIONs subcutaneously. At different time points, the mice were subjected to bioluminescence imaging. As shown in Figure 3.18, 24 hours after injection, luciferase was detectable at the injection site. In contrast, a single application of either LPS or Poly(I:C) which are classical inflammation inducing agents results in systemic distribution of IFNs, predominantly visible in liver[66]. Thus, injection with LPS-loaded SPIONs results in a specific luciferase signal indicating that the inflammation induced was local and no systemic distribution of the injected material is obvious during observation time.

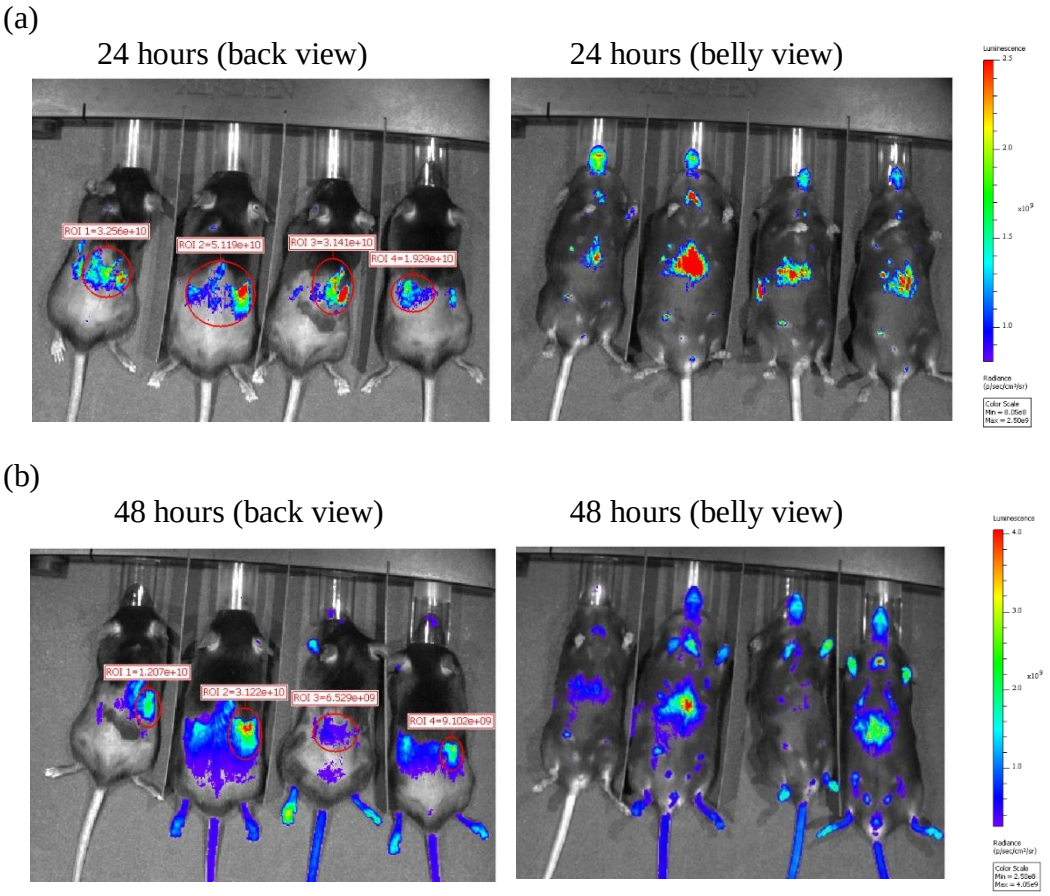

Figure 3-18In vivo local subcutaneous inflammation model. Mx2-Luc mice were injected with LPS and SPIONs subcutaneously. After 24 hours (a) and 48 hours (b) post-injection, the mice were imaged with IVIS. Signal was detectable at the site of LPS injection after 24hours and was sustained till 48 hours. As seen in the belly view, there is negligible systemic signal, suggesting the inflammation is local.

3.2.3 In vivo targeting of macrophages to a local inflammation site

To investigate whether the macrophages will migrate to the site of inflammation, bone marrow-derived macrophages were isolated from Mx2-Luc mice. The macrophages were either polarized to the M2 state by incubating with IL4 and IL10 or left at M0 state 7 days after differentiation. Upon tail vein injection, both M0 and M2 macrophages home to the site of inflammation (Figure 3.19). Of note, also when macrophages were loaded with SPIONs at a concentration of 20µg/mL, both loaded M0 and M2 macrophages were homing at the site of inflammation 24 hours after tail vein injection Figure 3.20). In contrast, no luciferase expressing macrophages were seen at the belly of the mice where no inflammation was induced. 48 hours post injection, the luciferase signal decreased at the site of inflammation in the group injected with M0 macrophages while luciferase activity at the belly increased in this group. In contrast, M2 cells did not show increased activity at the belly but rather showed ongoing luciferase activity at the site of inflammation. Thus, both

types of macrophages migrate to inflammatory sites in the body but M2 polarized cells showed prolonged activity or retention time at the site of inflammation.

(a)

(b)

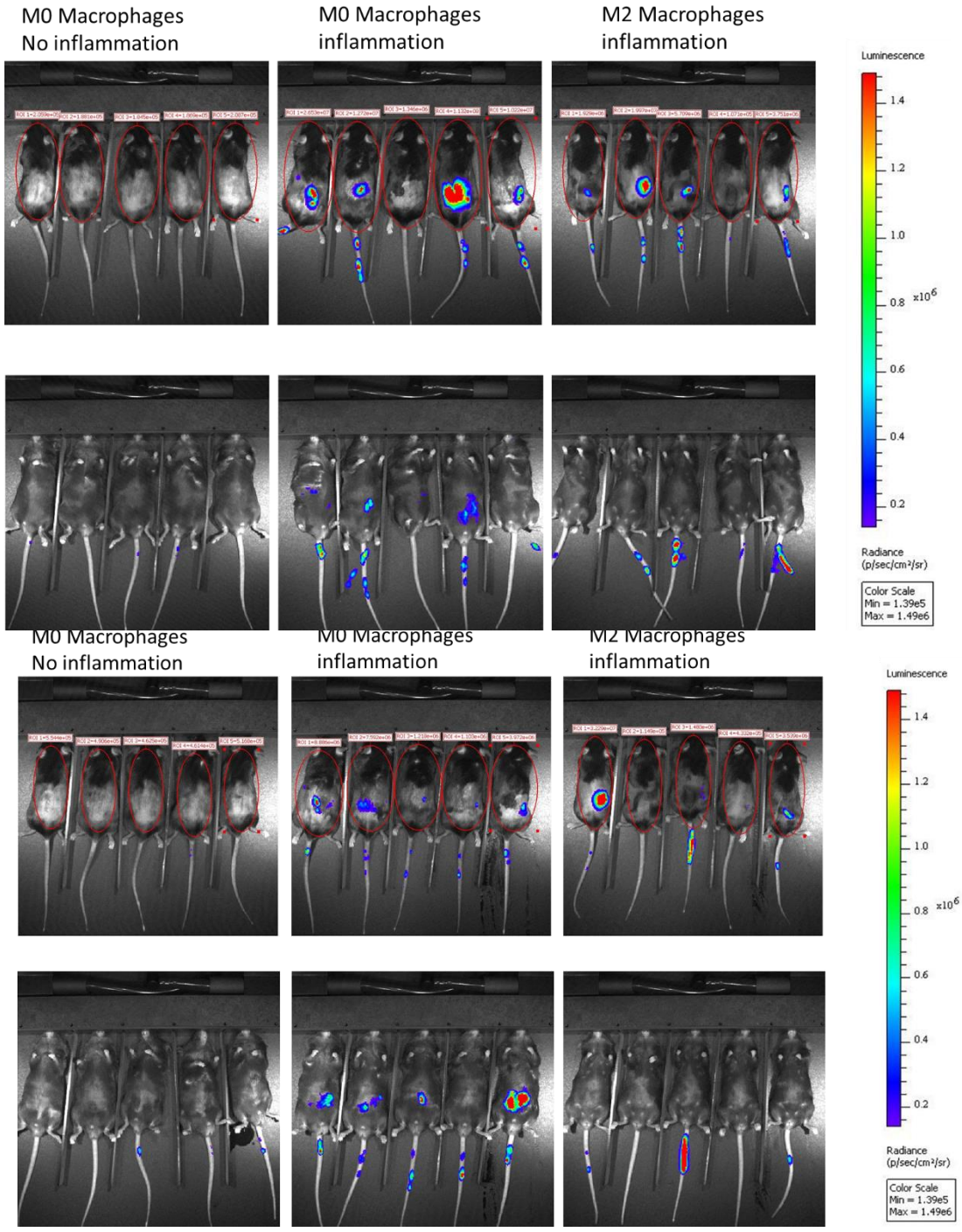

Figure 3-19In vivo homing of macrophages to inflammation site. (a) 24 hours post-injection (b) 48 hours post-injection. Inflammation was induced in the back of Rag2-/-yc-/- mice by subcutaneous injection of LPS and SPION mix. 10^6 macrophages were injected in eachcase by tail vein injection 1 hour after induction of inflammation. Animals were imaged at each time point, 5 minutes after intraperitoneal injection of 100µL D-Luciferin. All animals per group were treated similarly.

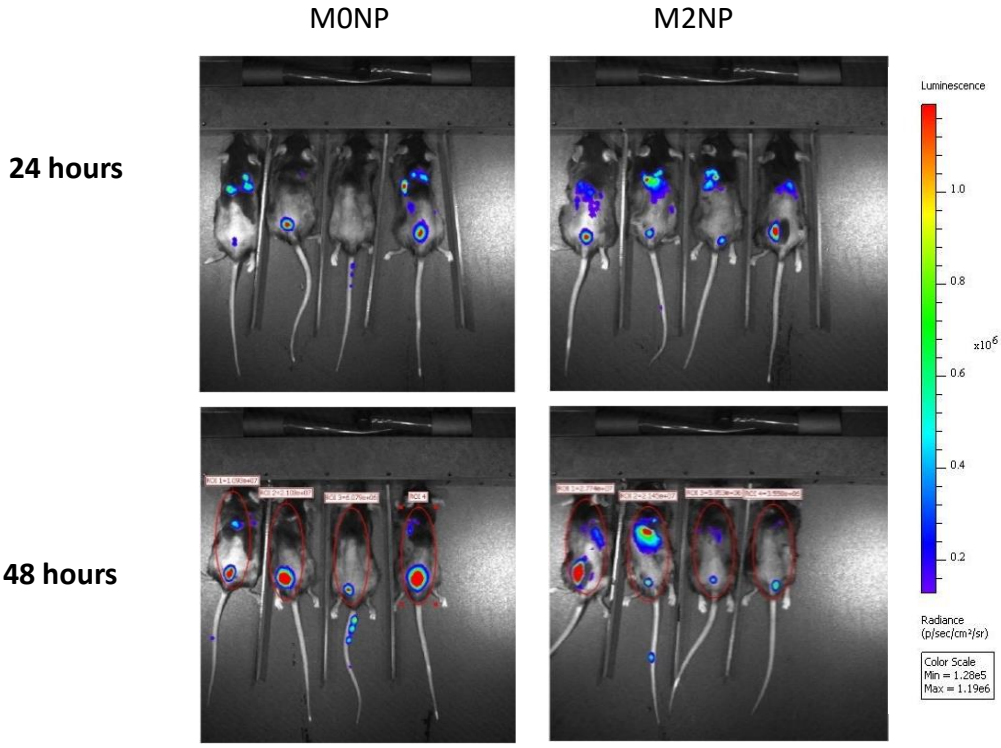

Figure 3-20Homing of in vitro loaded macrophages to inflammation site. Inflammation was induced in the back of Rag2-/-γc-/- with subcutaneous injection of LPS and SPION mix. One million macrophages, previously loaded with 20μg/mL SPIONs were injected in each caseby tail vein injection, 1 hour after induction of inflammation. Animals were imaged at each time point, 5 minutes after intraperitoneal injection of 100μL D-Luciferin. All animals per group were treated similarly.

3.3 In vivo targeted and controlled release of cargo from cell entrapped SPIONs

To visualize site specific release of cargo *in vivo*,(Z)-4-hydroxytamoxifen ((Z)-4-OHT) was chosen as a cargo for loading nanoparticles. (Z)-*4-OHT* inducesactivationofCreERT2. CreERT2[i]s a fusion protein where the Cre recombinase and the estrogen receptor binding domain are linked together. At physiological conditions, the fusion protein resides as an inactive form in the cytoplasm but upon exposure of cell to (Z)-4-OHT, it undergoes a conformational change and is able to translocate to the nucleus and recognize its specific target DNA sequence, so-called loxP. Cre binds to loxP sites and induces recombination; Depending on the orientation of the loxP sites inversion or excision will occur. Here, to permanently achieve transient release of (Z)-4-OHT and subsequent activation of CreERT2, two inverted loxP sequences were used to flank the respective reporter gene which was integrated downstream a promoter in antisense orientation, resulting in a silent, non-expressed state. In this situation, Cre recombinase will lead to an inversion of the reporter gene, and the gene will get activated. A schematic representation of the mechanism is shown in Figure 3.21a.

To generate (Z)-4-OHT responsive mice, mice expressing CreER^{T2}under the ubiquitously expressing ROSA26 promotor were bred with RosaAntiluc (luciferase framed by two loxP sites) expressing animals [74]. The offsprings having both CreER^{T2}and RosaAntiluc were selected (so called Cre-Luc animals). Fibroblast cells (hereafter referred as Cre-Luc) were isolated from these animals and immortalized using T-antigen.

Further, to achieve a reporter cell line that allows single cell detection of (Z)-4-OHT-mediated Cre activity, Cre-GFP cells were established upon stable transfection of the CreER^{T2} expression construct and a floxedVenusGFP reporter gene in antisense orientation.

Both Cre-Luc and Cre-GFP cells were treated with varying concentration of (Z)-4-OHT (1 to 20 ng/mL) for 48 hours and then either luciferase expression was assessed in cell extracts (Figure 3.21b) or the percentage of GFP expressing cells was determined using flow cytometry (Figure 3.22). Results indicate that both cell models were sensitive to concentrations of (Z)-4-OHT at as low as 1ng/mL. The use of Cre-GFP reporter cells clearly indicate that mainly the number of cells increases at higher concentration of (Z)-4-OHT added to the cells, as expected from the underlying mechanism.

(a)

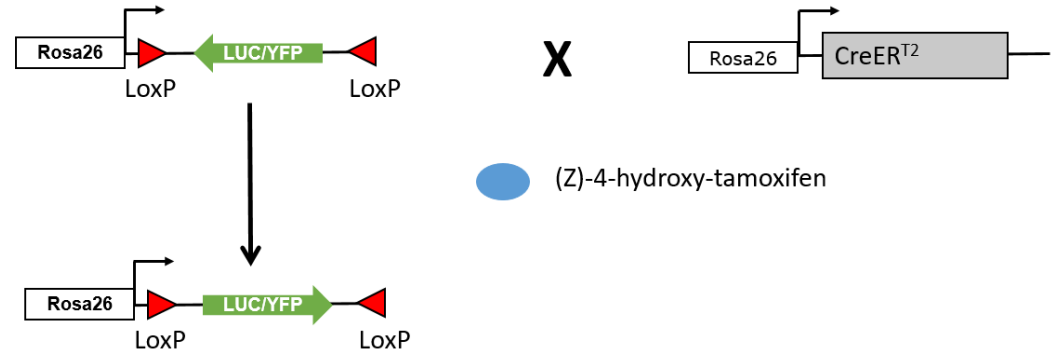

(b)

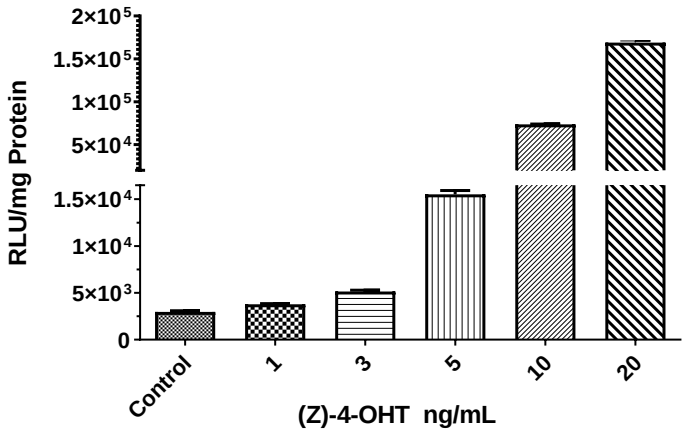

Figure 3-21(Z)-4-OHT titration with Cre-Luc cells. (a) Schematic representation of Cre-LoxP system. (b) 10^5 cells were cultured in a 24-well plate and incubated with different concentrations of (Z)-4-OHT for 48 hours. The luciferase expression was measured with invitro luminescence assay. Each sample wasmeasured in triplicate.

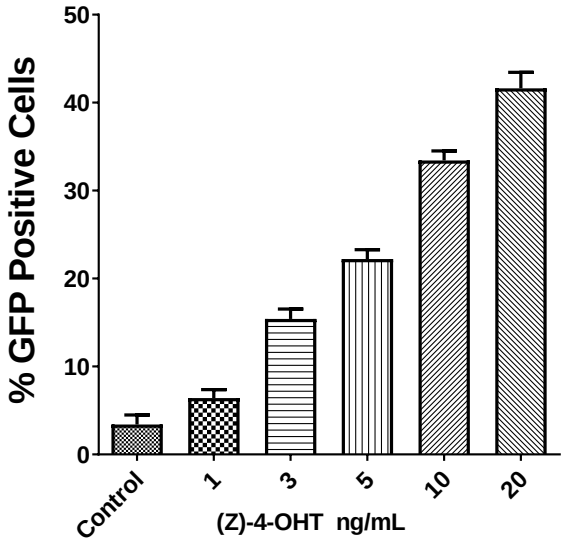

Figure 3-22(Z)-4-Hydroxytamoxifen ((Z)-4-OHT) titration with Cre-GFP cells. 10^5 cells were cultured in a 24-well plate, incubated with different concentrations of (Z)-4-OHT for 48 hours and GFP expression was measured with FACS.Each sample wasmeasured in triplicate.

Next, the kinetics of reporter gene induction was compared for the two cell lines. Therefore, Cre-Luc and Cre-GFP cells were treated with 20ng/mL of (Z)-4-OHT and expression of both reporter genes was analyzed after each 24 hours till 120 hours. As shown in Figure 3.23 and Figure 3.24, both luciferase and GFP expression increased uniformly over time after addition of (Z)-4-OHT. For both cells lines a robust increase in reporter gene activity is obvious after 24 hours, suggesting that both cell models offer the comparable sensitivity and temporal control towards (Z)-4-OHT.

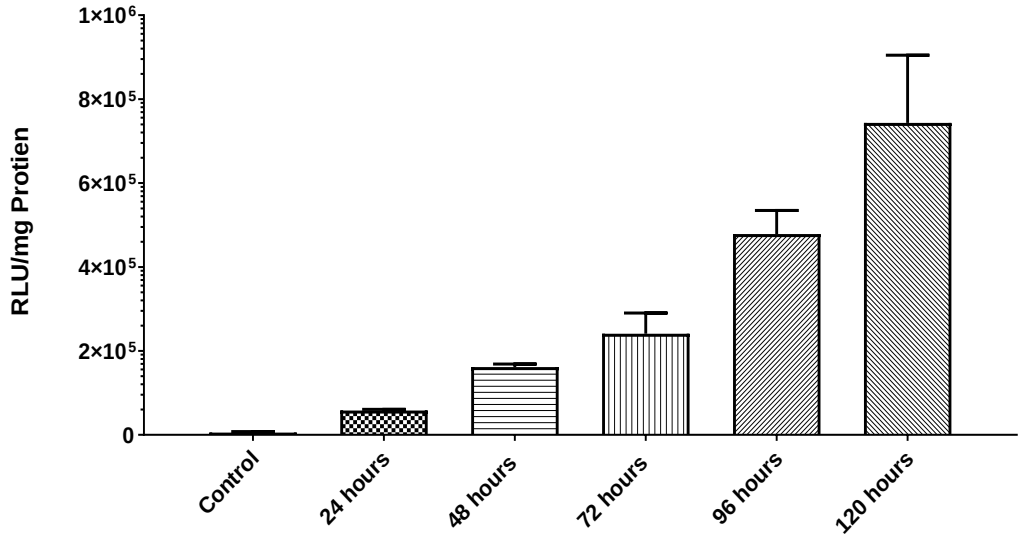

Figure 3-23Kinetics of luciferase induction after exposure of Cre-Luc cells to (Z)-4-Hydroxytamoxifen. 10^5Cre-Luc cells were incubated with 20ng/mL of (Z)-4-Hydroxytamoxifen for 24, 48, 72, 96 or 120 hours and measured for luciferase expression (n=3).

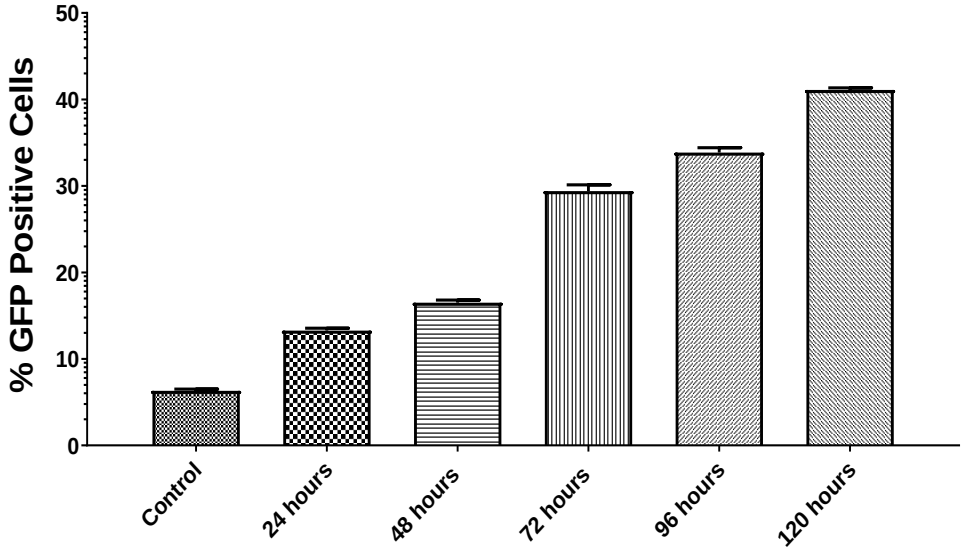

Figure 3-24Kinetics of GFP expression after exposure of Cre-GFP cells to (Z)-4-Hydroxytamoxifen. 105 Cre-GFP cells were incubated with 20ng/mL of (Z)-4-Hydroxytamoxifen for 24, 48, 72, 96 or 120 hours and analyzed for GFP expression with FACS (n=3).

3.3.1 Magnetic hyperthermia induced controlled release of (Z)-4-Hydroxytamoxifen

Reporter cell lines allow sensitive measurement of (Z)-4-OHT in the supernatant of cells and hence are attractive candidates for controlled release studies. To achieve heat induced release of (Z)-4-OHT from SPIONs, in the laboratory of Andreas Kirschning, LUH Hannover, (Z)-4-OHT was decorated on magnetic silica nanoparticles by using a heat sensitive linker (for details see PhD Thesis of Sibel Türkkan, Leibniz University Hanover). These particles were kindly provided for further analysis.

First, it was tested whether the ability of the linker-modified (Z)-4-OHT to activate $CreER^{T2}$ is affected. (Z)-4-OHT-Linker strongly activated both reporter systems, indicating that the nanoparticle-free modification did not influence activity of the molecule (Figure 3.25).

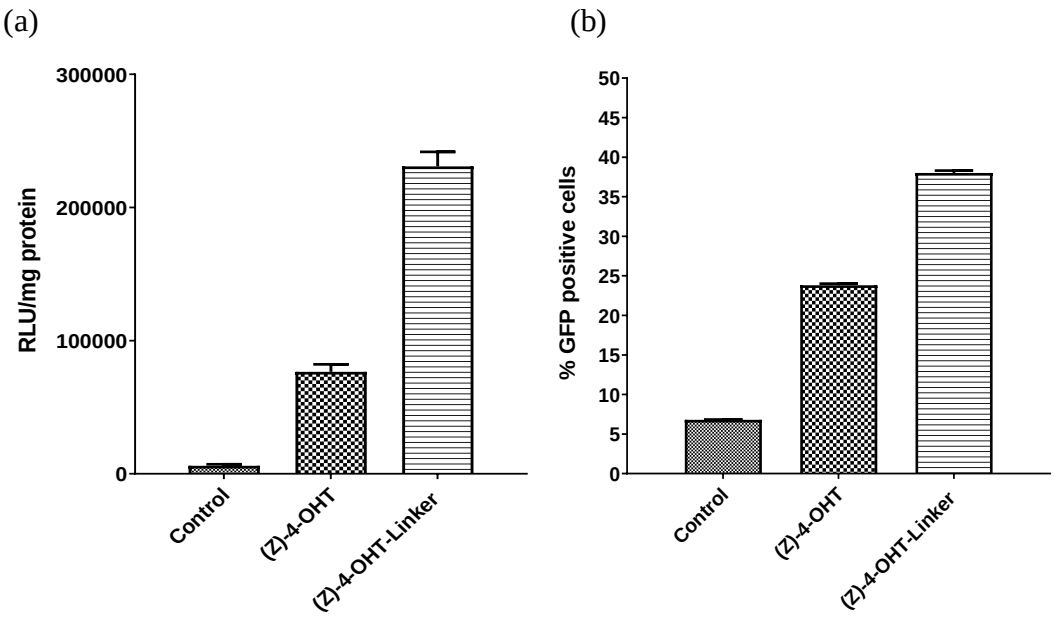

Figure 3-25Luciferase and GFP induction in Cre-Luc (a) and Cre-GFP (b) cells after incubation with linker coupled (Z)-4-Hydroxytamoxifen. 10^5 cells were incubated with 20 ng/mL of either (Z)-4-OHT or (Z)-4-OHT-Linker for 48 hours. Then, cells were analyzed for luciferase activity (a) or subjected to flow cytometry (b). All samples were analyzed in triplicates.

To investigate if (Z)-OHT can be decoupled from SPIONs by AMF, 1mg/mL of suspended (Z)-4-OHT-SPIONs were exposed to an alternating magnetic field for 45 minutes and 50µL of supernatant was taken from the solution every 5 minutes. Cre-GFP reporter cells were used to determine (Z)-4-OHT activity in the supernatant. As shown in Figure 3.26, the number of GFP-positive cells increased from 6.5% to maximal 16.3%, indicating (Z)-4-OHT activity in the supernatant. The arise of (Z)-4-OHT activity started as early as after 5 minutes exposure to magnetic field and induced GFP expression in 14% of cells. However, a maximal increase of 10% of cells showing induced conversion of the reporter gene was detectable corresponding to only 3 ng/mL of released (Z)-4-OHT. This was much less than expected, given the fact that the (Z)-4-OHT-SPIONs were decorated with as much as 1 µg of (Z)-4-OHT and that the reporter cells can reach a maximum expression of 45% with 20ng of (Z)-4-OHT (Figure 3.22). Thus, this indicates that either the drug was not efficiently released and/or released (Z)-4-OHT was partially inactivated by the heat on the surface of nanoparticles generated by magnetic hyperthermia.

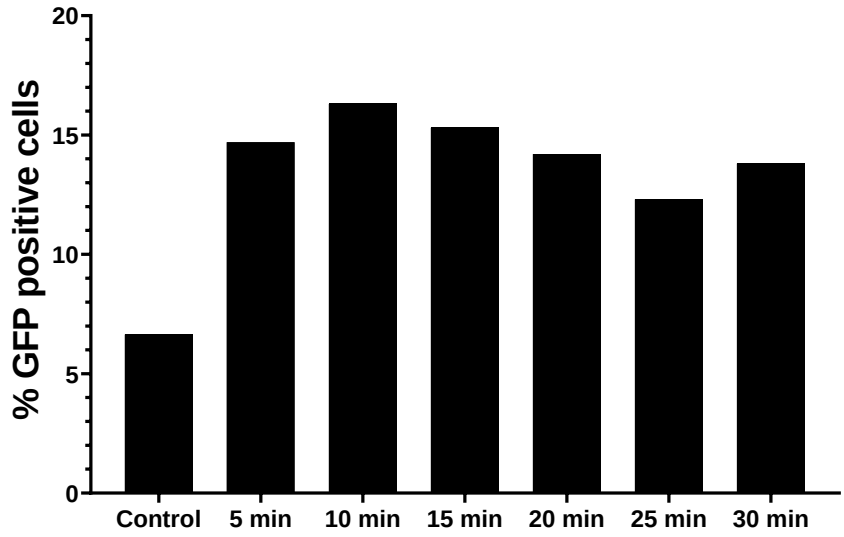

Figure 3-26Controlled release of (Z)-4-OHT from (Z)-4-OHT-SPIONs after exposure to magnetic field. 1mg/mL of suspended (Z)-4-OHT-SPIONs were exposed to magnetic field for up to 30 min. 50µL of supernatant was at indicated time points collected for analysis on Cre-GFP cells.

HPLC based analysis of AMF-induced release of (Z)-4-OHT from SPIONs in the laboratory of the group of Prof.A.Kirschning, LUH, showed that the hyperthermia produced from SPION after magnetic field leads to isomerization of the compound, i.e. changes the conformation of (*Z*)-4-OHT to the (E)-4-OHT form which was shown to be significantly less active. Thus, the unexpected low activation from after AMF-induced release is presumably a consequence of heat induced inactivation of the drug.

This was further confirmed with the Cre-Luc reporter cells. Briefly, the activity of (Z)-4-OHT and (Z)-4-OHT incubated for 24 hours at either 25°C or 37°C was compared upon incubation with Cre-Luc reporter cells for 48 hours. As shown in Figure 3.27, the activity of (Z)-4-OHTdrops as it is exposed to elevating temperatures which is shown as drop in luciferase expression by reporter cells.

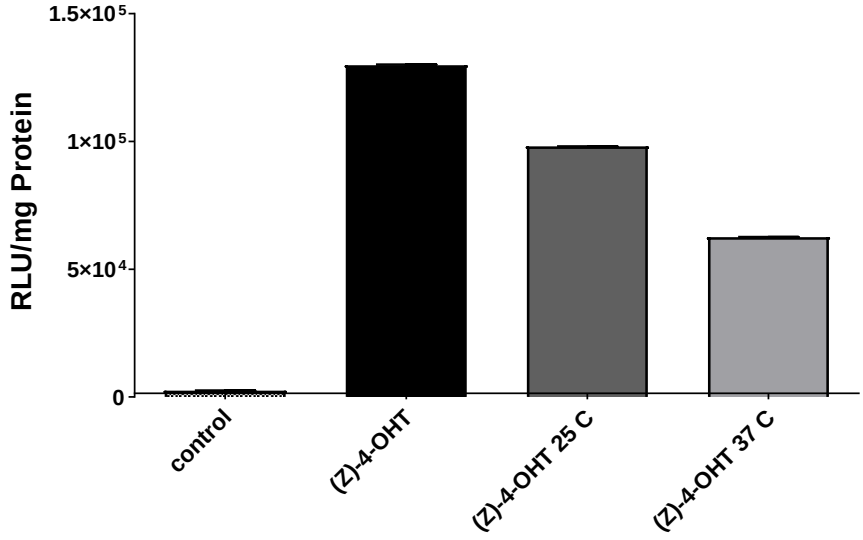

Figure 3-27Effect of temperature increase on activity of (Z)-4-Hydroxytamoxifen. 100,000 Cre-Luc cells were treated with 20ng/mL (Z)-4-hydroxytamoxifen and incubated for 30 minutes at different temperatures. Luciferase assay was performed 48 hours after incubation. Results are shown as mean ± SD of triplicates.

3.3.2 Cargo release from large pore silica nanoparticles

From section 3.3.2, it was evident that magnetic hyperthermia induces*Z* to *E* isomerizationof (Z)-4-OHT, thereby inactivating it. Thus, in order to achieve site specific drug release, as an alternative, non-paramagnetic large pore silica nanoparticles (LPSNP) were used to non-covalently bind (Z)-4-OHT. By adsorption of the compound, spontaneous release of (Z)-4-OHT is expected. To this end, LPSNP were incubated in a solution of 1mg/mL of (Z)-4-OHT for 24 hours and washed extensively. To evaluate the kinetics of release of (Z)-4-OHT from LPSNP, loaded LPSNP were suspended in culture media and supernatant was collected at different time points (6, 12 and 24 hours) and applied on Cre-Luc cells. Luciferase expression in reporter cells was analyzed after 48 hours of incubation. As shown in Figure 3.28, as soon as after 6 hours, luciferase activity was detected which further increased over time, together indicating spontaneous release of (Z)-4-OHT from loaded LPSNP.

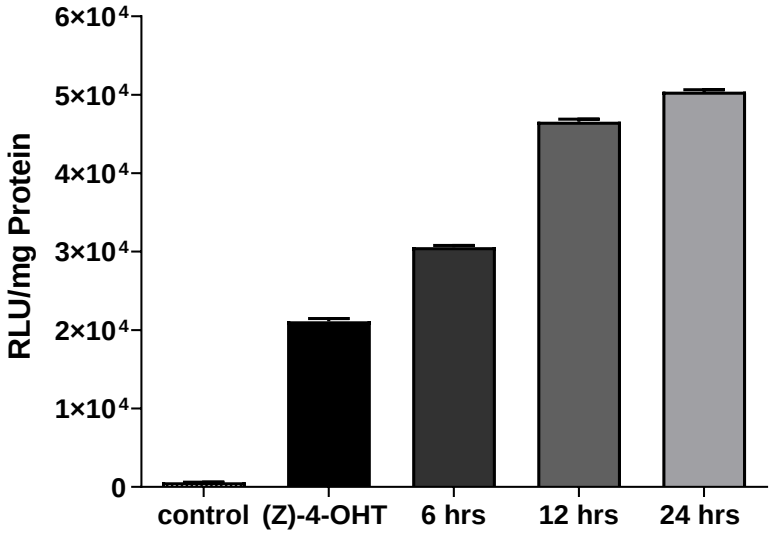

Figure 3-28Spontaneous release of (Z)-4-OHT from large pore silica nanoparticles at different time points. 1mg/mL of (Z)-4-OHT-LPSNP were suspended in culture media and after each time point the suspension was centrifuged and supernatant was applied on 1 x 105 Cre-Luc cells. The expression was analyzed after 48 hours. Results are shown as mean ± SD of triplicates.

3.3.3 Magnetic hyperthermia induced cargo release from large pore silica nanoparticles loaded macrophages

In order to achieve site-specific cargo release from macrophages, the spontaneous release of (Z)-4-OHT from macrophages loaded with (Z)-4-OHT-LPSNPs was tested. To this end, J774a.1 cells were loaded with (Z)-4-OHT-LPSNPs and placed in the upper well of a transwell insert. In the lower well, Cre-Luc reporter cells were cultured. The cells were co-cultured for 24, 48 and 72 hours and luciferase activity was assayed at the end of the respective cultivation period. Co-cultivation with control loading of the upper well and addition of (Z)-4-OHT into the upper was performed for 48 hours. As shown in Figure 3.29, after 24 hours of co-cultivation a release of (Z)-4-OHT is detectable in the separated reporter cells, indicating a fast cargo release from carrier macrophages. Luciferase activity further increase at 48 hours and declined at 72 hours of co-culturing.

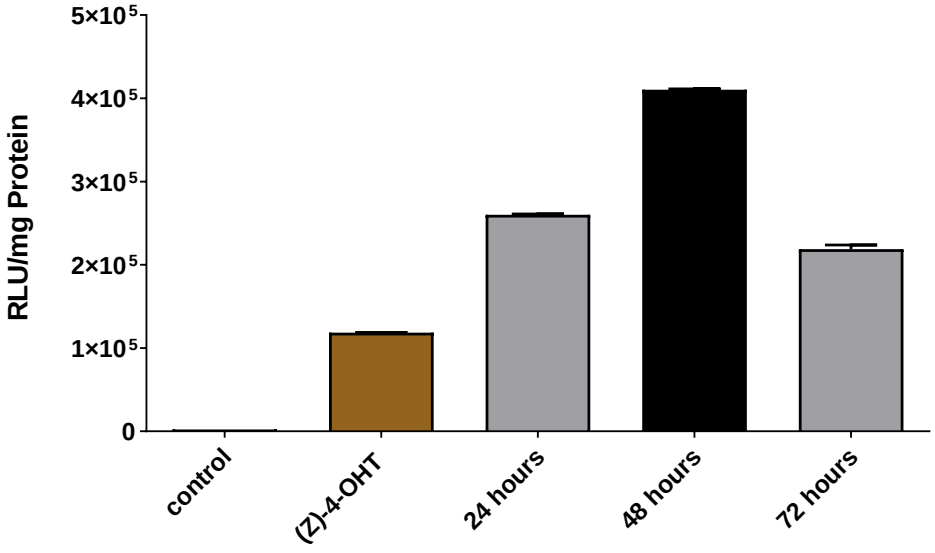

Figure 3-29Spontaneous release of (Z)-4-OHT form macrophages loaded with (Z)-4-OHT -LPSNP. 20µg/mL of (Z)-4-OHT-LPSNP were loaded in 1x 105 J774a.1 cells and co-cultured with Cre-Luc cells for varying amount of time. The results show mean ± SD of triplicates.

Next, it was hypothesized that if the macrophages are loaded with both SPIONs and (Z)-4-OHT- LPSNP and exposed to AMF, the generated magnetic hyperthermia will contribute to burst release of (Z)-4-OHT from macrophages. The magnetic hyperthermia will induce macrophage cell death and hence the release of (Z)-4-OHT from macrophages will be accelerated. To check the effect of magnetic hyperthermia on (Z)-4-OHT release from LPSNP, macrophages were loaded with heat producing SPIONs and cargo containing LPSNP. First cells were loaded with SPIONs and after 6 hours, (Z)-4-OHT-loaded LPSNP were added. The double loaded macrophages were then subjected to magnetic field for 30 minutes and co-cultured with Cre-Luc reporter cells for different amounts of time (24, 48 and 72 hours) in a transwell system. Double loaded control macrophages were mock-treated for 30 minutes and then added into transwell insert. Co-cultivation with control loading of the upper well and addition of (Z)-4-OHT into the upper was performed for 48 hours. In contrast to the situation without magnetic hyperthermia, exposure of double loaded cells to AMF induced a strong release of (Z)-4-OHT which was maximal after 24 hours of co-cultivation (Figure 3.30). (Z)-4-OHT dependent luciferase activity declined at 48 hours and reached low values at 72 hours of co-cultivation. This can be explained from results presented in Figure 3.5, where AMF application induced apoptosis of SPION-loaded macrophages within 24 hours. Here, it can be assumed that apoptosis was induced in the double loaded macrophages through magnetic hyperthermia and thereby the release rate of

(Z)-4-OHT from the cells was increased. Sequential loading of the two kinds of nanoparticles might separate the heat producing SPIONs from the cargo carriers in independent endosomes and thereby heat production would not induce (Z)-4-OHT isomerization strongly. However, without AMF-induced magnetic hyperthermia luciferase reporter gene activity did not reach maximal levels at 24 hours of co-cultivation. As evident from Figure 3.5, when SPIONs loaded macrophages are exposed to AMF, cell death is induced. The induced cell death contributes to rapid release of both LPSNPs and (Z)-4-OHT from the macrophages and hence the burst release at 24 hours is detected from AMF treated cells. This is further confirmed at 48 hours time point as most of (Z)-4-OHT is already released at 24 hours and little (Z)-4-OHT is left in the cells or LPSNPs. Together these results indicate that AMF-induced magnetic hyperthermia can boost cargo release from macrophages in a timely controlled manner.

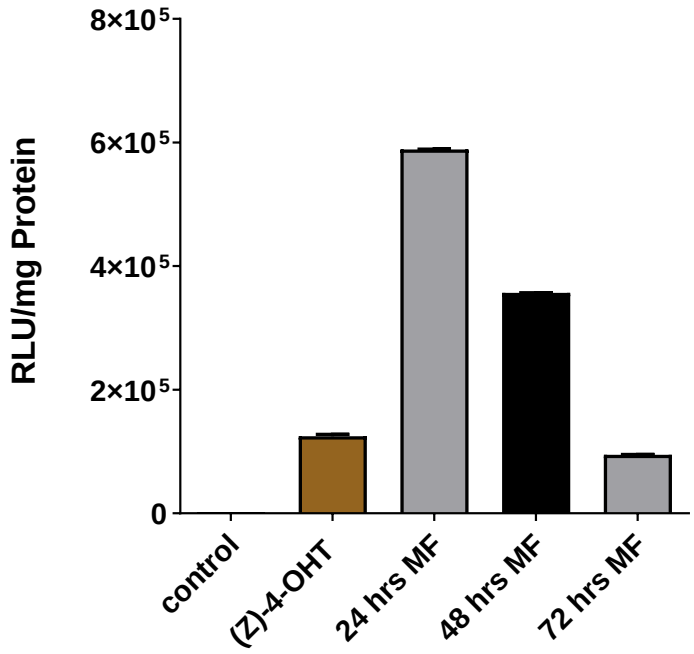

*Figure 3-30Magnetic hyperthermia-mediated bulk release of (Z)-4-OHT from double loaded macrophages. 1 x 105 J774a.1 cells were loaded with 20µg/mL of (Z)-4-OHT-LPSNP and 20µg/mL of SPIONs. An AMF with 779kHz frequency was applied to the cells and incubated with 1*x 10^5Cre-Luc cells for varying amount of time. Bulk release at 24 hours after AMF is seen. Results are presented as mean ± SD of triplicates.

3.3.4 Spontaneous cargo release from large pore silica nanoparticles *in vivo*

After having proven that spontaneous release of active (Z)-4-OHT from large pore silica nanoparticles engulfed in macrophages is possible, release was studied *in vivo*. First, Cre-Luc mice were subcutaneously injected with two different doses of (Z)-4-OHT loaded

LPSNP (25µg or 50µg). Release of (Z)-4-OHT was determined *in vivo* by monitoring luciferase reporter gene activity. Bioluminescent imaging was performed 24, 48 and 72 hours after LPSNP injection. As controls free (Z)-4-OHT (20µg) and blank LPSNPs were injected subcutaneously. As shown in Figure 3.31, 24 hours after injection, luciferase activity was detectable at the site of LPSNP injection indicating that (Z)-4-OHT was released from nanoparticles and activated the $CreER^{T2}$ system in the living organism. While injection of unloaded LPSNPs did not induce luciferase expression at all, direct injection of free (Z)-4-OHT induced a fast and prolonged reporter gene activity. Although 24 hours after injection of (Z)-4-OHT-LPSNP the luciferase signal was detectable at the injection site, this signal decreased over time as opposed to injection of (Z)-4-OHT. The reason for this decline can be that as silica nanoparticles induce inflammation, the inflammatory environment at (Z)-4-OHT-LPSNP injection site might have contributed to elimination of luciferase expressing cells and hence the signal dropped over time.

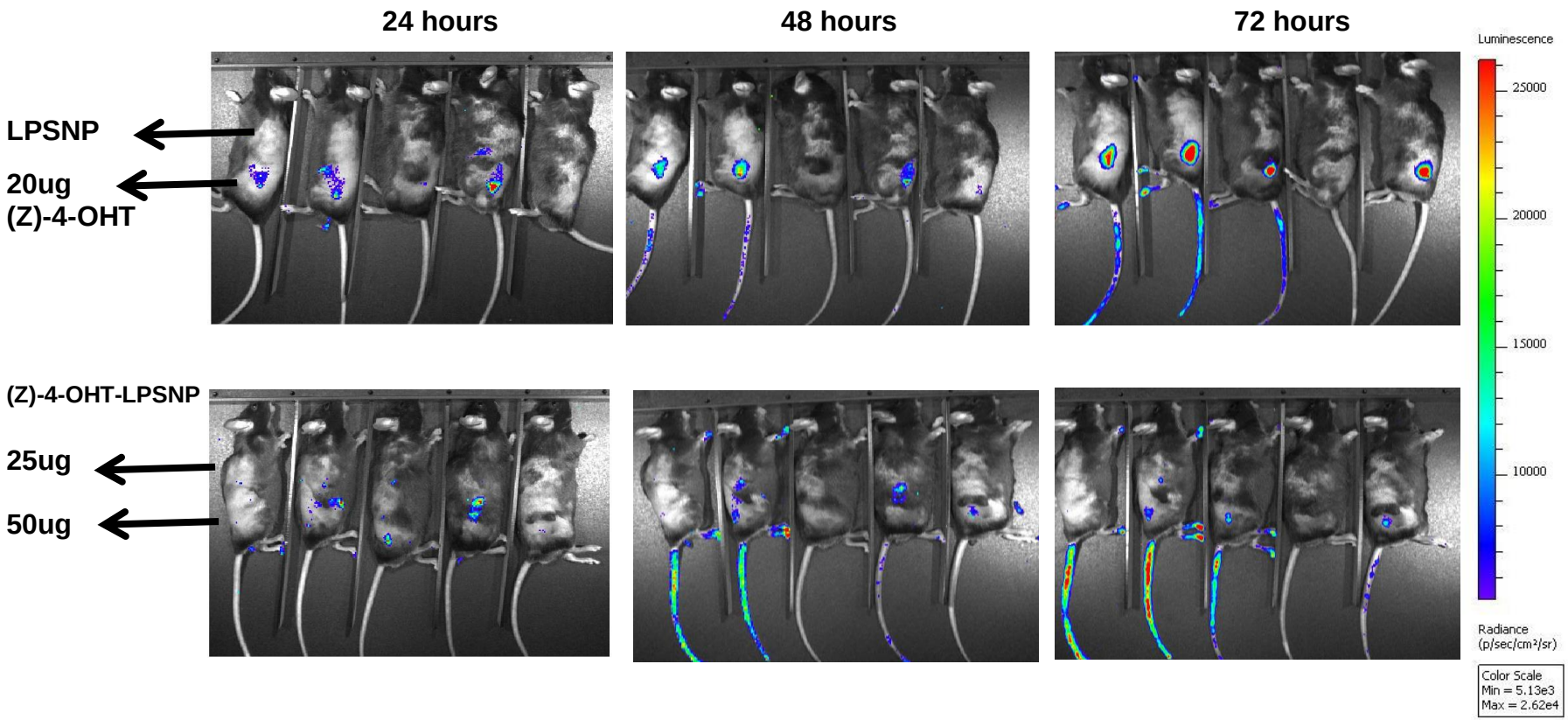

Figure 3-31Spontaneous release of (Z)-4-Hydroxytamoxifen after subcutaneous injection of LPSNP. Cre-Luc mice were injected with either naked LPSNPs or 20 µg of (Z)-4-OHT or 25 or 50µg of (Z)-4-OHT-LPSNP subcutaneously. The arrows show the site of injections. The animals were injected with D-luciferin intra-peritoneally after 24 or 48 or 72 hours post subcutaneous injection and imaged using in vivo imaging system.

3.3.5 Site specific cargo release from large pore silica nanoparticles loaded macrophages *in vivo*

After having established that (Z)-4-OHT can be spontaneously released from LPSNP *in vivo*, targeted release studies were performed. From in vitro data (section 3.2.1) it is evident that M2 macrophages travel faster and over a longer distance when loaded with nanoparticles as compared to either M0 or M1 macrophages. Based on this data, for *in vivo* targeted release experiments, M2 macrophages were used. Briefly, bone marrow derived macrophages were polarized to M2 state by IL4 and IL10 stimulation and then loaded with (Z)-4-OHT containing LPSNPs. Local inflammation was induced in Cre-Luc mice subcutaneously and macrophages were injected intravenously. Whole body bioluminescent imaging of mice was performed 24 and 48 hours after injection of cells. Imaging was performed at the site of inflammation (back view) to visualize specific release and at the belly site to determine also the extent of (Z)-4-OHT release at unspecific sites in the body. As shown in Figure 3.32, at the back site of mice luciferase activity could be detected only at the site of inflammation indicating that macrophages were attracted and active (Z)-4-OHT was released specifically. The luciferase signal declined at 48 hours probably because of the inflammation itself as much of the (Z)-4-OHT target cells might have been killed by the inflammatory microenvironment. This indicates accumulation and release of (Z)-4-OHT. In addition to targeted release, also non-specific or off-target release of (Z)-4-OHT was seen in the liver and spleen (belly view). This might be attributed to the fact that i.v injected macrophages would also be distributed to the liver, spleen and lungs. Importantly, the luciferase signal at the off-targets (i.e. liver and spleen) was comparatively low at 24 hours and increased drastically at 48 hours. In contrast, with regard tothe release at target site the strongest signal was seen at 24 hours. This further supports the hypothesis that the inflammation itself might have triggered the release of (Z)-4-OHT from the macrophages, e.g. by macrophage cell death at target site. These results are further summarized in Figure 3.33.

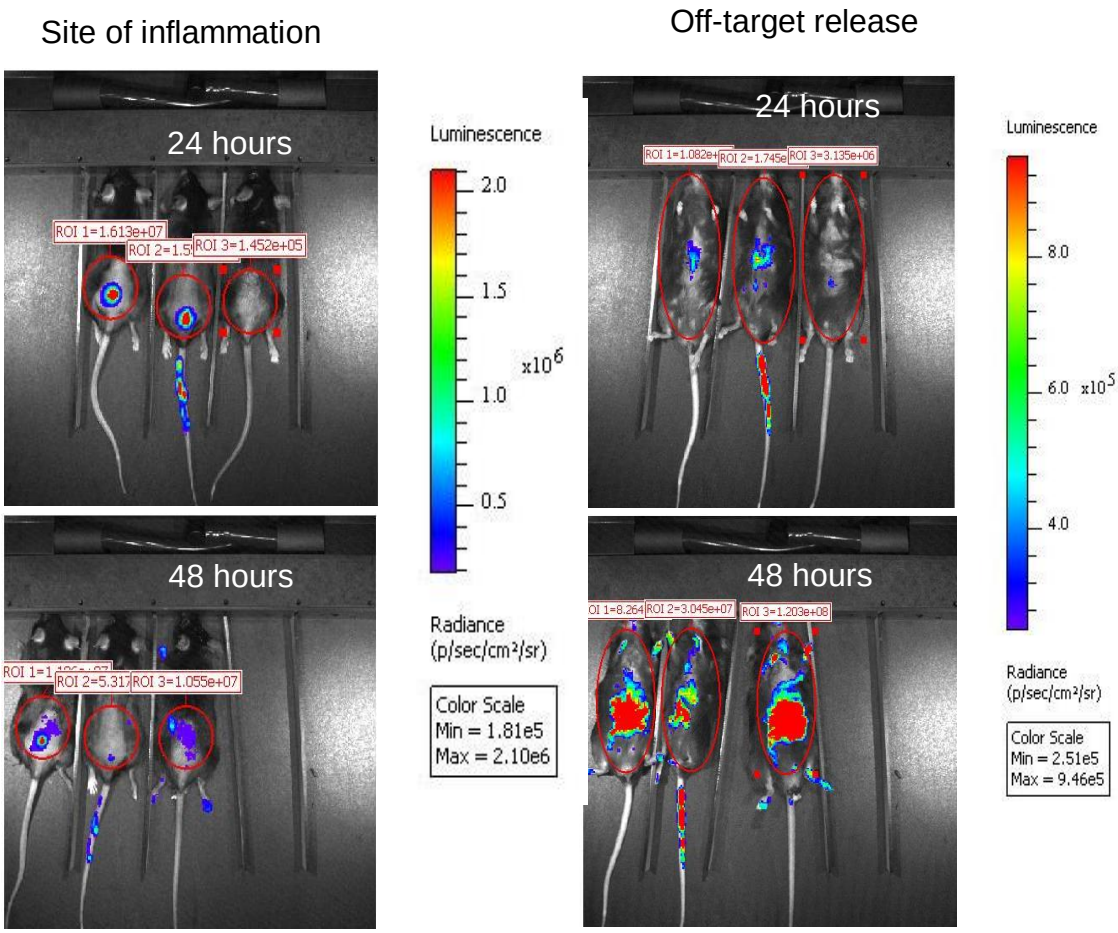

Figure 3-32Release of (Z)-4-OHT after intravenous injection of loaded macrophages into mice with local inflammation. Inflammation was induced in Cre-Luc mice by subcutaneous injection of LPS+SPION mix in the back. 1 x 105 BMD macrophages loaded with 30µg of nanoparticles were injected i.v by tail vein injection. The animals were imaged after i.p injection of 100µL D-Luciferin at 24 hours and 48 hours post i.v injection.

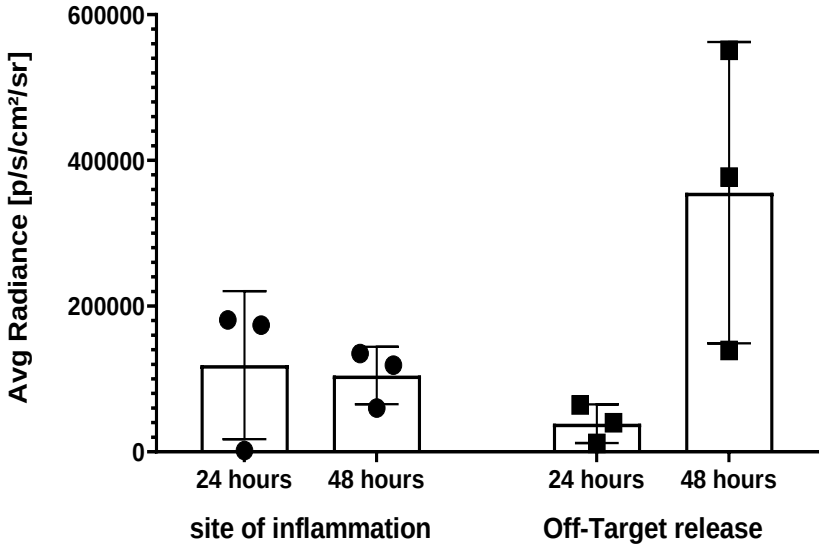

Figure 3-33Quantification of luciferase induced light (see Figure 3-32 for details) at the target site after intravenous injection of loaded macrophages to local inflammation induced model (Cre-Luc mice).

4 DISCUSSION

Targeted delivery of drugs to specific locations in the body and controlled release has been in demand for decades[78]. Recent advances in nanoparticle based drug delivery has opened new dimensions in the field. New strategies have been proposed to achieve better drug release from nanoparticles. These include encapsulation of drugs inside nanoparticles, doping the drugs in mespores as well as covalent bonding of drugs to nanoparticles surface [79]. Different systems for release of cargo molecules from nanoparticles have been introduced over the past 2 decades. However, unspecific release of the therapeutic payload at non-target sites has been reported in a number of cases[11]. Of many release mechanisms described in the literature, the use of hyperthermia as a stimulus for drug release has attracted much attention. Superparamagnatic iron oxide nanoparticles, when subjected to an alternating magnetic field, can generate hyperthermia that can be used as a stimulus for drug release. In general, thermo-sensitive polymers such as poly (N-isopropylacrylamide) [80] or heat sensitive linkers such as elastin like polypeptides [81] are coated on the surface of iron oxide nanoparticles. In addition, drugs that are conjugated to these thermos-sensitive polymers are released when the nanoparticles are exposed to a magnetic field[82]. In addition, magnetic hyperthermia can also have a synergistic effect in cancer therapy[83].

In addition, poor body circulation, rapid clearance or in some cases undesired deposition, inefficient targeting and reduced ability to cross biological barriers has all been the obstacles for which the answers are being sought. Of these, limited ability to cross biological barriers and poor targeting has been of immense importance [84]. These limitations can be addressed with the use of cells as vehicles for transportation of therapeutics. Different cell types that include bacteria, immune cells, and hematopoietic stem cells have been used to deliver drugs to sites of disease. The main challenge that arises with the use of cells as transporting vehicles is the loading of therapeutics and specific accumulation of these cells at site of disease [85]. Macrophages have the natural ability to take up molecules such as nanoparticles through phagocytosis, allowing easy and rapid loading. In addition, macrophages can cross biological barriers and accumulate at therapeutic target site (cancer, inflammation or infection) thus making them a suitable candidate for drug delivery. During the onset of inflammation, (hallmark of cancer) monocytes from bone marrow are released into the circulation that moves to the inflammatory site where they mature and become macrophages [86]. Circulatory

macrophages as well as become active and migrate to the inflammation site. Based on these intrinsic abilities of macrophages to take up nano-sized particles and to migrate to inflammation sites, some studies have exploited them for use as cellular vehicles for transport of drugs [87].

The objective of the current study was to design a drug delivery system that combines targeting of nanoparticles and controlled release of enclosed therapeutics. For this purpose, silica-coated, super-paramagnetic iron oxide nanoparticles were used in which model drugs had been mounted via a thermo-sensitive linker. These drug containing nanoparticles were in turn loaded into macrophages. When subjected to magnetic field, the heat-sensitive linker was cleaved and the cells were killed, together enabling the release of the cargo. It was further shown that loaded macrophages maintain their intrinsic homing property enabling them to migrate to inflammatory sites *in vivo*. Finally, delivery and specific release of cargo molecules by macrophages to sites of inflammation was demonstrated.

4.1 Cellular uptake and in vitro cytotoxicity

Immune cells represent an option for successful targeted drug delivery based on their natural ability of homing to pathogenic site within the body. As well, cells like monocytes, macrophages and dendritic cells can be loaded with therapeutic payloads [88]. In this study, super-paramagnetic iron oxide nanoparticles with silica shell were used. To determine the uptake efficacy they were loaded with FITC molecules. Different macrophage cell lines as well as primary monocytes differentiated into macrophages were tested and all of them, except RAW264.7 cells, showed that as much as 95% of cells phagocytosed the nanoparticles as confirmed with flow cytometry. Confocal microscopic analysis and transmission electron microscopy further confirmed the phagocytosis of nanoparticles and indicated that single cells show massive loading inside endosomal structures. This is in agreement with previous studies which demonstrated that macrophages phagocytose foreign particles which are mostly localized in endosomes or endo-lysosomes [89]. Depending on the size and shape, it has been shown that silica nanoparticles can be toxic to cells [90]. 100-200 nm silica nanoparticles with circular shapes have been shown to be biocompatible with different cell types [91, 92]. In the present study, it was shown that the used nanoparticles did not elicit any cytotoxicity or cell death at as high as 100ug/ml loading concentration and at least 48 hours of subsequent cultivation. This clearly indicates that efficient loading of the used nanoparticles comes along with high biocompatibility.

Macrophages represent plastic cells that can exhibit different polarization abilities depending on the stimulus. For example, macrophages can be polarized to the pro-inflammatory M1 state using LPS and IFN-γ or to the anti-inflammatory M2 state upon IL4 and IL10 treatment [93]. It has been reported that different size silica nanoparticles have different effects on the macrophage polarization states and hence on the functionality of macrophages [94]. Silica nanoparticles reveal inflammatory effects both in vivo and in vitro independent of the route of administration [95]. In the present study, the effect of SPIONs on the polarization state of macrophages was evaluated *in vitro*. When incubated with 100 nm magnetic silica nanoparticles, the BM derived M0 macrophages were polarized to the M1 state as evident from the qRT-PCR expression analysis of M1 and M2 markers in Figure 3.17. This is in accordance with previous studies [96] where RAW265.7 or BMDM cells were used. Different views regarding the uptake capacity of both macrophage types are presented in the literature. For instance, it has been shown that 25 nm silica nanoparticles are efficiently taken up by M1 macrophages as compared to M2 macrophages [97]. In other studies, it has been shown that regardless of the size of silica nanoparticles, the uptake efficiency is higher in the M1 state as compared to the M2 state [98]. In the present study, it was shown that uptake efficiency is not reduced in M2 macrophages and is comparable with both M0 and M1 state. From these results, I suggest that different polarization status of macrophages does not effect on their uptake capability.

4.2 Targeted delivery of macrophages to sites of inflammation

In the present study, macrophages were used as transporting vehicles for drug-loaded nanoparticles. Uptake of SPIONs induced the M1 polarization state with characteristic expression profiles of the respective pro-inflammatory marker genes. Recent knowledge indicates that M1 macrophages display a good phagocytic capacity but have less chemotactic or migratory activities. In contrast, M2 macrophages reveal a pronounced migratory potential [99]. In addition, loaded macrophages are characterized by an increased volume that might further decrease their migratory capacity. Thus, it was important to assess the migration ability of loaded polarized macrophages both in vitro and in vivo.

4.2.1 In vitro migration properties of macrophages

Monocytes and macrophages have been previously evaluated for their transmigration abilities in vitro using different assays. In the present study, as evident from the chemotaxis assay, SPION-loaded M0 macrophages covered the same distance with the same velocity as

loaded M1 macrophages (Figure 3.16). In contrast, nanoparticle-loaded M2 macrophages displayed still a higher migratory potential covering a distance of 550µm at 3.1µm/sec velocity as shown in Figure 3.18. Together these results indicate that M2 macrophages when loaded with silica nanoparticles retained their migratory capacity as opposed to M0 macrophages. To the best of my knowledge, in the present study, the ability of M2 macrophages to transport drug-loaded nanoparticles across membranes (Figure 3.17) have been shown for the first time. Several studies demonstrated that monocytes and macrophages are able to carry nanoparticles across trans-endothelial membranes. For instance, it has been shown that as much as 35% of PMA differentiated THP monocytes crossed transwell membranes after 24 hours towards C5a when decorated with backpacks on their membranes [100]. This was also true when macrophages were loaded with drugs containing liposomes. In this case as much as 30% of loaded macrophages could cross transwell membrane after 24 hours [101]. Nanoparticles are frequently decorated with mannose moieties to target them to cancer cells [102]. Mannose binds to the surface of cancer cells and hence the nanoparticles subsequently release the encapsulated drug [103]. However, because of the spontaneous release of drugs from nanoparticles, the strategy has still to be perfected [104]. M2 macrophages highly express mannose-binding C-type lectin receptors [105]. If loaded with drug-loaded nanoparticles, the M2 macrophages can be promising candidates to be used as targeting vehicles for cancer therapy.

Macrophages and monocytes have been shown to penetrate deep into cancer tissues *in vivo*, even targeting the tumor hypoxic region [43]. This intrinsic ability of macrophages was also evaluated in the present study with the aim to examine if loading macrophages with silica nanoparticles could affect its penetration properties. Therefore, I made use of a 3D co-culturing assay based on spheroid co-cultures of KSHV-infected endothelial cells or MCF-7 cancer cells with labeled macrophages. Laser scanning confocal microscopy revealed that macrophages could penetrate deep into the 3D tumor spheroid independently of SPION loading, indicating little or no effect of silica nanoparticles on the penetration ability of macrophages (Figure 3.15). Macrophages have been previously shown to penetrate as much as 54µm depth into glioma spheroids even when loaded with nanoparticles [106]. Cancer spheroids are resistant to chemotherapy as compared to 2D cultures, which mimic the in vivo situation [107]. In addition, nanoparticles display no or marginal ability to penetrate into cancer spheroids and thus making the chemotherapy unsuccessful [106]. With current results, it can be concluded that penetration of SPION-loaded macrophages gives a new

opportunity to target drugs to unreachable parts of cancer tissue and thus making this region accessible for chemotherapy.

4.2.2 In vivo targeting of inflammation sites

4.2.2.1 Mouse local inflammation model

Inflammation is an adaptive response to infection and has been acknowledged also as an important hallmark of cancer[108]. For this reason, in vivo studies were carried out using a local inflammation model in mice. Lipopolysaccharides (LPS) are known to induce acute inflammation at a sub-lethal dose [109]. Although, when injected subcutaneously, LPS induces systemic inflammation affecting liver, lungs and kidneys [110]. The same is true for poly(I:C) injections [111]. Silica nanoparticles, as evident from this study, are inflammatory in nature as they induce the polarization of M0 macrophages to the M1 state. In addition, it was shown that silica nanoparticles induce IFN induction through activation of the MAVS pathway [112]. Based on this observation, I hypothesized that subcutaneous injection of silica nanoparticles will induce local inflammation, as nanoparticles do not migrate to vital organs after subcutaneous injection. To validate the hypothesis, I made use of an existing mouse model Mx2-Luc that contains the luciferase gene under control of the Mx2 promoter [66]. Mx2 represents a tightly regulated IFN-stimulated gene (ISG) [113]. The rationale behind using this model was that IFNs are known to be induced during the onset of inflammation [114]. Upon silica nanoparticle-induced inflammation in Mx2-Luc mice, type I IFN will be produced which ultimately will trigger the activation of ISG promoters and thereby luciferase activity will be detected by in vivo imaging. When injected subcutaneously into Mx2-Luc mice, silica nanoparticles induced inflammation which was seen with luciferase induction at site of injection. Of importance, no sign of systemic inflammation was observed in these conditions. This induction was even stronger when LPS was mixed silica nanoparticles and injected subcutaneously (Figure 3.19). It is noteworthy that the silica nanoparticles used were mesoporous in nature and LPS incubation with nanoparticles presumably resulted in accumulation of LPS in the nanoparticles. This supports the idea that LPS was released slowly from the nanoparticles over time. When imaging the animals over an extended period and the luciferase signal at injection site peaked at 48 hours (Figure 3.19), confirming this hypothesis.

4.2.2.2 Targeting macrophages to inflammation sites

Monocytes and bone marrow-derived macrophages as well as macrophage cell lines like RAW264.7 have been shown to home at cancer sites upon intravenous injection [43, 59, 114]. This has been particularly true for the delivery of peptides and nanoparticles to mouse brains in a Parkinson disease animal model [44]. This tumor-associated accumulation depends on chemotactic cytokines such as chemokines and complement factors, which are released into the tumor microenvironment by many different cell types such as tumor cells, endothelial cells, mesenchymal stem cells (MSC), cancer-associated fibroblasts, myeloid cells, and neutrophils[115]. In the present study, macrophages were isolated from Mx2-Luc mice and injected via the tail vein into wild type mice in which local inflammation had been induced. The presence of Mx2-Luc macrophages at the site of inflammation was obvious as soon as 24 hours after cell injection. This accumulation also occurred when SPION-loaded macrophages were injected. At the same time point (24 hours after cell injection) the Mx2 dependent luciferase signal was low in the liver and spleen of recipient mice. Literature suggests that only 10% of the injected monocytes home at the tumor site after 24 hours of administration [116]. In the present study, high luciferase signal was seen at the inflammation site as compared to other organs. As in the current model the inflammation was particularly induced locally, it can be expected that other sites such as the liver were devoid from inflammatory signals and thus for macrophages in the liver and that can be the reason why low signal for macrophages was seen in the liver and spleen.

In *in vitro* studies, it was shown that silica nanoparticles induce the polarization of macrophages from M0 to M1 and that M1 macrophages travel less and with low speed as compared to its M0 or M2 counterparts (section 3.2.1). I hypothesized that if M2 macrophages are loaded with silica nanoparticles, in an in vivo setting, they will accumulate with a higher rate and in higher numbers at the site of inflammation as compared to loaded M0 macrophages. To test this hypothesis, macrophages were polarized to the M2 state by IL4 and IL10 treatment and injected to the local inflammation model. Interestingly, after 24 hours of intravenous administration of M2 macrophages, they already travelled to the inflammation site which was comparable to M0 macrophages (Figure 3.19 and 3.20). However, M2 macrophages were present at inflammation site even at 48 hours while in mice transplanted with M0 macrophages showed no accumulation at this time point. To my knowledge, this is the first time M2 macrophages have been shown as vehicles for *in vivo* delivery. The accumulation of M2 macrophages over longer periods of time was

particularly true when the macrophages were loaded with silica nanoparticles and injected intravenously, which results in systemic distribution. Thus, while further work is needed to improve the specificity, as a proof of principle, this study shows that macrophages can be used as vehicle for site specific delivery of cargo loaded nanoparticles.

4.3 Magnetic hyperthermia induced cell death and cargo release

In recent years, controlled drug delivery or controlled release of drugs from nanoparticles has drawn much attention in the field of biomedical science. There are significant advances in the formulation of materials that can be responsive to specific stimuli such as pH, enzymes, light or temperature [61]. One such stimulus is the alternating magnetic field that can be used not only for targeted accumulation of magnetic nanoparticles at a particular site but also for controlled release of drugs [117]. For this purpose, SPIONs have been extensively investigated for their superparamagnetic properties [118]. These superparamagnetic iron oxide nanoparticles when placed in alternating magnetic field start oscillating by Brownian motion and hence produce hyperthermia. Depending on the size of nanoparticles and the strength of the magnetic field, the hyperthermia produced can reach to temperatures as high as 110℃ [35]. This hyperthermia is extremely local to the surface of nanoparticles. Thus, when such nanoparticles are within cellular compartments, the intracellular temperature raise can reach as much as 41-43℃ [119]. Of note, this temperature raise is enough to induce carrier cell killing. In addition, the temperature raise also affects the surrounding tumor cells directly. Accordingly, this strategy is sought extensively in cancer research in combination with chemotherapy, as the hyperthermia alone is not sufficient to eradicate tumor [120].

To increase the drug loading capacity of iron oxide nanoparticles, a number of coating options have been explored such as coating with polymers or inorganic molecules [121-123]. Silica shell iron oxide nanoparticles are recently drawing much attention for their surface functionalization properties and higher drug loading capacity [124].

4.3.1 Magnetic hyperthermia induced cell killing

Magnetic hyperthermia induced cell death has been reported in a number of different cell lines. Upon internalization of superparamagnetic nanoparticles and application of AMF, cell death is induced [125]. In most of the experimental models where tumor cell killing is the primary objective, cancer cells are incubated directly with superparamagnetic nanoparticles in media and upon AMF application, a temperature raise to 44-46℃ is

observed, which is sufficient to activate an apoptotic pathway [126]. This magnetic hyperthermia induced cell killing was also shown for monocytes and dendritic cells [127, 128]. However, detailed information's that elucidate the effect of magnetic hyperthermia on macrophages are missing. In the present study, different macrophage cell lines as well as primary BMDM were loaded with SPION and exposed to magnetic field. As shown in section 3.1.3, all the cell lines as well as primary macrophages were sensitive to magnetic hyperthermia as evident from the induction of apoptosis and decline in metabolic activity with primary cells being the most sensitive. Interestingly, one macrophage cell line, IC21 was resistant to magnetic hyperthermia induced apoptosis. Literature suggests that hyperthermia upregulates the expression of HSP70 which then contributes to apoptosis and necrosis of cells [129]. One explanation for resistance of IC21 cell line to magnetic hyperthermia can be the inability to strongly upregulate HSP70 in response to heat shock. This also indicates that not all cell lines can be used for magnetic hyperthermia and that proper care should be taken in selection of cell lines before proceeding to such studies. In the present study, effect of varying concentration of SPION and the length of magnetic field treatment on hyperthermia induced cell death was investigated. It was observed that SPION-mediated magnetic hyperthermia induces cell death at a concentration as low as 2µg/mL/100,000 cells. Still, the effect increases with increasing concentration of SPION per cells. Interestingly, in a theoretical study it has been reported that to fulfill the requirement of hyperthermia, only a few clusters of SPIONs are needed [130]. In the present study, transmission electron microscopy of macrophages loaded with 20µg/mL SPION showed clumps or clusters of nanoparticles within the cells (Figure 3.1). This partly explains why low amounts of intracellular SPION can induce apoptosis via magnetic hyperthermia. It has also been reported that the duration of AMF or the intensity of AMF affects the outcome of generated hyperthermia [128]. It has been proposed that the initial heat shock produced from the hyperthermia generated by application of high frequency AMF is sufficient to induce apoptosis in dendritic cells [130]. In the present study, high frequency AMF was applied to cells for different lengths of time. It was shown that even as low as 5 minutes of AMF exposure is enough to induce cell death in loaded macrophages (Figure 3.6).

4.3.2 Magnetic hyperthermia induced cargo release

Extensive work has been done for the development of smart delivery system that can trigger controlled release of drugs upon exposure to specific stimuli. One such approach is the use

of hyperthermia induced from magnetic nanoparticles [82]. Based on the approach many nanoparticle systems have been designed, primarily focusing on hydrogels or polymeric composites. These polymeric composites undergo structural changes when exposed to elevated temperatures, which leads to the release of encapsulated drugs [61]. Although, with the use of polymeric composites, comes unspecific drug release at off-targets as the polymers are generally responsive to pH changes. Once in the systemic circulation, these nanoparticles are exposed to different pH in the blood, liver and spleen that induces non-specific release [10]. Alternatively, zinc-doped iron oxide nanocrystals with mesoporous silica coating have shown promising results in vitro [131]. When exposed to magnetic field, the hyperthermia induced from zinc doped iron oxide core causes relaxation of the gate sealing molecules with silica shell and releasing the drugs in the mesopores [132, 133]. SPIONs have currently drawn much attention due to their biocompatibility and ability to generate hyperthermia as much as 110℃. In the present study, model drugs (anticancer Maytansin toxin and/or (Z)-4-OHT) were covalently conjugated via heat sensitive linker to silica shell of superparamagnetic iron oxide nanoparticles. Magnetic hyperthermia induced cargo release was then shown both in vitro and in vivo.

4.3.2.1 Magnetic hyperthermia induced Maytansin release

Hyperthermia induced drug release has been reported as an efficient alternative for controlled drug delivery [82]. There are a number of studies where the release of surface bounded drugs or peptides has been shown upon elevation of temperature. Primarily these include hydrogel based nano-systems where the surface deformation leads to enhanced drug release [134]. Alternatively, magnetic core, mesoporous silica shell nanoparticles have also been demonstrated to release drugs upon exposure to hyperthermia generated by electromagnetic field stimulations [124]. In context of magnetic silica nanoparticles, many strategies have been focused on gating the mesopores of the silica shell with heat labile polymers like PIPAM [135]. Although in such systems, hyperthermia induced drug release have been reported there is always non-specific release of drugs even at physiological temperature. As much as 50% of the conjugated drug can be released even without exposure to hyperthermia. To overcome these problems, in the current study, the silica shell of the nanoparticles were grafted with thermos-sensitive linkers by covalent bonding. These thermosensitive linkers were on turn covalently attached to highly toxic anti-cancer drug, Maytansin. It was shown both in 2D and 3D cell culture systems that there is minimal release of Maytansin at physiological conditions (section 3.1.4). When these toxin-loaded

nanoparticles (T-SPIONs) were loaded into macrophages, exposed to an alternating magnetic field and co-cultured with KSHV infected endothelial cells or MCF-7 breast cancer cells, it induced cancer cell killing. Of interest, there was negligible non-specific release of toxin in the absence of magnetic field. These results were in turn translated in to a 3D cell culture model using KSHV infected endothelial cells in co-culture with T-SPIONs loaded macrophages to make spheroids which mimic in vivo conditions [70, 125]. When these spheroids were exposed to a magnetic field, complete disruption of spheroid structure was observed. From these studies, it was concluded that hyperthermia based cleavage of heat sensitive linkers for the release the attached drug represents a promising alternative for controlled drug release.

4.3.2.2 Magnetic hyperthermia induced (Z)-4-Hydroxytamoxifen release

To visualize the release of drugs in vivo, the Cre-loxP system was exploited. In another strategy, (Z)-4-Hydroxytamoxifen was covalently linked with magnetic silica nanoparticles using4-[Allyl(tert-butoxycarbonyl)amino]butanoic acidheat sensitive linker. Surprisingly, supernatant from OH-TAM-SPIONs exposed to AMF, could not activate luciferase or venusGFP in the reporter cells. As the magnetic hyperthermia leads to a temperature increase of almost 110°C on the particle surface, it was hypothesized that the elevated temperature could lead to the isomerization of (Z)-4-Hydroxytamoxifen from the *Z* to the *E* form. Since the E form is not able to bind and activate CreERT2, this would result in the deactivation of (Z)-4-Hydroxytamoxifen. Indeed, when (Z)-4-Hydroxytamoxifen was exposed to varying elevating temperatures (25, 37, 60 and 90°C) a significant drop in the expression of luciferase was observed (section 3.3.2), which confirms heat sensitivity. This is in line with a previous study [136]. Moreover, an in depth HPLC based analysis performed by Sibel Türkkan, Leibniz University, Hannover, revealed that after exposure of OH-SPIONs to magnetic field, most of the released molecules show the E configuration.

For this reason, an alternative strategy was adopted for targeted delivery of (Z)-4-Hydroxytamoxifen. To this end, (Z)-4-Hydroxytamoxifen was non-covalently entrapped in large pore silica nanoparticles ((Z)-4-OHT-LPSNP). Spontaneous release of (Z)-4-Hydroxytamoxifen was shown after incubation of nanoparticles in culture media for different intervals of time. To achieve induced release from macrophages, both (Z)-4-OHT-LPSNPand SPIONs were combined. After exposure of macrophages carrying both types of particles to a magnetic field, a robust release at 24 hours was observed, while in absence of

the magnetic field low spontaneous release of OH-Tam into the culture media was detectable. This suggests magnetic hyperthermia increased the release of (Z)-4-Hydroxytamoxifen from (Z)-4-OHT-LPSNPloaded macrophages in a synergistic way. As discussed in section 4.3.1, exposure of SPION loaded macrophages to magnetic field induces apoptosis in loaded cells which might have contributed to the rapid release of (Z)-4-Hydroxytamoxifen from the double loaded macrophages.

4.4 Targeted drug delivery *in vivo*

The major aim of the current study was on demand site-specific drug delivery. In the previous section, the targeting of macrophages to inflammation sites*in vivo* and controlled release of model drugs *in vitro*were highlighted. To combine both approaches together, inflammation was induced in Cre-Luc animals. Macrophages were polarized to the M2 phenotype and loaded with either OH-TAM-NP alone or with (Z)-4-OHT-LPSNPand SPION together. As evident from section 3.3.6, macrophages migrated to inflammation sites and released (Z)-4-Hydroxytamoxifen as early as at 24 hours post injection. Opposed to previous studies where macrophages were used to deliver drugs site specifically [106, 116, 137], minor spontaneous release was seen at off-targets. When site-specific magnetic field was applied to the injected animals, a sudden increase of luciferase activity was observed at the inflammation sites suggesting that TAM was released. Systemic [91] or intratumoral[138, 139] injections of nanoparticles rely on passive migration of nanoparticles to diseased site [140]. With the current approach, active targeting of inflammation sites has been achieved with macrophages. In another strategy where nanoparticles were conjugated to monocytes as cellular backpacks, 10% of loaded monocytes were able to reach the target site [43]. In contrast, in the current study, based on the increase of the luciferase signal at the inflammation site, most of the macrophages accumulated at the target site and released the drug. In the last, for most therapeutic studies, multiple injections of nanoparticle-loaded monocytes or macrophages [141] and dendritic cells [142] are needed to gain the therapeutic effect. In the present study, much higher luciferase activity was seen at inflammation site after single injection of (Z)-4-OHT-LPSNP loaded M2 macrophages. It can be safely proposed that the current strategy if adopted for drug release in disease model, the multiple injections can be avoided.

One concern about the use of M2 macrophages is that they are pro-inflammatory and hence might accelerate the inflammation process. In the current strategy, however, macrophages

are used as carrier cells: when SPIONs loaded macrophages reach inflammation sites and magnetic hyperthermia is applied, this also leads to cell death and the macrophages are destroyed. Thus, harmful effects of the carrier M2 macrophages are not envisaged.

5 OUTLOOK

In this study a targeted and controlled drug delivery system was established. Superparamagnetic nanoparticles with covalently attached drugs were mounted in macrophages and the drug release was shown in vitro using both 2D and 3D cell culture system. Macrophages loaded with nanoparticles were also shown to home at the site of inflammation in a mouse model. Although plasticity exists between different macrophage phenotypes, it was shown that both M0 and M2 loaded macrophages can migrate to inflammation site after systemic administration. At the inflammation site, the drug release was shown using (Z)-4-hydroxytamoxifen as model drug. However, it was shown in this thesis that (Z)-4-hydroxytamoxifen was inactivated after magnetic hyperthermia treatment.

This strategy can be further improved when OH-TAM-NP are coated with heat sensitive polymers like PNIPAM where the hydrogel can be dissolved at a small elevation 44-46°C. If macrophages are double loaded with such nanoparticles and SPION and exposed to magnetic field, more controlled release of (Z)-4-Hydroxytamoxifen can be expected. This could solve the problems associated with hyperthermia induced isomerization of (Z)-4-Hydroxytamoxifen as it will be away from the SPIONs and the heat produced by SPIONs is locally on the nanoparticle surface. Further, spontaneous or non-specific release would also be minimized as the OH-TAM-NP would be coated with hydrogels and hence there would be little chance for (Z)-4-Hydroxytamoxifen to go out of the nanoparticle complex. Also, if the distance of drug from the heat center (superparamagnetic iron oxide molecules) is increased, the effect of heat on drug can be minimized. Alternatively, more model drugs such as nafoxidineshould be explored as the current study highlights that magnetic hyperthermia induce drug release strategy is limited to heat resistant drugs. The current strategy can be not only used for site specific drug release but also for visualization of early inflammation or cancer using labelled nanoparticles.

6 REFERENCES

1. Haley, B. and E. Frenkel, *Nanoparticles for drug delivery in cancer treatment.*Urol Oncol, 2008. **26**(1): p. 57-64.

2. Arayne, M.S. and N. Sultana, *Review: nanoparticles in drug delivery for the treatment of cancer.* Pak J Pharm Sci, 2006. **19**(3): p. 258-68.

3. Tiwari, G., et al., *Drug delivery systems: An updated review.* Int J Pharm Investig, 2012. **2**(1): p. 2-11.

4. Muller, R.H. and C.M. Keck, *Challenges and solutions for the delivery of biotech drugs--a review of drug nanocrystal technology and lipid nanoparticles.* J Biotechnol, 2004. **113**(1-3): p. 151-70.

5. Mora-Huertas, C.E., H. Fessi, and A. Elaissari, *Polymer-based nanocapsules for drug delivery.* Int J Pharm, 2010. **385**(1-2): p. 113-42.

6. Gaucher, G., R.H. Marchessault, and J.C. Leroux, *Polyester-based micelles and nanoparticles for the parenteral delivery of taxanes.* J Control Release, 2010. **143**(1): p. 2-12.

7. Barbato, F., et al., *Biodegradable microspheres of novel segmented poly(ether-ester-amide)s based on poly(epsilon-caprolactone) for the delivery of bioactive compounds.* Biomaterials, 2001. **22**(11): p. 1371-8.

8. Liu, N., et al., *A pH- and thermo-responsive poly(amino acid)-based drug delivery system.* Colloids Surf B Biointerfaces, 2015. **136**: p. 562-9.

9. Peppas, N.A., et al., *Poly(ethylene glycol)-containing hydrogels in drug delivery.* J Control Release, 1999. **62**(1-2): p. 81-7.

10. Knipe, J.M. and N.A. Peppas, *Multi-responsive hydrogels for drug delivery and tissue engineering applications.* Regen Biomater, 2014. **1**(1): p. 57-65.

11. Kumari, A., S.K. Yadav, and S.C. Yadav, *Biodegradable polymeric nanoparticles based drug delivery systems.* Colloids Surf B Biointerfaces, 2010. **75**(1): p. 1-18.

12. Langner, M. and T.E. Kral, *Liposome-based drug delivery systems.* Pol J Pharmacol, 1999. **51**(3): p. 211-22.

13. Torchilin, V.P., *Multifunctional, stimuli-sensitive nanoparticulate systems for drug delivery.* Nat Rev Drug Discov, 2014. **13**(11): p. 813-27.

14. Chen, Y., H. Chen, and J. Shi, *Inorganic nanoparticle-based drug codelivery nanosystems to overcome the multidrug resistance of cancer cells.* Mol Pharm, 2014. **11**(8): p. 2495-510.

15. McBain, S.C., H.H. Yiu, and J. Dobson, *Magnetic nanoparticles for gene and drug delivery.* Int J Nanomedicine, 2008. **3**(2): p. 169-80.

16. Wang, K., et al., *Iron-Oxide-Based Nanovector for Tumor Targeted siRNA Delivery in an Orthotopic Hepatocellular Carcinoma Xenograft Mouse Model.* Small, 2016. **12**(4): p. 477-87.

17. Suriyanto, E.Y. Ng, and S.D. Kumar, *Physical mechanism and modeling of heat generation and transfer in magnetic fluid hyperthermia through Neelian and Brownian relaxation: a review.* Biomed Eng Online, 2017. **16**(1): p. 36.

18. Mahmoudi, M., et al., *Superparamagnetic iron oxide nanoparticles (SPIONs): development, surface modification and applications in chemotherapy.* Adv Drug Deliv Rev, 2011. **63**(1-2): p. 24-46.

19. Estelrich, J., et al., *Iron oxide nanoparticles for magnetically-guided and magnetically-responsive drug delivery.* Int J Mol Sci, 2015. **16**(4): p. 8070-101.

20. Yu, M.K., et al., *Drug-loaded superparamagnetic iron oxide nanoparticles for combined cancer imaging and therapy in vivo.*Angew Chem Int Ed Engl, 2008. **47**(29): p. 5362-5.

21. Duncan, B., C. Kim, and V.M. Rotello, *Gold nanoparticle platforms as drug and biomacromolecule delivery systems.* J Control Release, 2010. **148**(1): p. 122-127.

22. Madhusudhan, A., et al., *Efficient pH dependent drug delivery to target cancer cells by gold nanoparticles capped with carboxymethyl chitosan.* Int J Mol Sci, 2014. **15**(5): p. 8216-34.

23. Han, G., P. Ghosh, and V.M. Rotello, *Functionalized gold nanoparticles for drug delivery.* Nanomedicine (Lond), 2007. **2**(1): p. 113-23.

24. Bianco, A., et al., *Biomedical applications of functionalised carbon nanotubes.* Chem Commun (Camb), 2005(5): p. 571-7.

25. Hassan, H.A., et al., *Dual stimulation of antigen presenting cells using carbon nanotube-based vaccine delivery system for cancer immunotherapy.* Biomaterials, 2016. **104**: p. 310-22.

26. He, Q., et al., *A pH-responsive mesoporous silica nanoparticles-based multi-drug delivery system for overcoming multi-drug resistance.* Biomaterials, 2011. **32**(30): p. 7711-20.

27. Slowing, II, et al., *Mesoporous silica nanoparticles as controlled release drug delivery and gene transfection carriers.* Adv Drug Deliv Rev, 2008. **60**(11): p. 1278-88.

28. Ali, A., et al., *Synthesis, characterization, applications, and challenges of iron oxide nanoparticles.*Nanotechnol Sci Appl, 2016. **9**: p. 49-67.

29. Schwaminger, S.P., et al., *Formation of iron oxide nanoparticles for the photooxidation of water: Alteration of finite size effects from ferrihydrite to hematite.* Sci Rep, 2017. **7**(1): p. 12609.

30. Perlstein, B., et al., *Synthesis and characterization of functionalized magnetic maghemite nanoparticles with fluorescent probe capabilities for biological applications.* J Biomed Mater Res B Appl Biomater, 2010. **92**(2): p. 353-60.

31. Roca, A.G., et al., *Design strategies for shape-controlled magnetic iron oxide nanoparticles.* Adv Drug Deliv Rev, 2019. **138**: p. 68-104.

32. Albinali, K.E., et al., *A perspective on magnetic core-shell carriers for responsive and targeted drug delivery systems.* Int J Nanomedicine, 2019. **14**: p. 1707-1723.

33. Zhu, N., et al., *Surface Modification of Magnetic Iron Oxide Nanoparticles.* Nanomaterials (Basel), 2018. **8**(10).

34. Kim, J., et al., *Multifunctional uniform nanoparticles composed of a magnetite nanocrystal core and a mesoporous silica shell for magnetic resonance and fluorescence imaging and for drug delivery.*Angew Chem Int Ed Engl, 2008. **47**(44): p. 8438-41.

35. Wang, L.L., et al., *A Bio-Chemosynthetic Approach to Superparamagnetic Iron Oxide-Ansamitocin Conjugates for Use in Magnetic Drug Targeting.* Chemistry, 2017. **23**(10): p. 2265-2270.

36. Timin, A.S., et al., *Cell-Based Drug Delivery and Use of Nano-and Microcarriers for Cell Functionalization.* Adv Healthc Mater, 2018. **7**(3).

37. Yong, S.B., et al., *Recent challenges and advances in genetically-engineered cell therapy.* J Pharm Investig, 2018. **48**(2): p. 199-208.

38. Litvinov, R.I. and J.W. Weisel, *Role of red blood cells in haemostasis and thrombosis.* ISBT Sci Ser, 2017. **12**(1): p. 176-183.

39. Ihler, G.M., R.H. Glew, and F.W. Schnure, *Enzyme loading of erythrocytes.* Proc Natl Acad Sci U S A, 1973. **70**(9): p. 2663-6.

40. Anselmo, A.C. and S. Mitragotri, *Cell-mediated delivery of nanoparticles: taking advantage of circulatory cells to target nanoparticles.* J Control Release, 2014. **190**: p. 531-41.

41. Xue, J., et al., *Neutrophil-mediated anticancer drug delivery for suppression of postoperative malignant glioma recurrence.* Nat Nanotechnol, 2017. **12**(7): p. 692-700.

42. Yoo, J.W., et al., *Bio-inspired, bioengineered and biomimetic drug delivery carriers.* Nat Rev Drug Discov, 2011. **10**(7): p. 521-35.

43. Huang, W.C., et al., *Tumortropic monocyte-mediated delivery of echogenic polymer bubbles and therapeutic vesicles for chemotherapy of tumor hypoxia.* Biomaterials, 2015. **71**: p. 71-83.

44. Brynskikh, A.M., et al., *Macrophage delivery of therapeutic nanozymes in a murine model of Parkinson's disease.* Nanomedicine (Lond), 2010. **5**(3): p. 379-96.

45. Hirayama, D., T. Iida, and H. Nakase, *The Phagocytic Function of Macrophage-Enforcing Innate Immunity and Tissue Homeostasis.* Int J Mol Sci, 2017. **19**(1).

46. Hettinger, J., et al., *Origin of monocytes and macrophages in a committed progenitor.* Nat Immunol, 2013. **14**(8): p. 821-30.

47. Gordon, S. and A. Pluddemann, *Tissue macrophages: heterogeneity and functions.* BMC Biol, 2017. **15**(1): p. 53.

48. Leopold Wager, C.M. and F.L. Wormley, Jr., *Classical versus alternative macrophage activation: the Ying and the Yang in host defense against pulmonary fungal infections.* Mucosal Immunol, 2014. **7**(5): p. 1023-35.

49. Gordon, S. and F.O. Martinez, *Alternative activation of macrophages: mechanism and functions.* Immunity, 2010. **32**(5): p. 593-604.

50. Fleming, B.D. and D.M. Mosser, *Regulatory macrophages: setting the threshold for therapy.* Eur J Immunol, 2011. **41**(9): p. 2498-502.

51. Classen, A., J. Lloberas, and A. Celada, *Macrophage activation: classical versus alternative.* Methods Mol Biol, 2009. **531**: p. 29-43.

52. Mosser, D.M. and J.P. Edwards, *Exploring the full spectrum of macrophage activation.* Nat Rev Immunol, 2008. **8**(12): p. 958-69.

53. Weissleder, R., M. Nahrendorf, and M.J. Pittet, *Imaging macrophages with nanoparticles.* Nat Mater, 2014. **13**(2): p. 125-38.

54. Nakamura, M., et al., *Time-lapse fluorescence imaging and quantitative single cell and endosomal analysis of peritoneal macrophages using fluorescent organosilica nanoparticles.* Nanomedicine, 2013. **9**(2): p. 274-83.

55. Kwon, Y.M., et al., *Dose-dependent cytotoxicity of clinically relevant cobalt nanoparticles and ions on macrophages in vitro.* Biomed Mater, 2009. **4**(2): p. 025018.

56. McWhorter, F.Y., C.T. Davis, and W.F. Liu, *Physical and mechanical regulation of macrophage phenotype and function.* Cell Mol Life Sci, 2015. **72**(7): p. 1303-16.

57. Oh, N. and J.H. Park, *Endocytosis and exocytosis of nanoparticles in mammalian cells.* Int J Nanomedicine, 2014. **9 Suppl 1**: p. 51-63.

58. Barker, R.N., et al., *Antigen presentation by macrophages is enhanced by the uptake of necrotic, but not apoptotic, cells.* Clin Exp Immunol, 2002. **127**(2): p. 220-5.

59. Zhao, Y., et al., *Active Targeted Macrophage-mediated Delivery of Catalase to Affected Brain Regions in Models of Parkinson's Disease.* J NanomedNanotechnol, 2011. **S4**.

60. Dreaden, E.C., et al., *Small molecule-gold nanorod conjugates selectively target and induce macrophage cytotoxicity towards breast cancer cells.* Small, 2012. **8**(18): p. 2819-22.

61. Sood, N., et al., *Stimuli-responsive hydrogels in drug delivery and tissue engineering.* Drug Deliv, 2016. **23**(3): p. 758-80.

62. Pu, X., et al., *Mesoporous Silica Nanoparticles as a Prospective and Promising Approach for Drug Delivery and Biomedical Applications.*Curr Cancer Drug Targets, 2019. **19**(4): p. 285-295.

63. Gandhi, S., S. Sethuraman, and U.M. Krishnan, *Synthesis, characterization and biocompatibility evaluation of iron oxide incorporated magnetic mesoporous silica.* Dalton Trans, 2012. **41**(40): p. 12530-7.

64. Zhao, B., et al., *The effects of thermo-mechanical load on the vibrational characteristics of ultrasonic vibration system.*Ultrasonics, 2019. **98**: p. 7-14.

65. Goodman, A.M., et al., *Near-infrared remotely triggered drug-release strategies for cancer treatment.* Proc Natl Acad Sci U S A, 2017. **114**(47): p. 12419-12424.

66. Pulverer, J.E., et al., *Temporal and spatial resolution of type I and III interferon responses in vivo.* J Virol, 2010. **84**(17): p. 8626-38.

67. Ralph, P. and I. Nakoinz, *Phagocytosis and cytolysis by a macrophage tumour and its cloned cell line.* Nature, 1975. **257**(5525): p. 393-4.

68. Raschke, W.C., et al., *Functional macrophage cell lines transformed by Abelson leukemia virus.* Cell, 1978. **15**(1): p. 261-7.

69. Mauel, J. and V. Defendi, *Infection and transformation of mouse peritoneal macrophages by simian virus 40.* J Exp Med, 1971. **134**(2): p. 335-50.

70. Dubich, T., et al., *An endothelial cell line infected by Kaposi's sarcoma-associated herpes virus (KSHV) allows the investigation of Kaposi's sarcoma and the validation of novel viral inhibitors in vitro and in vivo.* J Mol Med (Berl), 2019. **97**(3): p. 311-324.

71. Soule, H.D., et al., *A human cell line from a pleural effusion derived from a breast carcinoma.* J Natl Cancer Inst, 1973. **51**(5): p. 1409-16.

72. Sundstrom, C. and K. Nilsson, *Establishment and characterization of a human histiocytic lymphoma cell line (U-937).* Int J Cancer, 1976. **17**(5): p. 565-77.

73. Hameyer, D., et al., *Toxicity of ligand-dependentCre recombinases and generation of a conditional Credeleter mouse allowing mosaic recombination in peripheral tissues.*Physiol Genomics, 2007. **31**(1): p. 32-41.

74. Sandhu, U., et al., *Strict control of transgene expression in a mouse model for sensitive biological applications based on RMCE compatible ES cells.* Nucleic Acids Res, 2011. **39**(1): p. e1.

75. Song, J., et al., *A mouse model for the human pathogen Salmonella typhi.* Cell Host Microbe, 2010. **8**(4): p. 369-76.

76. Trouplin, V., et al., *Bone marrow-derived macrophage production.* J Vis Exp, 2013(81): p. e50966.

77. Matsuda, T. and C.L. Cepko, *Controlled expression of transgenes introduced by in vivo electroporation.* Proc Natl Acad Sci U S A, 2007. **104**(3): p. 1027-32.

78. Rizvi, S.A.A. and A.M. Saleh, *Applications of nanoparticle systems in drug delivery technology.* Saudi Pharm J, 2018. **26**(1): p. 64-70.

79. Kalaydina, R.V., et al., *Recent advances in "smart" delivery systems for extended drug release in cancer therapy.* Int J Nanomedicine, 2018. **13**: p. 4727-4745.

80. Peng, C.L., et al., *Development of thermosensitive poly(n-isopropylacrylamide-co-((2-dimethylamino) ethyl methacrylate))-based nanoparticles for controlled drug release.* Nanotechnology, 2011. **22**(26): p. 265608.

81. Narain, R., et al., *Synthesis of monodisperse biotinylated p(NIPAAm)-coated iron oxide magnetic nanoparticles and their bioconjugation to streptavidin.* Langmuir, 2007. **23**(11): p. 6299-304.

82. Brazel, C.S., *Magnetothermally-responsive nanomaterials: combining magnetic nanostructures and thermally-sensitive polymers for triggered drug release.* Pharm Res, 2009. **26**(3): p. 644-56.

83. Espinosa, A., et al., *Duality of Iron Oxide Nanoparticles in Cancer Therapy: Amplification of Heating Efficiency by Magnetic Hyperthermia and Photothermal Bimodal Treatment.* ACS Nano, 2016. **10**(2): p. 2436-46.

84. Hoet, P.H., I. Bruske-Hohlfeld, and O.V. Salata, *Nanoparticles - known and unknown health risks.* J Nanobiotechnology, 2004. **2**(1): p. 12.

85. Vyas, S.P., A. Singh, and V. Sihorkar, *Ligand-receptor-mediated drug delivery: an emerging paradigm in cellular drug targeting.*Crit Rev Ther Drug Carrier Syst, 2001. **18**(1): p. 1-76.

86. Libby, P., *Inflammatory mechanisms: the molecular basis of inflammation and disease.*Nutr Rev, 2007. **65**(12 Pt 2): p. S140-6.

87. Visser, J.G., A.D.P. Van Staden, and C. Smith, *Harnessing Macrophages for Controlled-Release Drug Delivery: Lessons From Microbes.* Front Pharmacol, 2019. **10**: p. 22.

88. Su, Y., et al., *Design strategies and applications of circulating cell-mediated drug delivery systems.* ACS Biomater Sci Eng, 2015. **1**(4): p. 201-217.

89. Foroozandeh, P. and A.A. Aziz, *Insight into Cellular Uptake and Intracellular Trafficking of Nanoparticles.* Nanoscale Res Lett, 2018. **13**(1): p. 339.

90. Sukhanova, A., et al., *Dependence of Nanoparticle Toxicity on Their Physical and Chemical Properties.* Nanoscale Res Lett, 2018. **13**(1): p. 44.

91. Li, L., et al., *Biodistribution, excretion, and toxicity of mesoporous silica nanoparticles after oral administration depend on their shape.* Nanomedicine, 2015. **11**(8): p. 1915-24.

92. Kim, I.Y., et al., *Toxicity of silica nanoparticles depends on size, dose, and cell type.* Nanomedicine, 2015. **11**(6): p. 1407-16.

93. Huang, X., et al., *Polarizing Macrophages In Vitro.* Methods Mol Biol, 2018. **1784**: p. 119-126.

94. Miao, X., X. Leng, and Q. Zhang, *The Current State of Nanoparticle-Induced Macrophage Polarization and Reprogramming Research.* Int J Mol Sci, 2017. **18**(2).

95. Park, E.J. and K. Park, *Oxidative stress and pro-inflammatory responses induced by silica nanoparticles in vivo and in vitro.*Toxicol Lett, 2009. **184**(1): p. 18-25.

96. Herd, H.L., et al., *Macrophage silica nanoparticle response is phenotypically dependent.* Biomaterials, 2015. **53**: p. 574-82.

97. Gallud, A., et al., *Macrophage activation status determines the internalization of mesoporous silica particles of different sizes: Exploring the role of different pattern recognition receptors.* Biomaterials, 2017. **121**: p. 28-40.

98. Binnemars-Postma, K.A., et al., *Differential uptake of nanoparticles by human M1 and M2 polarized macrophages: protein corona as a critical determinant.* Nanomedicine (Lond), 2016. **11**(22): p. 2889-2902.

99. Vogel, D.Y., et al., *Macrophages migrate in an activation-dependent manner to chemokines involved in neuroinflammation.* J Neuroinflammation, 2014. **11**: p. 23.

100. Anselmo, A.C., et al., *Monocyte-mediated delivery of polymeric backpacks to inflamed tissues: a generalized strategy to deliver drugs to treat inflammation.* J Control Release, 2015. **199**: p. 29-36.

101. Bartneck, M., et al., *Liposomal encapsulation of dexamethasone modulates cytotoxicity, inflammatory cytokine response, and migratory properties of primary human macrophages.* Nanomedicine, 2014. **10**(6): p. 1209-20.

102. Zhu, S., et al., *Targeting of tumor-associated macrophages made possible by PEG-sheddable, mannose-modified nanoparticles.* Mol Pharm, 2013. **10**(9): p. 3525-30.

103. Shibaguchi, K., et al., *MannosylatedPolyrotaxanes for Increasing Cellular Uptake Efficiency in Macrophages through Receptor-Mediated Endocytosis.* Molecules, 2019. **24**(3).

104. Shi, G.N., et al., *Enhanced antitumor immunity by targeting dendritic cells with tumor cell lysate-loaded chitosan nanoparticles vaccine.* Biomaterials, 2017. **113**: p. 191-202.

105. Kerrigan, A.M. and G.D. Brown, *C-type lectins and phagocytosis.* Immunobiology, 2009. **214**(7): p. 562-75.

106. Madsen, S.J., et al., *Macrophages as cell-based delivery systems for nanoshells in photothermal therapy.* Ann Biomed Eng, 2012. **40**(2): p. 507-15.

107. Kunz-Schughart, L.A., *Multicellular tumor spheroids: intermediates between monolayer culture and in vivo tumor.* Cell Biol Int, 1999. **23**(3): p. 157-61.

108. Colotta, F., et al., *Cancer-related inflammation, the seventh hallmark of cancer: links to genetic instability.* Carcinogenesis, 2009. **30**(7): p. 1073-81.

109. Hamesch, K., et al., *Lipopolysaccharide-induced inflammatory liver injury in mice.* Lab Anim, 2015. **49**(1 Suppl): p. 37-46.

110. Copeland, S., et al., *Acute inflammatory response to endotoxin in mice and humans.* Clin Diagn Lab Immunol, 2005. **12**(1): p. 60-7.

111. Lever, A.R., et al., *Comprehensive evaluation of poly(I:C) induced inflammatory response in an airway epithelial model.*Physiol Rep, 2015. **3**(4).

112. Xia, X., et al., *Porous silicon microparticle potentiates anti-tumor immunity by enhancing cross-presentation and inducing type I interferon response.* Cell Rep, 2015. **11**(6): p. 957-966.

113. Kim, M.S., K.S. Min, and K. Imakawa, *Regulation of Interferon-stimulated Gene (ISG)12, ISG15, and MX1 and MX2 by Conceptus Interferons (IFNTs) in Bovine Uterine Epithelial Cells.* Asian-Australas J Anim Sci, 2013. **26**(6): p. 795-803.

114. Kopitar-Jerala, N., *The Role of Interferons in Inflammation and Inflammasome Activation.* Front Immunol, 2017. **8**: p. 873.

115. Nagarsheth, N., M.S. Wicha, and W. Zou, *Chemokines in the cancer microenvironment and their relevance in cancer immunotherapy.* Nat Rev Immunol, 2017. **17**(9): p. 559-572.

116. Combes, F., et al., *Off-Target and Tumor-Specific Accumulation of Monocytes, Macrophages and Myeloid-Derived Suppressor Cells after Systemic Injection.* Neoplasia, 2018. **20**(8): p. 848-856.

117. Tziveleka, L.A., et al., *Development of multiple stimuli responsive magnetic polymer nanocontainers as efficient drug delivery systems.*MacromolBiosci, 2014. **14**(1): p. 131-41.

118. Yoffe, S., et al., *Superparamagnetic iron oxide nanoparticles (SPIONs): synthesis and surface modification techniques for use with MRI and other biomedical applications.*Curr Pharm Des, 2013. **19**(3): p. 493-509.

119. Simeonidis, K., et al., *In-situ particles reorientation during magnetic hyperthermia application: Shape matters twice.* Sci Rep, 2016. **6**: p. 38382.

120. Yang, H.W., et al., *Non-invasive synergistic treatment of brain tumors by targeted chemotherapeutic delivery and amplified focused ultrasound-hyperthermia using magnetic nanographene oxide.* Adv Mater, 2013. **25**(26): p. 3605-11.

121. LaConte, L.E., et al., *Coating thickness of magnetic iron oxide nanoparticles affects R2 relaxivity.* J MagnReson Imaging, 2007. **26**(6): p. 1634-41.

122. Krajewski, M., et al., *High temperature oxidation of iron-iron oxide core-shell nanowires composed of iron nanoparticles.* Phys Chem Chem Phys, 2016. **18**(5): p. 3900-9.

123. Zhou, Z., et al., *Iron/iron oxide core/shell nanoparticles for magnetic targeting MRI and near-infrared photothermal therapy.* Biomaterials, 2014. **35**(26): p. 7470-8.

124. Bumb, A., et al., *Synthesis and characterization of ultra-small superparamagnetic iron oxide nanoparticles thinly coated with silica.* Nanotechnology, 2008. **19**(33): p. 335601.

125. Ullah, S., et al., *Macrophage entrapped silica coated superparamagnetic iron oxide particles for controlled drug release in a 3D cancer model.* J Control Release, 2019. **294**: p. 327-336.

126. Song, A.S., A.M. Najjar, and K.R. Diller, *Thermally induced apoptosis, necrosis, and heat shock protein expression in 3D culture.* J BiomechEng, 2014. **136**(7).

127. Marcos-Campos, I., et al., *Cell death induced by the application of alternating magnetic fields to nanoparticle-loaded dendritic cells.* Nanotechnology, 2011. **22**(20): p. 205101.

128. Asin, L., et al., *Controlled cell death by magnetic hyperthermia: effects of exposure time, field amplitude, and nanoparticle concentration.* Pharm Res, 2012. **29**(5): p. 1319-27.

129. Grimmig, T., et al., *Upregulated Heat Shock Proteins After Hyperthermic Chemotherapy Point to Induced Cell Survival Mechanisms in Affected Tumor Cells From Peritoneal Carcinomatosis.* Cancer Growth Metastasis, 2017. **10**: p. 1179064417730559.

130. Rabin, Y., *Is intracellular hyperthermia superior to extracellular hyperthermia in the thermal sense?* Int J Hyperthermia, 2002. **18**(3): p. 194-202.

131. Chen, F., et al., *Hydrothermal synthesis of a highly sensitive T2-weigthed MRI contrast agent: zinc-doped superparamagnetic iron oxide nanocrystals.* J NanosciNanotechnol, 2011. **11**(12): p. 10438-43.

132. Moise, S., et al., *The cellular magnetic response and biocompatibility of biogenic zinc- and cobalt-doped magnetite nanoparticles.* Sci Rep, 2017. **7**: p. 39922.

133. Thomas, C.R., et al., *Noninvasive remote-controlled release of drug molecules in vitro using magnetic actuation of mechanized nanoparticles.* J Am Chem Soc, 2010. **132**(31): p. 10623-5.

134. Chatterjee, S., P.C. Hui, and C.W. Kan, *Thermoresponsive Hydrogels and Their Biomedical Applications: Special Insight into Their Applications in Textile Based Transdermal Therapy.* Polymers (Basel), 2018. **10**(5).

135. Yu, E., et al., *Improved controlled release of protein from expanded-pore mesoporous silica nanoparticles modified with co-functionalized poly(n-isopropylacrylamide) and poly(ethylene glycol) (PNIPAM-PEG).* Colloids Surf B Biointerfaces, 2017. **149**: p. 297-300.

136. Manns, J.E.H., S.; Brown, J.E.; Double, J.A., *Methods for liquid chromatographic analysis of tamoxifen, tamoxifen metabolites and their geometric isomers in biological samples.* Analytical Proceedings, 1993. **30**(3): p. 161-163.

137. Haney, M.J., et al., *Cell-mediated transfer of catalase nanoparticles from macrophages to brain endothelial, glial and neuronal cells.* Nanomedicine (Lond), 2011. **6**(7): p. 1215-30.

138. Shi, M., et al., *Increased radiosensitivity of colorectal tumors with intra-tumoral injection of low dose of gold nanoparticles.* Int J Nanomedicine, 2016. **11**: p. 5323-5333.

139. Wang, F., et al., *Injectable and thermally contractible hydroxypropyl methyl cellulose/Fe3O4 for magnetic hyperthermia ablation of tumors.* Biomaterials, 2017. **128**: p. 84-93.

140. Danhier, F., O. Feron, and V. Preat, *To exploit the tumor microenvironment: Passive and active tumor targeting of nanocarriers for anti-cancer drug delivery.* J Control Release, 2010. **148**(2): p. 135-46.

141. Basel, M.T., et al., *Cell-delivered magnetic nanoparticles caused hyperthermia-mediated increased survival in a murine pancreatic cancer model.* Int J Nanomedicine, 2012. **7**: p. 297-306.

142. Rosalia, R.A., et al., *CD40-targeted dendritic cell delivery of PLGA-nanoparticle vaccines induce potent anti-tumor responses.* Biomaterials, 2015. **40**: p. 88-97.

7 APPENDIX

7.1 Abbreviations

(Z)-4-OHT	(Z)-4-hydroxytamoxifen
µL	Micro litre
µM	Micro molar
2D	2-dimensional
3D	3-dimensional
Act	Actin
AMF	Alternating magnetic field
Arg	Arginase
AuNPs	Gold nanoparticles
BBB	Blood brain barrier
BMDM	Bone marrow derived macrophages
CR	Controlled release
Cre	Cyclic recombinase
DMEM	Dulbecco's modified eagle medium
EF1α	Elongation factor 1 alpha
ER^{T2}	Estrogen Receptor mutant
FBS	Fetal bovine serum
FCS	Fetal calf serum
GFP	Green Flourescent protein
HEPES	4-(2-hydroxyethyl)-1-piperazineethanesulfonic acid
HSP70	Heat shockprotein 70
IFNγ	Interferon gamma
IL	Interleukin
IMDM	Iscove's modified dulbecco's media
iNOS	Inducible Nitric oxide synthases
IONs	Iron oxide nanoparticles
ISG	IFN-stimulatedgene
IVIS	In vivo imaging system
K-EC	KSHV infected endothelial cells

KSHV	Kaposi's sarcoma-associated herpesvirus
LC50	Median lethal concentration
LPS	Lipopolysaccharide
LPSNP	Large poresilicananoparticles
Luc	Luciferase
MEM	Minimal essential medium
MHT	Magnetic hyperthermia
mL	Milli litre
MSC	Mesenchymal stemcells
MSNs	Mesoporous silica nanoparticles
nm	Nano meter
PGA	Polyglycolic acid
pH	Power of Hydrogen
PIPAM	Poly(N-isopropylacrylamide-co-4-vinylpyridine) [poly(NIPAM-co-4-VP)]
PLA	Polylactic acid
PLGA	Poly lactic-co-glycolic acid
PMA	Para-Methoxyamphetamine
Poly I:C	Polyinosinic:polycytidylic acid
RBCs	Red blood cells
RPMI	Fetal calfserum
SPIONs	Superparamagnetic iron oxidenanoparticles
SV40	Simian vacuolating virus 40
TDD	Targeted drug delivery
TEM	Transmission electron microscopy
TGF	Tumor growth factor
T-SPIONs	Toxin conjugated spions
WST-1	Water soluble tetrazolium salts

7.2 List of figures

7.3 List of tables

ACKNOWLEDGMENTS

It would have been not possible for me to complete this PhD research without the help of so many. They definitely deserve to be acknowledged.

First I would like to thank my supervisor, Prof Dr Dagmar Wirth, for her guidance and encouragement throughout my PhD. She always offered generous and honest support whenever needed. I learned a lot of new things under her supervision.

There are no words to thank Dr Mario Koester. He is one of the best person I have met in Germany. I found him a true genius and intellectual. He put up with me with calmness and patience on almost daily basis whenever I annoyed him with many questions. He taught me how to break down complex problems into simple pieces.

I would also like to thank Dr Hansjorg Hauser for his advice and scientific inputs during our group discussions or in my thesis committees. With this, I would like to thank my thesis committee members Prof Dr Andreas Krischning and Prof Dr Ingo Schmitz for their valuable inputs during our meetings. Thanks to my PhD Thesis reviewer Prof Dr Melanie Brinkmann for accepting to review my thesis on such a short notice.

I would like to thank all the members of MSYS for the wonderful atmosphere, support and the laughs we shared. The moments spent with you are beautiful memories that I will always remember. Dr Ivana Kutle, Dr Natascha Goedeke, Anne Dittrich, Aileen Bleisch, Artur Wilhelm and Sandhya Kumar thanks to all of you for all the support you have given me all these years. Special thanks to my dear friend and colleague Kingsley Kumashie for being there for me whenever I needed him. Off course, I cannot forget the help and support given by Petra Beuhr, Sabrina Herrmann and Sara Behme. I would also like to thank all the members of Inscreenex for the enlightening scientific discussions in our

brainstorming and meetings. Dr Tobias helped me in cell culture and provided me many cell types.

I would like to specially mention DAAD for granting me the fellowship to pursue my doctoral degree in Germany.

The graduate school of HZI offered very organised and structured PhD program which I want to specially appreciate. Apart from this, the graduate school also sponsored some of the conferences for me. For all of which I am thankful.

During my PhD, I became friend with so many amazing people, met a lot of intellectuals and got to know many of my colleagues from other Helmholtz institutes. I cannot name all of them but I would specially thank Vasiliki Anastasopouloufor putting up with me all this time, encouraging and believing in me.

Off course, I cannot forget the support from Theresa Wegner. She was always there for me whenever I needed her despite how many arguments and fights we had. She is one of the best person I met in Germany.

Finally I would like to thank my family for their love, encouragement, belief and patience. Without whose understanding, I would have never been able to come this far.

Sami Ullah

SchöppenstedterStraße 2, 38100, Braunschweig, Germany
Date of Birth: 28/11/1986 **Gender**: Male **Email:** samibiotech@gmail.com

Education:

PhD in Biotechnology **2015-2019**

Exploiting Macrophages and Nanoparticles for Targeted and Controlled Drug Delivery
Model System for Infection and Immunity,
Helmholtz center for infection research, Braunschweig, Germany.

MPhil in Virology and Immunology **2010-2012**

Evaluation of Expression Pattern of miRNA-146a in Rheumatoid Arthritis Patients
Atta-ur-Rehman School of Applied Biosciences,
National University of Science and Technology, Islamabad, Pakistan

BS (Hons) in Biotechnology **2005-2009**

Effects of gasoline engine emissions on health status of auto rickshaw drivers at DIR (L) KpK
Department of Biotechnology,
University of Malakand, Chakdara, Pakistan

Experience:

IT manager **1st Jul 2017-1st Dec 2019**
Model System for Infection and Immunity,
Helmholtz Centre for Infection Research, Braunschweig (Germany)

Leader of communication working group **1st Jan 2018-1st Feb 2019**
Helmholtz Juniors (Helmholtz-Gemeinschaft Deutscher Forschungszentren), Berlin

Lecturer (Biotechnology) **5thNov,28th may 2015**
Shaheed Benazir Bhutto University, Sheringal, Dir Upper, KP, Pakistan

Research Officer (Immuno-Genetics) **1stFeb, 2011-1st Oct 2012**
National University of Science and Technology, Islamabad, Pakistan

Research Officer (Molecular Biology) **1stJan, 2010-1st Oct 2010**
Department of Biotechnology, University of Malakand, Chakdara, Pakistan

List of Publications:

PhD Publications:

1. **Sami Ullah**, Sibel Türkkan, Hansjörg Hauser, Andreas Kirschning, and Mario Köster, Dagmar Wirth (2019): Macrophage and silica nanoparticles mediated targeted delivery of (Z)-4-Hydroxytamoxifen*in vivo*, **(Manuscript in preparation)**
2. **Sami Ullah**, Katja Seidel, Sibel Türkkan, Dawid Peter Warwas, Tatyana Dubich, Manfred Rohde, Hansjörg Hauser, Peter Behrens, Andreas Kirschning, and Mario Köster, Dagmar Wirth (2019): Macrophage entrapped silica coated superparamagnetic iron oxide particles for controlled drug release in a 3D cancer model, *Journal of controlled Release*. 294:327-336
3. Muhammad Imran Rahim, **Sami Ullah**, Peter P Mueller (2018). Advances and Challenges of Biodegradable Implant Materials with a Focus on Magnesium-Alloys and Bacterial Infections, *Metals*. 8(7), 532

Previous Publications:

4. **Sami Ullah**, Muhammad Akram Khan, Shafiq Ur Rahman, Imran Khan, Fazal Akbar, Anshu Babbar (2018). Molecular characterization and clinical epidemiology of HCV in District Dir (Lower), Pakistan, *Virus Disease***.**29 (3):369-374
5. S. Umar, **Sami Ullah**, M. Yaqoob, M.A.A. Shah (2018). Chicken infectious anemia, an immunosuppressive disease of poultry birds, *World Poultry Science Journal*. 70(4):759-766
6. **Sami Ullah,** Attya Bhatti, Peter John (2012): MicroRNAs with a role in gene regulation and in human diseases, *molecular biology reports.41:225–232*
7. **Sami Ullah**, Muhammad Ali A. Shah, Nosheen Riaz (2012): Recent advances in development of DNA Vaccines against HCV, *Indian Journal of Virology* , 23 (3): 253-260
8. **Sami Ullah**, Muhammad Ali A. Shah, and Nosheen Riaz, Sajid Umar (2012): DNA Vaccines against Influenza: Recent Research and future prospects, *World Poultry Sciences journal,69, pp 125-134.*
9. Sajid Umar, Muhammad Younus, Muti Ur Rehman, Asim Aslam, Muhammad Ali Abdullah Shah, Muhammad Tanveer Munir, Sajjad Hussain, Farooq Iqbal, Muhammad Saleem Fiaz, **Sami Ullah** (2015). Role of aflatoxin toxicity on transmissibility and pathogenicity of H9N2 avian influenza virus in turkeys. *Avian Pathology*. 44(4): 305-310
10. **Sami Ullah**, Ayaz Ali Khan, Mir Azam Khan &Iltaf Ahmed (2011): Effects of gasoline engine emissions on health status of auto rickshaw drivers at DIR (L) Khyber Pakhtunkhwa, *Toxicological & Environmental Chemistry*. 94 (2): 411-422